



LUND UNIVERSITY

Primary Production in African Drylands

Quantifying Supply and Demand Using Earth Observation and Socio-ecological Data

Abdi, Abdulhakim

2017

Document Version:

Publisher's PDF, also known as Version of record

[Link to publication](#)

Citation for published version (APA):

Abdi, A. (2017). *Primary Production in African Drylands: Quantifying Supply and Demand Using Earth Observation and Socio-ecological Data*. [Doctoral Thesis (compilation), Dept of Physical Geography and Ecosystem Science]. Lund University, Faculty of Science, Department of Physical Geography and Ecosystem Science.

Total number of authors:

1

Creative Commons License:

CC BY-NC-ND

General rights

Unless other specific re-use rights are stated the following general rights apply:

Copyright and moral rights for the publications made accessible in the public portal are retained by the authors and/or other copyright owners and it is a condition of accessing publications that users recognise and abide by the legal requirements associated with these rights.

- Users may download and print one copy of any publication from the public portal for the purpose of private study or research.
- You may not further distribute the material or use it for any profit-making activity or commercial gain
- You may freely distribute the URL identifying the publication in the public portal

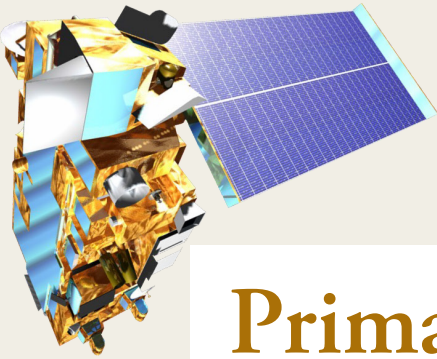
Read more about Creative commons licenses: <https://creativecommons.org/licenses/>

Take down policy

If you believe that this document breaches copyright please contact us providing details, and we will remove access to the work immediately and investigate your claim.

LUND UNIVERSITY

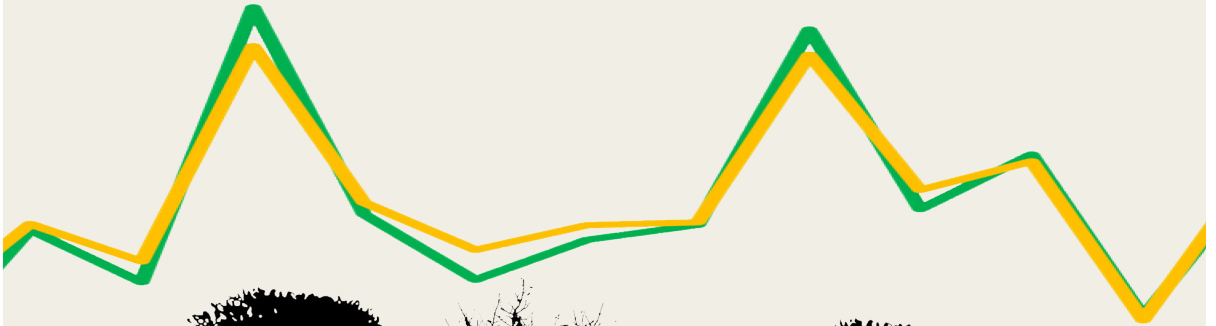
PO Box 117
221 00 Lund
+46 46-222 00 00



Primary Production in African Drylands

Quantifying Supply and Demand Using Earth
Observation and Socio-ecological Data

ABDULHAKIM MOHAMED ABDI | FACULTY OF SCIENCE | LUND UNIVERSITY



Primary Production in African Drylands

Primary Production in African Drylands

Quantifying Supply and Demand Using Earth
Observation and Socio-ecological Data

Abdulahakim Mohamed Abdi



LUND
UNIVERSITY

DOCTORAL DISSERTATION

by due permission of the Faculty of Science, Lund University, Sweden.
To be defended at Auditorium Pangea, Geocentrum II, Sölvegatan 12, Lund.

Friday, March 3rd 2017 at 10:00 am.

Faculty opponent

Professor Steven W. Running

Numerical Terradynamics Simulation Group

University of Montana

Organization LUND UNIVERSITY		Document name DOCTORAL DISSERTATION	
Department of Physical Geography and Ecosystem Science Sölvegatan 12, SE-22362, Lund, Sweden		Date of issue 2017-02-07	
Author: Abdulkhakim Mohamed Abdi		Sponsoring organization: Swedish National Space Board	
Title and subtitle Primary Production in African Drylands: Quantifying Supply and Demand Using Earth Observation and Socio-ecological Data			
<p>Abstract</p> <p>The human-environment connection in the mostly rural drylands of sub-Saharan Africa forms a complex, interlinked system that provides ecosystem services. This system is susceptible to climatic variability that impacts the supply of its products, and high population growth, which impacts the demand for these products. When plants remove carbon dioxide from the atmosphere through the process of photosynthesis, they use some of this carbon to maintain plant cellular structure. The rest is stored as plant tissue and forms plant biomass. The annual accumulation of this plant biomass is called net primary production (NPP). On an annual basis, NPP supplies the provision of crops, animal feed and pasture. The societal implications of reduced NPP can be severe, possibly leading to crop failure and eventual food insecurity. The trends in NPP supply over sub-Saharan Africa between 2000 and 2013 are significant over 32% of the area (4.7 million km²). However, they are concentrated in three distinct regions: the western Sahel (2 g C m⁻² yr⁻¹), central Africa (30 g C m⁻² yr⁻¹) and parts of Zambia, Malawi and Mozambique (-25 g C m⁻² yr⁻¹). In contrast, the mean overall trend in NPP demand is 3.5 g C m⁻² yr⁻¹, though in urban areas it averages approximately 50 g C m⁻² yr⁻¹. The tradeoffs between NPP supply and demand (i.e. change in one quantity relative to another) are locally constrained and linked to the prevailing climate, population growth and net migration. The demand-supply balance of NPP is influenced by climate, such as variability caused by the El Niño – Southern Oscillation. The greatest sensitivity to El Niño occurs in Southern Africa. Here, a +1°C shift in the Niño 3.4 index (as a measure of El Niño) causes a mean change in the NPP supply of -6.6 g C m⁻² yr⁻¹. Despite the fact that there were more La Niña events than El Niño events during the period of this study, the negative impact of El Niño on Southern Africa is strong enough to tip the balance toward the negative. Climatic variability influences the rate of carbon uptake and in sub-Saharan drylands all plants undergo photosynthesis at the expense of losing moisture to the atmosphere. The two main moisture related biophysical limitations, plant available water and vapor pressure deficit, together limit plant carbon uptake by influencing the greening and browning phases of vegetation phenology. The combination of Earth observation data (Land Surface Temperature, Enhanced Vegetation Index, and shortwave infrared surface reflectance) in a multiple regression model was able to explain 89% of the variability of in situ measured carbon uptake across three Sahelian sites. Testing the new Plant Phenology Index (PPI) to get better estimates of sub-Saharan carbon uptake showed that a PPI-based model was able to capture the magnitude of in situ carbon uptake relatively well ($R^2 = 0.75$, 1.39 g C m⁻² d⁻¹) compared to the other tested models. However, the performance of PPI in these semi-arid systems can be further improved through the inclusion of total chlorophyll content as it is a principal factor influencing carbon assimilation.</p>			
Key words: Vegetation, Earth Observation, Drylands, Africa, Net Primary Production, Coupled Human and Natural Systems			
Classification system and/or index terms (if any)			
Supplementary bibliographical information		Language	
ISSN and key title		ISBN: 978-91-85793-77-8	
Recipient's notes	Number of pages 180	Price	
	Security classification		

I, the undersigned, being the copyright owner of the abstract of the above-mentioned dissertation, hereby grant to all reference sources permission to publish and disseminate the abstract of the above-mentioned dissertation.

Signature

Date 2017-01-24

Primary Production in African Drylands

Quantifying Supply and Demand Using Earth
Observation and Socio-ecological Data

Abdulhakim Mohamed Abdi



LUND
UNIVERSITY

Cover Illustrations: *Front cover:* Rendering of the Terra spacecraft by Reto Stöckli, NASA Earth Observatory (used with permission). Time series graph of leaf area index (green line) and fraction of absorbed photosynthetically active radiation (yellow line). *Back cover:* The trend in NPP demand for African drylands (2000 – 2011), larger circles denote higher trend in demand for NPP. The gray color denotes arid, semi-arid and dry sub-humid areas.

© Abdulhakim Mohamed Abdi, 2017

Faculty of Science
Department of Physical Geography and Ecosystem Science

ISBN (print): 978-91-85793-77-8

ISBN (PDF): 978-91-85793-78-5

Printed in Sweden by Media-Tryck, Lund University, Lund 2017



war baa u gaajo xun

the worst hunger is the one for information

Somali proverb

Contents

Scientific Papers	10
Abstract	11
1. Introduction	13
1.1 The human-environment connection in African drylands	13
1.2 The supply of vegetation productivity	17
1.3 The demand for food, feed and fuel.....	20
1.4 The demand-supply balance of net primary production	23
1.5 Research objectives	26
2. Data and Methods.....	27
2.1 Satellite-derived NPP supply (Papers I and II).....	27
2.2 Computation of NPP demand (Papers I and II)	27
2.3 Modeling current and future African populations (Paper III).....	31
2.4 Standardization of Niño-3.4 anomalies (Paper II)	33
2.5 Calculation of water control variables (Paper IV)	34
2.6 Formulating a GPP model based on PPI (Paper V).....	35
3. Results and Discussion.....	37
3.1 Patterns and trends in NPP supply and demand (Papers I and II)	37
3.2 Role of ENSO in the demand-supply balance of NPP (Paper II)	40
3.3 Validation of African population projections (Paper III)	42
3.4 Water controls on Sahelian GPP (Paper IV).....	44
3.5 Potential of PPI to estimate GPP (Paper V).....	46
4. Conclusions and Broader Impacts	49
5. Outlook.....	53
Acknowledgements	55
References	57

Scientific Papers

- I. Abdi, A. M., Seaquist, J., Tenenbaum, D. E., Eklundh, L., & Ardö, J. (2014). The supply and demand of net primary production in the Sahel. *Environmental Research Letters*, 9(9), 094003.
- II. Abdi, A. M., Vrieling, A., Yengoh, G. T., Anyamba, A., Seaquist, J. W., Ummenhofer, C. C., & Ardö, J. (2016). The El Niño – La Niña cycle and recent trends in supply and demand of net primary productivity in African drylands. *Climatic Change*, 138(1), 111-125.
- III. Boke-Olén, N., Abdi, A. M., Hall, O., Lehsten, V. (2017). High-resolution African population projections from radiative forcing and socio-economic models, 2000 to 2100. *Scientific Data* 4: 160130.
- IV. Abdi, A. M., Boke-Olén, N., Tenenbaum, D. E., Tagesson, T., Cappelaere, B., & Ardö, J. (2017). Evaluating water controls on vegetation growth in the semi-arid Sahel using field and Earth observations data. *Submitted*.
- V. Abdi, A. M., Boke-Olén, N., Jin, Hongxiao, Eklundh, L., Lehsten, V., & Ardö, J. (2017). Estimating gross primary productivity in semi-arid Africa using the plant phenology index. *Manuscript*.

Contributions

Papers I & V: AMA designed the study, conducted the analysis, interpreted the results with the co-authors, and led the writing of the manuscript.

Papers II & IV: AMA conceived and designed the study, conducted the analysis, interpreted the results with the co-authors, and wrote the manuscript.

Paper III: AMA conceived the study with NBO, and contributed to the analysis and writing of the manuscript.

Paper I reprinted with permission from IOP Publishing.

Paper II reprinted with permission from Springer.

Paper III reprinted under a Creative Commons Attribution 4.0 License (CC-BY).

Abstract

The human-environment connection in the mostly rural drylands of sub-Saharan Africa forms a complex, interlinked system that provides ecosystem services. This system is susceptible to climatic variability that impacts the supply of its products, and high population growth, which impacts the demand for these products. When plants remove carbon dioxide from the atmosphere through the process of photosynthesis, they use some of this carbon to maintain plant cellular structure. The rest is stored as plant tissue and forms plant biomass. The annual accumulation of this plant biomass is called net primary production (NPP). On an annual basis, NPP supplies the provision of crops, animal feed and pasture. The societal implications of reduced NPP can be severe, possibly leading to crop failure and eventual food insecurity. The trends in NPP supply over sub-Saharan Africa between 2000 and 2013 are significant over 32% of the area (4.7 million km²). However, they are concentrated in three distinct regions: the western Sahel (2 g C m⁻² yr⁻¹), central Africa (30 g C m⁻² yr⁻¹) and parts of Zambia, Malawi and Mozambique (-25 g C m⁻² yr⁻¹). In contrast, the mean overall trend in NPP demand is 3.5 g C m⁻² yr⁻¹, though in urban areas it averages approximately 50 g C m⁻² yr⁻¹. The tradeoffs between NPP supply and demand (i.e. change in one quantity relative to another) are locally constrained and linked to the prevailing climate, population growth and net migration. The demand-supply balance of NPP is influenced by climate, such as variability caused by the El Niño – Southern Oscillation. The greatest sensitivity to El Niño occurs in Southern Africa. Here, a +1°C shift in the Niño 3.4 index (as a measure of El Niño) causes a mean change in the NPP supply of -6.6 g C m⁻² yr⁻¹. Despite the fact that there were more La Niña events than El Niño events during the period of this study, the negative impact of El Niño on Southern Africa is strong enough to tip the balance toward the negative. Climatic variability influences the rate of carbon uptake and in sub-Saharan drylands all plants undergo photosynthesis at the expense of losing moisture to the atmosphere. The two main moisture related biophysical limitations, plant available water and vapor pressure deficit, together limit plant carbon uptake by influencing the greening and browning phases of vegetation phenology. The combination of Earth observation data (Land Surface Temperature, Enhanced Vegetation Index, and shortwave infrared surface

reflectance) in a multiple regression model was able to explain 89% of the variability of in situ measured carbon uptake across three Sahelian sites. Testing the new Plant Phenology Index (PPI) to get better estimates of sub-Saharan carbon uptake showed that a PPI-based model was able to capture the magnitude of in situ carbon uptake relatively well ($R^2 = 0.75$) compared to the other tested models. However, the performance of PPI in these semi-arid systems can be further improved through the inclusion of total chlorophyll content as it is a principal factor influencing carbon assimilation.

1. Introduction

*This is a place without one patch of ground
Where the wild game herds could graze,
It is a place where beasts must pluck
Small mouthfuls here and there of scrub and straw,
It is a place of no abiding use,
A place where teeth will find no food to chew!*

“A Land of Drought” –Sayyid Maxamed Cabdille Xasan (1856 – 1920)

1.1 The human-environment connection in African drylands

The canto above, composed by a Somali pastoral leader in the Horn of Africa, exemplifies the relationship humans have with the land on which their livelihood depends. More than half of the African continent can be classified as a dryland system that is characterized by low rainfall and high evapotranspiration (Figure 1). Indeed, Africa contains some of the driest regions on Earth that constitute some of the oldest continually inhabited environments (Templeton, 2002). Understanding of these systems has changed over time. The Scottish philosopher Adam Smith posited in his 1776 work, *“The Wealth of Nations”*, that the natural progression of livelihoods was from hunter to pastoralist to farmer (Smith, 1776). However, it is now well-known that pastoralism evolved from agriculture as an alternative means of subsistence in arid and semi-arid regions during periods of drought (Lees and Bates, 1974). A considerable portion of the population of sub-Saharan Africa lives in rural drylands that form complex landscapes (Figure 2) where agriculture, pastoralism and agro-pastoralism are the principal livelihoods (Nicholson, 2011). Most of sub-Saharan Africa has one rainy season, except East Africa, which has two. Each rainy season lasts between one to three months and is the principal growing season for vegetation, both natural and farmed. The end of the rainy season heralds start of the dry season when drought conditions take hold and both

human and natural systems adopt measures that ensure their survival. In the natural system, herbaceous vegetation senesces, seeds remain dormant, and drought-deciduous trees shed leaves to minimize water loss (Nicholson, 2011). Some trees with deep roots and succulent shrubs with water storing mechanisms remain green during the dry season, and serve as forage for livestock and wild game. The people of sub-Saharan drylands have developed effective adaptation and mitigation strategies, rooted in indigenous knowledge, to cope with the high climatic variability. The dry season is the time for pastoralists and agro-pastoralists to move their livestock herds to where there are pastures. Farmers, on the other hand, exploit market opportunities during the dry season by engaging in activities such as seasonal economic migration, trade in arts and crafts, and artisanal mining (Batterbury, 2001; de Haan et al., 2002; Dovie, 2003). For example, during the dry season in central Sudan it is common for the majority of young men from farming villages to undertake economic migration to the capital Khartoum or to the gold mines in the north of the country¹.

Droughts are common in sub-Saharan Africa, and in the event of one the dry season can be prolonged causing extended drought conditions. Between 1900 and 2013, 642 droughts were reported across the world (Masih et al., 2014). Forty-five percent (291) of these droughts were in Africa and affected 362 million people, including 847,143 mortalities (Masih et al., 2014). That being said, it is important to note that mortalities coincident with periods of intense drought are not only a function of drought itself, but also the dominant political ecosystem (Sen, 1999). For example, the devastating drought of 1972-75 severely impacted the Horn of Africa and caused a minimum of 200,000 deaths² in Ethiopia (Degefu, 1988; Seaman, 1993). In contrast, during the same drought neighboring Somalia experienced a distinctly lower casualty level (~20,000 deaths) due to a relatively proactive intervention by the government (Samatar, 1989; Ahmed and Green, 1999). On the other hand, the rainy season can be intense, i.e. large amounts of rain falling over a relatively short period of time, and can cause widespread flooding as happened in 2007 when 45 heavy rainfall events displaced 2.5 million people across several sub-Saharan countries (Tschakert et al., 2010).

The human-environment connection in the drylands of sub-Saharan Africa forms a complex, interlinked system that provides ecosystem services. The majority of food consumed in the region comes from domestic sources (Barrett and Upton, 2013), making the natural system a crucial direct factor that acts both as a source

¹ Based on group interviews conducted in the village of Naseem (13.351°N, 30.499°E), North Kordofan, Sudan on January, 25th 2014.

² This estimate has been challenged by several authors, see for example: Caldwell JC. (1977) Demographic aspects of drought: An examination of the African drought of 1970-74. *African Environment Special Report* 6: 93-100..

of livelihood and nutrition. However, this system is susceptible to climatic variability that impacts the supply of its products, and high population growth, which impacts the demand for these products.

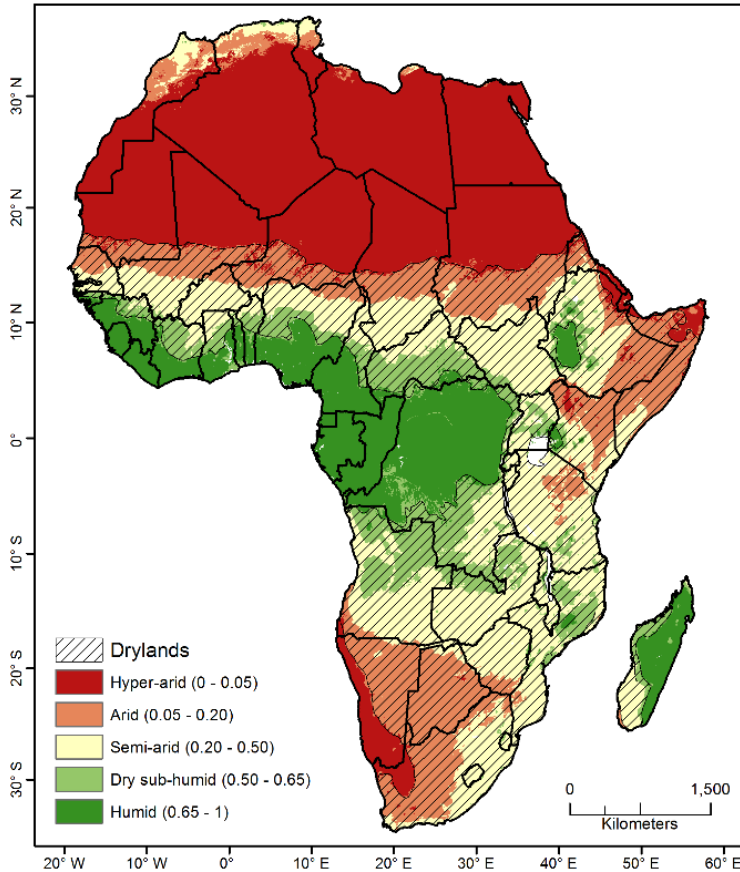


Figure 1: African dryland systems included in this dissertation.

The aridity index (AI) values in the parentheses were computed as the ratio of precipitation to potential evapotranspiration as per Budyko (1974). The shaded arid ($0.05 < AI < 0.20$), semi-arid ($0.20 < AI < 0.50$), and dry sub-humid ($0.50 < AI < 0.65$) regions are the main aridity zones considered in this dissertation. Data on precipitation from Funk et al. (2015) and potential evapotranspiration from Mu et al. (2011b) averaged for the period 2000 – 2014 were used to produce this figure.

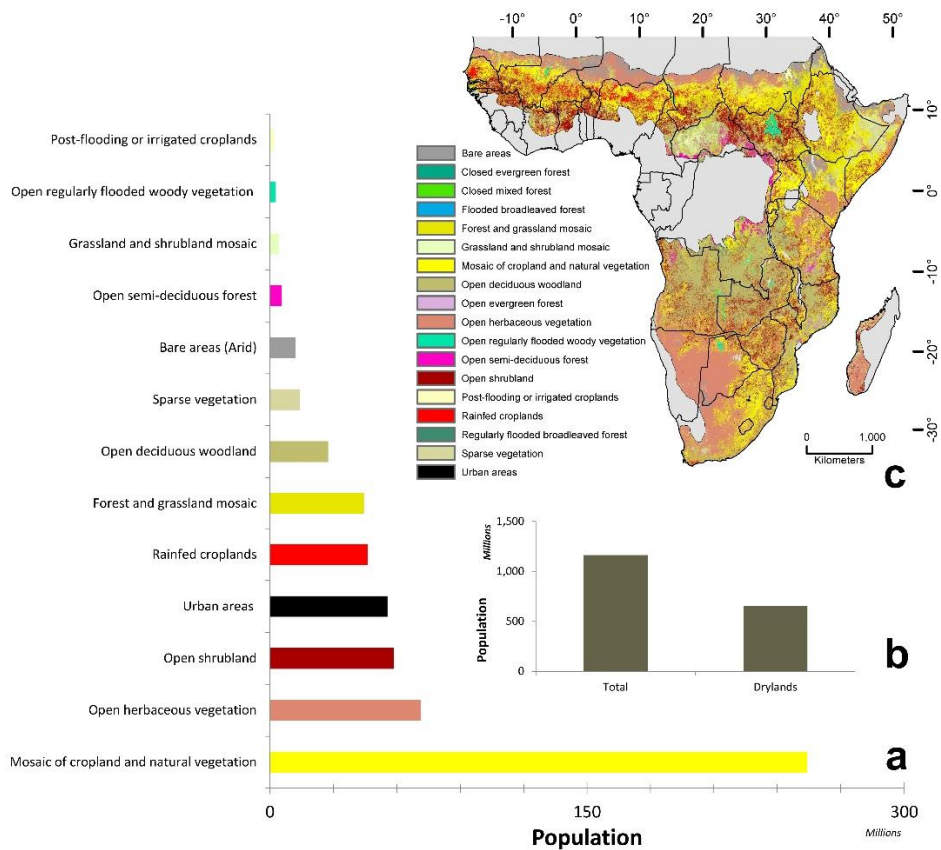


Figure 2: Population per land cover type in African drylands for the year 2010. An overview of (a) the population distribution per land cover type, (b) the population share of sub-Saharan drylands, (c) spatial distribution of the different land cover classes within the dryland extent. These values are based on gridded data on population from Linard et al. (2012) and land cover from Arino et al. (2012).

1.2 The supply of vegetation productivity

1.2.1 The role of climate

In the drylands of Africa both temperature and water availability control critical biogeochemical processes that are important for vegetation growth. Water is particularly important as a limiting factor for vegetation growth in drylands systems (Tucker et al., 1983; Prince, 1991; Verhoef et al., 1996; Moncrieff et al., 1997; Nicholson et al., 1998; Hickler et al., 2005; Sjöström et al., 2011). Merbold et al. (2009) found that mean annual rainfall is strongly correlated with maximum photosynthetic capacity and is the predominant factor driving the exchange of carbon dioxide (CO₂) between the land and the atmosphere over African ecosystems. Rainfall replenishes plant available water and reduces land surface temperature through latent heat loss from surface soil moisture (Cook, 1999). Rainfall also causes higher humidity levels and allows leaf stomata to stay open for longer periods (Nicholson, 2011). When plants transpire, the mixture of air and water exiting the stomata is saturated at a relative humidity of ~100% (Dingman, 2015). The difference between amount of water in the air and the maximum amount of water the air can hold when it is saturated at higher temperature is called the vapor pressure deficit (VPD) (Anderson, 1936). This deficit, along with plant available water, limits photosynthesis (and thereby plant growth) by causing extended closure of the stomata and prohibiting the flow of CO₂ into the leaf.

1.2.2 Gross and net primary production

Gross primary production (GPP) is the total amount of CO₂ plants extract from the atmosphere through the process of photosynthesis. Some of this carbon goes to maintain plant cellular structure and is thus lost through autotrophic respiration (Ra). The remaining carbon is stored as plant tissue, forming plant biomass (phytomass). The annual accumulation of phytomass is referred to as net primary production (NPP = GPP – Ra). On an annual basis, NPP supplies the provision of crops, animal feed and pasture. The societal implications of reduced NPP can be severe, possibly leading to crop failure and eventual food insecurity (Battisti and Naylor, 2009). The terms “*primary production*” and “*primary productivity*” are treated as synonymous in this dissertation³.

³ “*Production*” refers to the combination of inputs to create, or produce, an output during a given period of time, while “*productivity*” refers to the accretion of output in the production process.

Field estimation of terrestrial GPP can be done using infrared gas chambers (e.g. Johnson and Kelley (1970)) or leaf $^{14}\text{CO}_2$ assimilation studies (e.g. Szarek and Woodhouse (1977)). These studies are not only time consuming, but require repetitive field visits and are based on small samples of the landscape. A particular difficulty in the measurement of GPP is that growth and maintenance respiration is a continuous process that consumes some of the assimilated carbon. Micrometeorological techniques such as the eddy covariance (EC) method (Baldocchi et al., 1988) facilitated continuous measurements of CO_2 (and other) fluxes across larger areas. The EC method uses tower-mounted instruments to measure net ecosystem exchange (NEE), i.e. the exchange of CO_2 between terrestrial ecosystems and the atmosphere. This is done using the covariance between the oscillations in the vertical wind velocity and the CO_2 mixing ratio in the air above a vegetation canopy (Baldocchi et al., 1988).

Measuring NPP in the field involves harvesting the vegetation and calculating the annual growth of wood and the mass of foliage at the peak of annual leaf display (Schlesinger, 1997). It also involves measuring the difference in the mass of tissue harvested at the beginning and end of the growing season (Schlesinger, 1997). Since vegetation productivity varies spatially due to environmental conditions and, because fieldwork is both labor and cost intensive, it is expensive to conduct productivity measurements over large spatial extents. Thus, there is a need to estimate NPP at large scales in a relatively efficient way. One of the earliest applied methods was the use of empirical relationships. The first global estimates of primary production using this method was made by Lieth (1964), who related NPP with temperature and precipitation as limiting factors. This work was subsequently the foundation for the first computer-generated map of NPP (Lieth, 1972). Some of the latest methods of estimating observed primary production across large scales use Earth observation (EO) platforms, which is discussed in the next section.

1.2.3 Observing primary production from space

Rouse et al. (1973) introduced the normalized difference vegetation index (NDVI) using data from the newly launched ERTS-1 (later renamed Landsat-1) Multispectral Scanner System (MSS) satellite. The index is the difference between the near-infrared (700 – 1100 nm) and red surface (600 – 700 nm) reflectance divided by their sum, and is a measure of detecting live green vegetation using satellites. This early research was important on two levels: (1) it identified a configurable and broadly applicable satellite-driven concept that directly relates to biophysical properties of vegetation, and (2) it laid down the foundation for future research in NPP using EO data. Around the same time as the first applications of EO data, parallel research was being conducted on estimating terrestrial primary

production using the intrinsic properties of photosynthesis, i.e. the role of radiation (Monteith, 1972; Lieth, 1973; Lieth and Whittaker, 1975; Monteith and Moss, 1977). Subsequently, Tucker et al. (1981) proposed the direct use of satellite data in order to “*allow large-area assessment of net primary production or total dry matter accumulation.*” The advantages of using EO include, but are not limited to, (1) large-scale coverage, (2) frequent revisit times, (3) variable spatial resolutions, and (4) multispectral sensors that capture different segments of the electromagnetic spectrum.

The groundwork for production efficiency modeling (PEM) using EO data was laid by Running (1986) who refined the methodology to estimate NPP based on the light-use-efficiency (LUE) concept of Monteith (1981) and Monteith (1972). The basis of this concept is that GPP is the product of absorbed photosynthetically active radiation (APAR) (i.e. between 400 and 700 nm) and a factor that represents the efficiency (LUE) with which a plant converts this radiation into phytomass. The availability of EO data and flux measurements from EC towers paved the way for innovative methods that combine these two data sources. Running et al. (1994) outlined the derivation of vegetation products from the Moderate Resolution Imaging Spectroradiometer (MODIS) sensor onboard the Terra and Aqua satellites launched by the United States National Aeronautics and Space Administration (NASA). These products were included a biogeochemical model to produce GPP and NPP on a near-continuous basis, and validated at several EC flux tower sites representing different biomes (Running et al., 1999; Running et al., 2000; Turner et al., 2006). The MOD17 production efficiency model (Running et al., 2004) emerged out of these developments and provides near-real-time estimates of terrestrial carbon uptake. MOD17 uses MODIS spectral data, and climatic drivers in an LUE model (Heinsch et al., 2003).

In this dissertation, MOD17 has been used to provide an overall estimate of the NPP in the Sahel region of Africa (Abdi et al., 2014) and assess the impact of the El Niño – Southern Oscillation (ENSO) on NPP in sub-Saharan drylands (Abdi et al., 2016). That being said, MOD17 has been found to underestimate GPP (and by extension NPP) in African ecosystems, primarily due to an underestimation of the biome-specific optimum LUE parameter and inadequate accounting of water stress conditions (Sjöström et al., 2011; Sjöström et al., 2013). Two further studies in this dissertation (Abdi et al., 2017a; Abdi et al., 2017b) will attempt to improve GPP estimates in African drylands.

1.3 The demand for food, feed and fuel

1.3.1 Agricultural production

African agriculture is predominantly rain-fed (Figure 3) indicating that rural livelihoods are almost completely dependent on prevailing climatic conditions. Domestic production of staple foods contributes approximately 90% of overall food consumption in sub-Saharan Africa (Shapouri and Rosen, 1999; Barrett and Upton, 2013). Consumption statistics vary by country, but the underlying pattern is that most of the national supplies of staple crops are used for either food or feed (Elbehri et al., 2013). A recent study of the calorie delivery fraction of various agricultural products found that 80% of the crop calories produced in the region are used for food, 10% as feed, and 10% for other uses (Cassidy et al., 2013). Although imported foods are becoming popular, mainly in upper class urban households (Fox, 2015), they do not contribute to the national economy as much as domestic foods do. For example, in West Africa, each US\$ 1 spent on local produce boosts the local economy by US\$ 1.96 – 2.88 (Halweil, 2002). Additionally, most of the smallholder farms in sub-Saharan Africa can be construed as closed systems with inadequate transportation networks and the consumption of much of what is locally produced (Obayelu, 2011). Sustainable long-term food security depends on the development of the agricultural sector by providing access to markets to increase the resilience of domestic production.



Figure 3: A fallow agricultural field in North Kordofan, Sudan, during the dry season (January 2014).

Photo: Abdulhakim M. Abdi

1.3.2 Livestock and pastoralism

Livestock is an asset in sub-Saharan Africa, and is dependent upon on for their nutritional value and generation of economic growth (Jones and Thornton, 2009; Abdi et al., 2016). Pastoralists and agro-pastoralists across sub-Saharan rangelands depend on grassland and savanna productivity as forage for livestock production (Figure 4). The contribution of the livestock sector to the national gross domestic product (GDP) varies considerably depending on the country. In countries where livestock is an important commodity (e.g. Sudan, Somalia) its contribution ranges between 30 – 40% of GDP (Knips, 2004; Ickowicz et al., 2012). The high climatic variability, demonstrated by the succession of dry and wet periods, is characteristic for most of the continent. Pastoralists develop adaptations in response to climatic variability and persistent drought, for example, switching to a livestock breed that can withstand drought (Sperling, 1987) or has greater ability to digest browse (Blench, 1994).



Figure 4: A pastoralist from the *Shanabla* tribe with his herd of camels in North Kordofan, Sudan during the dry season (January 2014).

Photo: Abdulhakim M. Abdi.

Note: Permission was granted from the pastoralist for this photograph to be taken.

1.3.3 Household energy

In most parts of sub-Saharan Africa energy demand is met by woodfuels and is usually harvested in the form of dry or dead wood (Figure 5) (Hiemstra-van der Horst and Hovorka, 2009). First, a note on the terminology: (1) “fuelwood” refers to unprocessed woody biomass and is synonymous with “firewood”, (2) “woodfuel” refers to an energy source that is derived from woody biomass, (3) “charcoal” is created by burning fuelwood in a low-oxygen environment, the resulting substance, consisting primarily of carbon, produces more energy per kilogram than the fuelwood from which it is derived. Woodfuels meet 55% of the energy needs in Senegal (Pires, 2003), 72% in Mali (Maiga et al., 2008), 80% in Sudan (Hassan et al., 2009) and more than 90% in Chad (van der Plas and Abdel-Hamid, 2005). However, these resources are under pressure due to rising demand. In East Africa, the proportion of woody biomass harvested in excess of the mean annual growth exceeds 50% in 43 sub-national units where a quarter of the population lives (Bailis et al., 2015). In the southern parts of the Sahel, the average tree canopy cover decreased from 14% during the pre-drought 1960s to around 7% in the late 1980s, primarily due to the expansion of croplands (Breman and Kessler, 1995).



Figure 5: A donkey owned by a resident of the village of Luwaib in North Kordofan, Sudan laden with harvested wood (January 2014).

Photo: Abdulhakim M. Abdi.

1.4 The demand-supply balance of net primary production

NPP supplies the annual provision of crops, animal feed and pasture, and adds to annual increments of woody biomass. The societal implications of reduced NPP can be severe and could lead to crop failure and eventual food insecurity (Battisti and Naylor, 2009). In this dissertation, the concepts of “supply” and “demand” are adopted to demonstrate the linkage between ecosystem productivity, human livelihood, and inter-annual climatic variability in sub-Saharan drylands. On the one hand, the sub-Saharan population will continue to experience increase in demand for NPP, as a function of population growth and per capita consumption (Fetzel et al., 2015). On the other hand, forecasts of reduced productivity (up to -41%) of major sub-Saharan crops due to increases in temperature have been consistent across different studies (Jones and Thornton, 2003; Schlenker and Lobell, 2010; Thornton et al., 2011; Knox et al., 2012).

As demand for food, feed and fuel drives land use change, the proportion of NPP required by humans relative to climate-regulated supply (demand-supply ratio, DSR) (Figures 6 and 7) can serve as an integrated benchmark of human dependence on ecosystems. This is particularly essential for long-term trends in order to identify regions that are not vulnerable (e.g. Scenario 1 in Figure 6) and those that are vulnerable (e.g. Scenario 2 in Figure 6) to variations in NPP supply. A similar concept was used in North Kordofan, Sudan, by Olsson (1985) who found that the proximity to a population center influences the availability of biomass. This suggests that there is a direct locally-constrained connection between the supply of NPP and the demand for it. Olsson (1985) also found that overutilization of land is only evident during periods of drought, which means that during periods of restricted resource availability demand surpasses supply in those areas. The future effects of extreme climatic variability, and eventual shifts in the climate system, could have strong impacts on this balance, and intensified by the need to keep pace with an increasing population (Campbell et al., 2014).

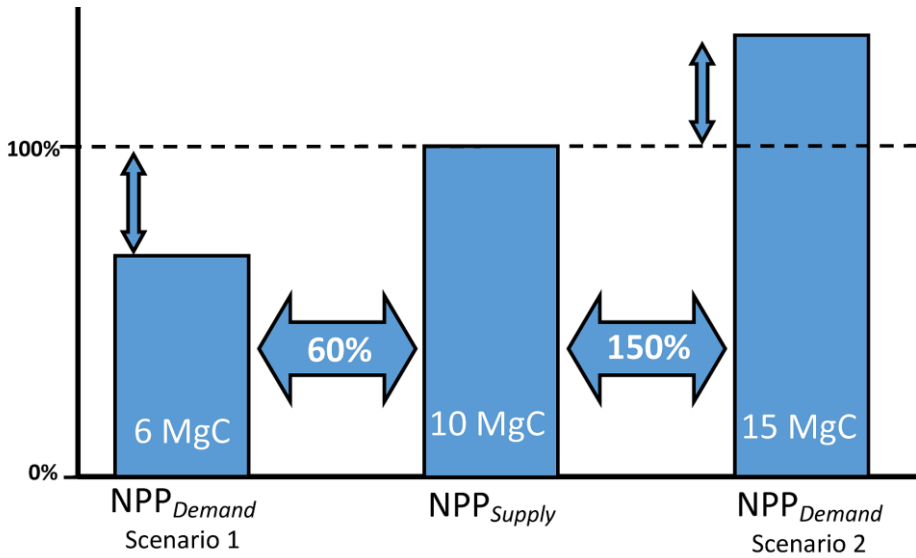


Figure 6: A general overview of NPP supply and two scenarios of NPP demand.

Scenario 1 shows a system where NPP demand is 60% of available supply. Scenario 2 shows a system where NPP demand has increased to is 150% of available supply, which means that NPP supply has to enter this system from elsewhere in order to satisfy demand.

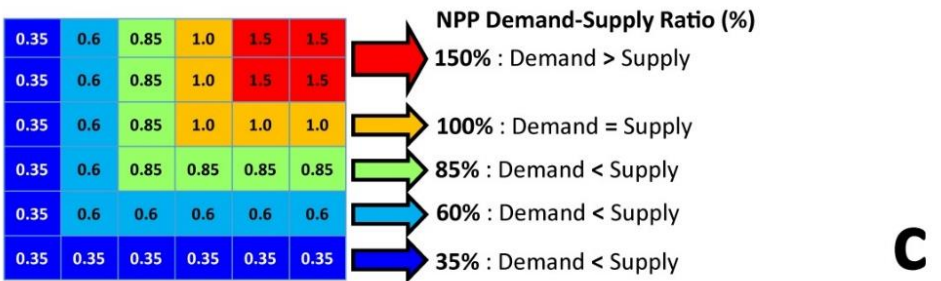
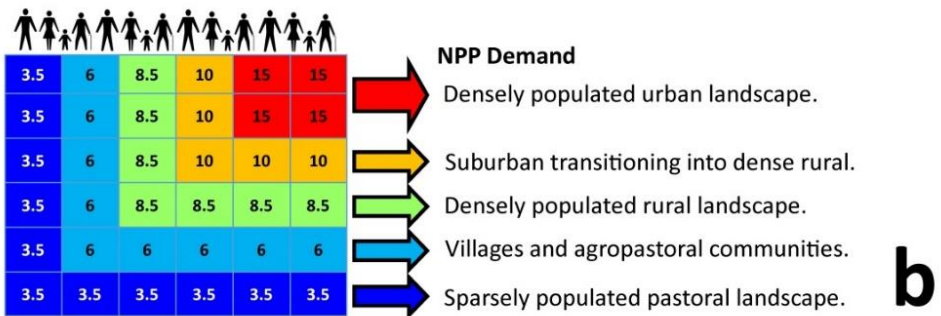
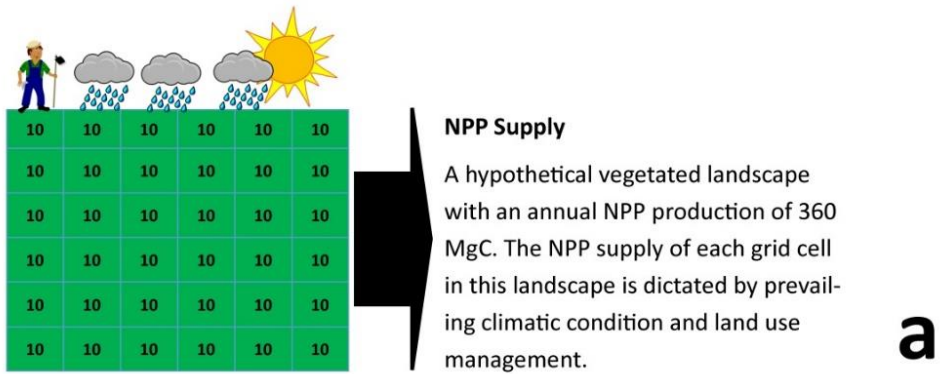


Figure 7: A spatial overview of the demand-supply balance of NPP

(a) The supply of NPP (MgC in this example) is governed either by climatic and land use conditions, while (b) the demand for NPP (MgC in this example) is a function of population density and dietary composition. (c) When these two concepts are spatialized and compared, it results in the demand-supply balance of NPP.

1.5 Research objectives

The principal aim of this dissertation is to understand the human-environment connection in the drylands of sub-Saharan Africa from the perspective of the provision and extraction of NPP. Accordingly, the two fundamental aspects of this connection, i.e. supply and demand, need to be analyzed, separately and together, in order to acquire a better understanding of their dynamics.

Therefore, this dissertation has the following objectives:

1. Assess the inter-annual variability of supply and demand of NPP in the greater Sahel as an example of a complex system where the balance between these two entities is in flux. (Paper I)
2. Examine the trends in the supply and demand of NPP across sub-Saharan drylands and evaluate the impact of the El Niño – Southern Oscillation on the demand-supply balance of NPP. (Paper II)
3. Develop a long-term, spatially-explicit, population dataset for the African continent that takes into account radiative forcing and socioeconomic pathways. (Paper III)
4. Evaluate the mechanisms that control GPP in sub-Saharan drylands and explore the potential of the new plant phenology index in estimating the GPP of these systems. (Papers IV and V)

2. Data and Methods

2.1 Satellite-derived NPP supply (Papers I and II)

The estimate of NPP supply used in this dissertation was acquired from the NASA Earth Observation System repository (www.ntsug.umd.edu/project/mod17). These data are based on the LUE approach as defined in Monteith (1972) and applied in the MOD17 algorithm of the MODIS sensor:

$$NPP_{Supply} = (PAR * FPAR * \epsilon_{max} * VPD * T_{min}) - Ra \quad (1)$$

where NPP_{Supply} is the NPP available in the ecosystem regardless of land use type in grams of carbon per meter square per year ($g C m^{-2} yr^{-1}$); PAR is incoming photosynthetically active radiation in megajoules per meter square per year ($MJ m^{-2} yr^{-1}$); FPAR is the fraction of incident PAR absorbed by the vegetation canopy; ϵ_{max} represents maximum light use efficiency, in grams of carbon per megajoule of PAR ($g C MJ^{-1}$), under hypothetical biome-specific ideal conditions; VPD and T_{min} are simple linear ramp functions of vapor pressure deficit and minimum temperature, respectively, which constrain maximum light use efficiency; Ra (autotrophic respiration) represents the amount of carbon respired, in $g C m^{-2} yr^{-1}$, during maintenance and growth respiration of leaves, fine roots and woody tissue. Further descriptions of the MOD17 algorithm are detailed in (Running and Zhao, 2015) and Zhao et al. (2011).

2.2 Computation of NPP demand (Papers I and II)

In this dissertation, the term “consumption” is defined as the actual amount of NPP extracted from the ecosystem as reported in the statistical database of the Food and Agriculture Organization of the United Nations (FAOSTAT, faostat3.fao.org/). The term “demand” is defined as the annual amount of NPP required by the sub-Saharan dryland population. A framework based on FAOSTAT was developed to calculate demand for NPP. The components of NPP

demand for each country were downloaded from the food balance sheets provided by FAOSTAT for 2000 – 2011. Abdi et al. (2014) used the total primary crop production for each country, which was modified in Abdi et al. (2016) by using domestic supply quantities to account NPP supply for domestic utilization.

The first component of NPP demand is domestically consumed food (NPP_{food}). This category includes twenty-seven types of regionally important primary crops, which represent 95% of all those that are domestically consumed by most of the countries in the study area (FAOSTAT, 2015) (see Supplementary Information in Abdi et al. (2014) for a complete list of crops). Additionally, meats sourced from six types of domestic animals (cattle, goats, sheep, pigs, camels, and poultry) and two non-meat animal products (eggs and milk) were also included.

$$NPP_{food} = \left[\overbrace{\left(\sum_{p=1}^{27} P_{p,y} + I_{p,y} - E_{p,y} + S_{p,y} \right) \times D_{p,y} \times C_{p,y}}^{\text{Crops}} \right] + \left[\overbrace{\left(\sum_{a=1}^7 M_{a,y} \right) \times K_{a,y} \times 0.45}^{\text{Non-crop}} \right]$$

where, P , I and E are produced, imported and exported quantities of crop type p , in year y ; S is the variation (positive or negative) in the stocks of crop type p , in year y ; D and C are the crop-specific dry matter and carbon conversion coefficients, respectively; M is the wet carcass weight (i.e. without internal organs) of animal type a , in year y , and K is the dry matter intake required to produce that weight, in year y . Crop tonnage was converted to carbon units using the conversion factors provided in Abdi et al. (2014).

Livestock are assets in sub-Saharan Africa. Pastoralists and agro-pastoralists depend on livestock for nutritional value and economic growth. NPP_{feed} represents the total amount of animal feed required to sustain the livestock population of the region.

$$NPP_{feed} = \left(\sum_{a=1}^6 T_{a,y} \right) \times R_{a,y} \times 0.45$$

where, T is the Tropical Livestock Unit (TLU) for livestock type a , in year y ; R is the annual dry matter requirement as provided in Abdi et al. (2014). A ratio of 0.45 was used to convert dry matter into carbon (Abdi et al., 2014).

Crop residues ($NPP_{residues}$) refer to the parts of the crop that are left over in a field after harvest. Thus, they are not part of the crop yield (i.e. edible seeds, roots, fruits, leaves, or stalks) and vary according to crop type.

$$NPP_{residues} = \sum_{p=1}^{23} H_{p,y} \times 0.45$$

where, H is the residue factor (proportion of non-yield contributing crop phytomass) of crop type p , in year y . See the Supplementary Information in Abdi et al. (2016) for the residue factors that were used.

In most parts of the sub-Saharan Africa household energy demand is met by woodfuels comprising fuel wood and wood charcoal (NPP_{fuel}) extracted from the region's dry woodlands. The demand for woodfuels across sub-Saharan Africa is variable and ranges from 55% in Senegal (Pires, 2003) to over 91% in Malawi (Zulu, 2010), but on average it is approximately 80% across the study area.

$$NPP_{fuel} = \left(\overbrace{\sum W_{NC,y} \times 0.58 \times 0.45}^{Non-coniferous} \right) + \left(\overbrace{\sum W_{CN,y} \times 0.43 \times 0.45}^{Coniferous} \right) + \left(\overbrace{\sum W_{CH,y} \times 0.75}^{Charcoal} \right)$$

where, NC , CN and CH represent non-coniferous, coniferous and wood charcoal. Dry matter conversion ratios of 0.58 and 0.43 were applied to the non-coniferous and coniferous fuel wood, respectively, and a ratio of 0.45 to convert dry matter into carbon. Wood charcoal was directly converted to carbon content by applying a ratio of 0.75 (See the Supplementary Information in Abdi et al. (2016)).

Landscape fires, both natural and anthropogenic, play an important role in sub-Saharan dryland ecosystems. One of the anthropogenic applications of burning in sub-Saharan Africa is to expand cropland area (Andela and van der Werf, 2014). Consequently, the amount of NPP lost to support human demand for food is taken into account. NPP_{burned} represents domestic human-driven NPP loss resulting from burning of both forest and savanna resources.

$$NPP_{burned} = \sum B_y \times 0.45$$

where, B is the total amount of dry matter burnt in year y . The data are presented as dry matter content, therefore a ratio of 0.45 was used to convert dry matter into carbon.

A homogeneous per capita consumption within each country was not assumed due to variations in diet, lifestyle and wealth between urban and rural populations in sub-Saharan Africa. Rather, ratio factors for urban and rural consumption were applied to national sums of each group of products based on statistics from peer-

reviewed literature and national household consumption surveys (See the Supplementary Information in Abdi et al. (2016)).

$$NPP_{demand_urban} = \overbrace{NPP_{food} + NPP_{feed} + NPP_{residues} + NPP_{fuel} + NPP_{burned}}^{Urban}$$

$$NPP_{demand_rural} = \overbrace{NPP_{food} + NPP_{feed} + NPP_{residues} + NPP_{fuel} + NPP_{burned}}^{Rural}$$

$$NPP_{demand} = NPP_{demand_urban} + NPP_{demand_rural}$$

Per capita NPP consumption was computed by dividing rural and urban consumption values by each country's rural and urban population. Grids of urban and rural consumption were then merged to produce a single map of total per capita consumption. Gridded population data from the WorldPop project (www.worldpop.org.uk) (Linard et al., 2012) were used. These data came in three time slices: 2000, 2005, 2010, which were then interpolated using growth rates from the United Nations Population Division (esa.un.org/unpd/wpp), and an extra year (2011) added to coincide with the FAOSTAT data. Then, the gridded population data was used as a spatial surrogate to disaggregate per capita demand to grid cells for each year between 2000 and 2011. The years 2012 and 2013 were not included because domestic supply data on food, feed and fuel from FAOSTAT were limited to 2011 at the time of writing. Urban and rural areas were separated from one another by masking the urban extent in WorldPop grids based on the "Artificial Areas" category in the GlobCover 2009 land cover map by Arino et al. (2012) ([doi.pangaea.de/10.1594/PANGAEA.787668](https://doi.org/10.1594/PANGAEA.787668)).

2.3 Modeling current and future African populations (Paper III)

One of the challenges that was encountered in mapping the demand for NPP in Papers I and II was the lack of annual gridded data on population distribution. The latest open-access gridded population product prior to the dataset presented here was the Gridded Population of the World, Version 4 (Doxsey-Whitfield et al., 2015). This product was published in 2015 and includes population data at 5-year intervals between 2000 and 2020, which means that the grids would still have to be interpolated at each interval to produce annual estimates (Abdi et al., 2014; Abdi et al., 2016). To the best of our knowledge the combination of Representative Concentration Pathways (RCPs) and Shared Socioeconomic Pathways (SSPs) scenarios for gridded population projections has not been done before. The RCPs and SSPs supersede the Special Report on Emissions Scenarios (SRES) and were adopted by the Intergovernmental Panel on Climate Change (IPCC) for its AR5 (van Vuuren et al., 2011; IPCC, 2014). Unlike the SRES, the four RCPs are not based on socioeconomic scenarios but on radiative forcing (i.e. the ability of greenhouse gases to affect the Earth's energy balance) and the simulated influences of land use, greenhouse gas and aerosol emissions. Therefore, a set of five SSPs were used in conjunction with the RCPs to develop future country level population distribution scenarios (O'Neill et al., 2014). Each SSP scenario is adjoined with a population projection and a proportion of the country population living in urban areas (Figure 8). The presented gridded population dataset can be useful when performing simulations dependent on gridded RCP land use and climate data, for example carbon flux studies, and assessments of supply and demand of NPP. The population distribution for Africa was modeled to follow the RCP-specific urban fraction dataset further described in Hurtt et al. (2011) and the country-specific SSP population and urban fraction scenarios from the SSP database of the International Institute for Applied Systems Analysis (IIASA). The urban fraction data is provided at a spatial resolution of 30 arc-minutes (0.5 degrees or approximately 50 kilometers at the equator) and represents annual projected global land use and land cover patterns until the year 2100. It is developed with a Global Land-use Model (Hurtt et al., 2006), which estimates future land use transitions and patterns within each 30 arc-minute grid cell using an accounting-based method by considering a range of parameters (i.e. spatial patterns, residency time, and land conversions). The five SSPs and four RCPs produce a set of 20 SSP-RCP scenario combinations that deliver a basis for future scenarios. Consequently, the 15 most probable SSP-RCP combinations defined in Engström et al. (2016) were used.

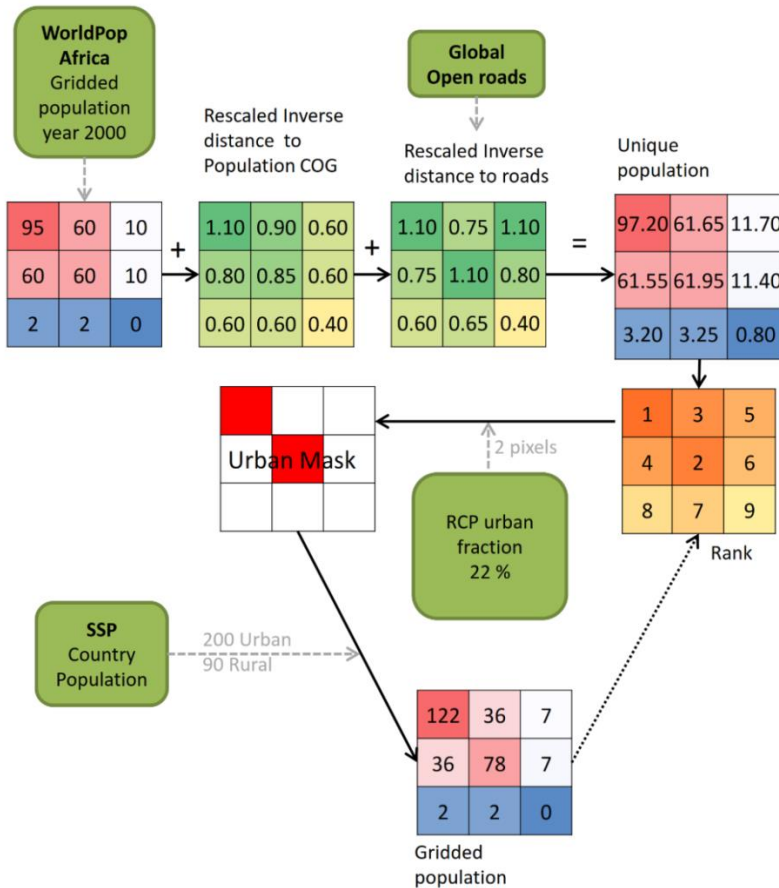


Figure 8: Flowchart of the method used to distribute the population.

The example shown here highlights the need to add inverse distance to population center of gravity (COG) and inverse distance to roads to the population data to be able to uniquely rank the pixels. The country SSP population is distributed for rural and urban separately based on an urban mask and the gridded population from the year before or unique population for the first year. The green boxes with rounded corners indicate input data.

2.4 Standardization of Niño-3.4 anomalies (Paper II)

The Niño-3.4 sea surface temperature index was used as a representation of ENSO to understand its role in the demand-supply balance of NPP in African drylands. To differentiate between positive, negative and neutral ENSO years, the threshold set by the National Oceanic and Atmospheric Administration was applied. Accordingly, an ENSO year is characterized by a minimum of five consecutive 3-month running mean of the Extended Reconstructed Sea Surface Temperature version 3b (ERSST.v3b) anomalies in the Niño 3.4 region based on a threshold of $\pm 0.5^\circ\text{C}$. The base period for computing the anomalies in ERSST.v3b is 1971 – 2000. To visualize differences in NPP between the three ENSO phases (El Niño, La Niña, Neutral), standardized anomalies (Z-scores) were calculated for NPP supply and DSR using equations 2 – 4. The ENSO cycle begins around July, peaks in December – February (of the following year), starts to decay in March – April, and enters the post-phase in May – June (Philippon et al., 2014). The monthly NPP supply anomalies reflect this July to June cycle and were summed to annual values spanning two calendar years. However, the data used to compute NPP demand are provided in calendar years. Therefore, NPP demand-supply anomalies correspond to the years in the second half of the ENSO cycle to account for the lagged effect of the peak and decay phases of ENSO.

$$Z_{El_Niño} = \sum_{t=1999/00}^{2010/11} \frac{OBS_{NPP,t} - MN_{NPP,t}}{SD_{NPP,t}}, \text{if } Nino3.4_t \geq +0.5$$

$$Z_{La_Niña} = \sum_{t=1999/00}^{2010/11} \frac{OBS_{NPP,t} - MN_{NPP,t}}{SD_{NPP,t}}, \text{if } Nino3.4_t \leq -0.5$$

$$Z_{Neutral} = \sum_{t=1999/00}^{2010/11} \frac{OBS_{NPP,t} - MN_{NPP,t}}{SD_{NPP,t}}, \text{if } -0.5 < Nino3.4_t < +0.5$$

where, $OBS_{NPP,t}$, $MN_{NPP,t}$, $SD_{NPP,t}$ are the observed, mean, and standard deviation, respectively, of NPP supply, demand or the demand-supply ratio at time t .

2.5 Calculation of water control variables (Paper IV)

In this study, we used three eddy covariance sites located in Sudan, Niger and Senegal. All three sites were in the Sahelian zone between 13°N and 15°N. A crucial first step in improving NPP estimates is to first improve estimates of GPP and understand the environmental controls linked to it. Since vegetation in dryland systems are by definition limited by the availability of water, we investigated the role different field-collected drought stress metrics and their relationship with eddy covariance gross primary productivity (EC GPP). Plant available water (PAW) represents the amount of water in the soil that can be extracted by plants. PAW is limited by the soil type, soil water content at field capacity (moisture left over after percolation) and permanent wilting point (soil moisture that is unavailable to plants). It is an important parameter in the terrestrial water cycle and may have a considerable influence on primary productivity (Pappas et al., 2013).

Volumetric soil moisture was recorded using CS616 water content reflectometers (Campbell Scientific) in Demokeya and Wankama, and HH2 probe (Delta T Devices) in Dahra. These parameters were recorded every 10 – 30 seconds and averaged for every 30 minutes. Measurement depths varied with site and were dependent on the field campaign. Accordingly, volumetric soil moisture was summed from top of soil to 50 cm depth in Dahra and Wankama, and 60 cm depth in Demokeya. Then, PAW was calculated as:

$$PAW = (SWC \times 100) - PWP \times D$$

where PAW is plant available water (mm); SWC is volumetric soil water content at field capacity ($\text{m}^3 \text{m}^{-3}$); PWP is the soil texture-dependent permanent wilting point (%) from Table 2 in Abdi et al. (2017b); D (mm) is the depth at which the soil moisture measurements were made.

Vapor pressure deficit (VPD) (Anderson, 1936), the difference between amount of water in the air and the maximum amount of water the air can hold when it is when it is saturated, is a potentially limiting factor for GPP (Maroco et al., 1997). VPD was calculated from field measured air temperature (T_a , °C) and relative humidity (RH, %) following Ward et al. (2015):

$$VPD = \left[0.611 \times e^{\frac{17.27 \times T_a}{T_a + 237.3}} \right] - \left[\frac{RH}{100} \times e^{\frac{17.27 \times T_a}{T_a + 237.3}} \right]$$

2.6 Formulating a GPP model based on PPI (Paper V)

Leaf chemical processes are likely to be influenced by the feedback between canopy, near-surface air, and actual leaf temperature (Hashimoto et al., 2008; Sims et al., 2008). EO-derived LST has been found to correlate well with VPD, and has been used as an environmental scalar in modeling GPP (Hashimoto et al., 2008; Sims et al., 2008; Wu et al., 2010). VPD was derived from daytime LST using Equation 4.

$$VPD_{LST} = -2.74 + (2.57 * 1.06^{LST_{Day}})$$

where VPD_{LST} is the vapor pressure deficit derived from LST; LST_{Day} is the 8-day MOD11A2 product. In a previous study, Abdi et al. (2017b) showed that GPP is significantly reduced in Sahelian ecosystems when VPD is above 2 kPa. Therefore, following the approach described in Sims et al. (2008), we used VPD instead of LST as a direct control on GPP. This was done by scaling VPD_{LST} so that GPP is reduced when $VPD > 20$ hPa:

$$VPD_{Scaled} = \min \left[5.22 - (0.14 \times VPD_{LST}); \frac{VPD_{LST}}{20} \right]$$

We define GPP as the product of PPI and VPD_{Scaled} :

$$GPP_{PPI} = PPI \times VPD_{Scaled}$$

All the EO data were smoothed with a Savitzky-Golay filter (Savitzky and Golay, 1964) in the software package TIMESAT (Jönsson and Eklundh, 2004) using: fitting method = 1, window size = 5, and seasonal parameter = 1. The full dataset containing all four sites was randomly split 50/50 into calibration (297 samples) and evaluation (297 samples) subsets. In order to compare the GPP models against EC GPP, we used the coefficient of determination (R^2) in an ordinary least-squares regression analysis. We also computed the root-mean-square error (RMSE) to assess their accuracy in relation to EC GPP.

We compared this model to two other vegetation index-based models: the “Temperature-Greenness” (T-G) model (Sims et al., 2008) and the “Greenness-Radiation” (G-R) model (Gitelson et al., 2006). We also compared it to the MOD17A2 GPP product. The T-G model was originally developed for North American ecosystems and uses the product of scaled LST and EVI (scaledLST *

scaledEVI) to estimate GPP. It is based on the idea that GPP has generally strong correlation with EVI, and that LST accounts for temperature controls on GPP. The scaling factor reduces scaledLST to 1 when $LST = 30^{\circ}\text{C}$ and to 0 when $LST = 0$, or reaches 50°C , while the EVI scaling factor reduces GPP to zero when $EVI \approx 0.1$ (Sims et al., 2008). The G-R model is based on the idea that total chlorophyll content of a canopy is the primary factor influencing the amount of PAR absorbed by green vegetation (Gitelson et al., 2006). It originally formulated GPP as the product of total chlorophyll (Chl) and top-of-canopy PAR (PAR_{TOC}), but was modified by Wu et al. (2011) who replaced Chl with EVI for scalability using EO data.

3. Results and Discussion

3.1 Patterns and trends in NPP supply and demand (Papers I and II)

In the Sahel, around 41% of the NPP supply is consumed by humans. The low regional inter-annual variability of NPP in this region, at 1.7% (Figure 9), is representative of the global trend over the past 35 years (Running, 2012) suggesting that the supply of NPP is at a near constant level. That being said, parts of the western Sahel exhibited a modest positive trend in NPP supply between 2000 and 2013 ($\mu = 2 \text{ g C m}^{-2} \text{ yr}^{-1}$, $P < 0.05$) (Figure 10), which could be due to sub-regional efforts to rehabilitate the land and increase productivity are may have a role (Kaboré and Reij, 2004). On the other hand, both population and NPP demand are increasing at similar annual rates of 2.8% and 2.2%, respectively. This supply-demand relationship is sensitive to systemic shocks such as droughts or pest infestations that might lower the regional NPP supply.

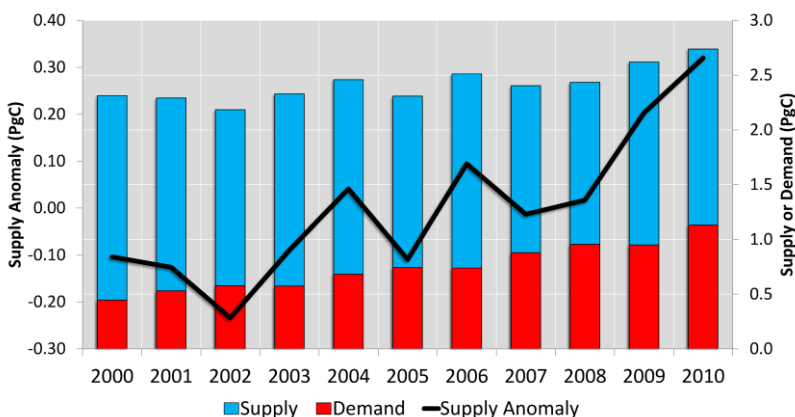


Figure 9: Inter-annual variability of NPP supply and demand in the Sahel.

Total NPP supply, NPP demand, and NPP supply anomalies in the greater Sahel region between 2000 and 2010. NPP supply anomalies were computed as differences of NPP supply from annual mean using the 11-year record.

There were two years that exhibited large negative NPP anomalies in Figure 9. The year 2002 was marked with a severe drought in Ethiopia and parts of Sudan that caused food and water deficit affecting 12 million people (Balogun et al., 2013) as well as localized food shortages in West Africa. In 2004, the largest desert locust (*Schistocerca gregaria*) infestation in 17 years reduced the regional NPP supply until the 2005 growing season (Ceccato et al., 2006). This infestation resulted from heavy rains the preceding year that created ideal breeding conditions for the locusts (Ceccato et al., 2006). Apart from the Sahel, NPP supply trends over 2000 – 2013 were also significant in central Africa ($\mu = 30 \text{ g C m}^{-2} \text{ yr}^{-1}$, $P < 0.05$) and parts of Zambia, Malawi and Mozambique ($\mu = -25 \text{ g C m}^{-2} \text{ yr}^{-1}$, $P < 0.05$) (Figure 10 a). By contrast, trends of NPP demand over 2000 – 2011 are significant in 48% of the area and roughly evenly distributed (Figure 10 b).

The mean overall trend in NPP demand is $3.5 \text{ g C m}^{-2} \text{ yr}^{-1}$, though in urban areas it averages approximately $50 \text{ g C m}^{-2} \text{ yr}^{-1}$. The tradeoffs between NPP supply and demand trends (i.e. change in one quantity relative to another) are locally constrained and linked to the prevailing climate, population growth and net migration. For instance, in the region of Sikasso in southern Mali, the trend of NPP supply averages $10 \text{ g C m}^{-2} \text{ yr}^{-1}$ (Figure 10 a-1) and that of demand is $1 \text{ g C m}^{-2} \text{ yr}^{-1}$ (Figure 10 b-1). This region is agriculturally productive and exhibits positive NPP supply anomalies (Figure 10 b). The low trend in NPP demand is surprising because the population of Sikasso grew 3.9% a year between 2000 and 2011 (FAO, 2013). This paradox of high land productivity, rapid population growth and low demand for NPP could be a sign that the population is not consuming adequate amounts of food, feed and fuel.

One of the fastest growing cities in sub-Saharan Africa is Addis Ababa, which grew by 40% between 2000 and 2010 due to economic migration from other parts of the country (Adugna and Hailemariam, 2011; Moller, 2012). Consequently, the observed average trend in demand for NPP in the Addis Ababa metropolitan area was $153 \text{ g C m}^{-2} \text{ yr}^{-1}$ for 2000 – 2011 (Figure 10 b-2), the highest in sub-Saharan Africa. The observed decrease in NPP supply in the vicinity of Addis Ababa over 2000 – 2013 (Figure 10 a-2) could be linked to the rapid growth of the city. Itannam and Olsson (2004) found that urbanization and industrialization resulting from Addis Ababa's rapid expansion contributed to land degradation in surrounding agricultural areas. This adversely affects the livelihoods of farmers prompting further economic migration into the city (Abdissa and Degefa, 2011). In Malawi, approximately 45% of the population lives in the southern part of the country (van Vuuren et al., 2011), where the vicinity of the country's second-largest city, Blantyre, has experienced an overall decrease in NPP supply ($-11 \text{ g C m}^{-2} \text{ yr}^{-1}$, Figure 10 a-3) over 2000 – 2013 and an increase of NPP demand ($0.80 \text{ g C m}^{-2} \text{ yr}^{-1}$).

$\text{C m}^{-2} \text{ yr}^{-1}$, Figure 10 b-3). The supply of NPP in this region is highly sensitive to ENSO events (Figure 11 a, b) with a net negative impact, this is discussed further in section 3.2.

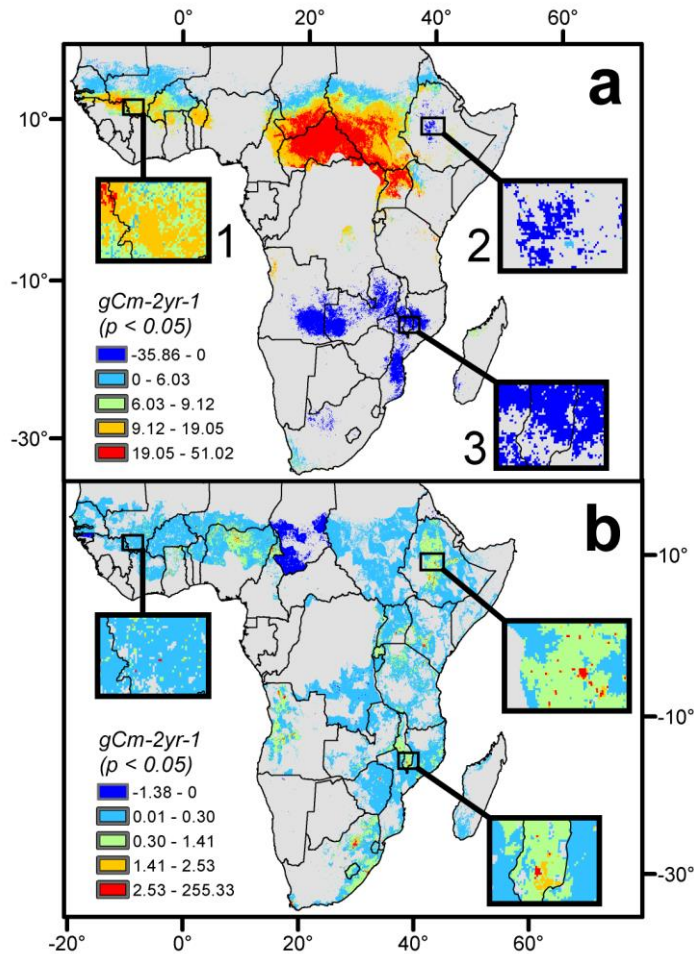


Figure 10: Trends in NPP supply (2000 – 2013) and demand (2000 – 2011).

(a) NPP supply, and **(b)** NPP demand. Detail showing pixel-level supply and demand trends for different urban and rural areas in sub-Saharan Africa: **(1)** the agricultural region of Sikasso in southern Mali, **(2)** the Addis Ababa metropolitan area, and **(3)** southern Malawi within the vicinity of the city of Blantyre. Since the units of NPP supply are generally denoted as quantity per unit area per unit time, and demand generally represents NPP required by the inhabitants in each pixel, each NPP demand pixel in **b** was divided by its area to facilitate comparability. Grey areas indicate both statistically insignificant ($P > 0.05$) and areas outside the study region.

3.2 Role of ENSO in the demand-supply balance of NPP (Paper II)

Demand for NPP is coupled with population growth and consumption patterns, but it is not linked to, nor does it change with, ENSO phases. Consequently, when NPP supply is reduced by El Niño, NPP demand increases relative to it, causing positive demand-supply ratio (DSR) anomalies. This is clearly visible in the mainly arid region of Southern Africa. The region exhibited the largest contiguous region of negative NPP supply anomalies during El Niño (Figure 11 a), and consequently also shows the largest positive DSR anomalies (Figure 11 d). The opposite effect can be seen during La Niña, when NPP supply anomalies in Southern Africa are positive and DSR anomalies are negative. Negative NPP supply anomalies during La Niña are concentrated around equatorial East Africa resulting in positive DSR anomalies (Figure 11 b, e).

The greatest sensitivity to El Niño occurs in Southern Africa. Here, a $+1^{\circ}\text{C}$ shift in the Niño 3.4 index causes a mean change in the NPP supply of $-6.6 \text{ g C m}^{-2} \text{ yr}^{-1}$. El Niño events in Southern Africa are associated with dry conditions, while La Niña events are associated with wet conditions. Most land cover types in Southern Africa exhibit negative NPP supply values relative to changes in the Niño 3.4 index. The exceptions, with either the median value or a large number of positive outliers, are the region's forests and woodlands that are adapted to prolonged dry seasons or droughts, and possess physiological mechanisms such as extensive roots allowing efficient deep water access or are drought deciduous (i.e. the trees lose leaves to conserve water) (Nicholson, 2011).

Despite the fact that there were more La Niña events than El Niño events between 2000 and 2011, the negative impact of El Niño on Southern Africa is strong enough to tip the balance toward the negative. This sensitivity, coupled with a $1.3 \text{ g C m}^{-2} \text{ yr}^{-1}$ trend in NPP demand, increases demand relative to available supply. This is troubling because the difference in NPP supply in Southern Africa between El Niño and La Niña years corresponds to what is required to feed approximately 15 million people for one year (Stige et al., 2006). Malawi exemplifies Southern Africa's sensitivity to El Niño events. The net negative effect of ENSO as a whole means that the negative correlation the region has with El Niño outweighs its positive correlation with La Niña. The strong El Niño of 2015/16 reduced the October 2015 – February 2016 rainy season to its lowest level since 1981 (FEWSNET, 2016). This severe drought condition caused below average crop production leading to low earnings from agricultural labor and high food prices (FEWSNET, 2016).

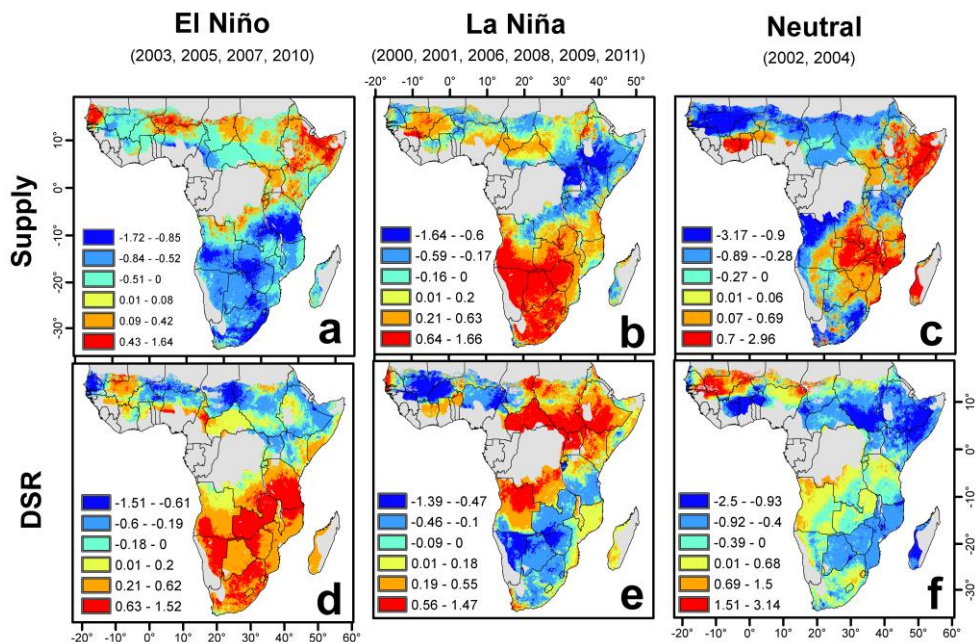


Figure 11: Standardized anomalies (2000 – 2011).

Standardized anomalies for NPP supply (a, b, c) and demand-supply ratio (d, e, f). Means were calculated for El Niño (a, d), La Niña (b, e) and neutral years (c, f). For each panel, the anomaly indicates the number of standard deviations an observation is above or below the mean. The ENSO cycle typically straddles two calendar years, beginning around July, with a peak in December – February, and begins to decay in March – April of the following year. The monthly NPP supply anomalies reflect this cycle and were summed to annual values. Since the FAOSTAT data is provided in calendar years, the demand-supply ratio (DSR) data reflects that nomenclature. Accordingly, DSR anomalies shown here represent the latter half of the ENSO cycle, e.g. for the ENSO-neutral years of 2001/02 and 2003/04, the corresponding DSR anomalies are the years 2002 and 2003. Grey areas are outside the study region.

3.3 Validation of African population projections (Paper III)

The technical validation of the dataset is performed by comparing the SSP 1 country populations with the gridded population dataset (for SSP1/RCP 4.5) aggregated to country levels. This is done for year 2005 since both SSP population projections and RCP land use projections do not deviate until after that year. Accordingly, we performed the technical validation on only one RCP–SSP combination.

To further evaluate the created dataset we compared the 2000 to 2005 population change for the created gridded dataset with the change for UN (2015) adjusted Gridded Population of the World version 4 (GPWv4) by Doxsey-Whitfield et al. (2015). This was done for a sample of six African countries (Benin, Madagascar, Morocco, Botswana, Ethiopia, and Tunisia) representing a wide variation in population density and spatial distribution. Then, the population was aggregated to level 2 administrative regions within each country. For most of the countries the change matches in general well but typically deviates more for a few of the level 2 administrative regions. A summary of the comparison to GPWv4 for the validation countries and year 2005 can be seen in Table 2 where it can be observed that the total distributed SSP population figures are not exactly the same as the population for GPWv4. However, the coefficient of determination is high ($R^2 > 0.8$) for most of the countries and administrative levels indicating that the spatial pattern is captured between the regions. This indicates that the method is well suited to capture the spatial variability in the population. However, due to considerable differences in the total population between GPWv4 and the SSP population data we do not expect the change to match perfectly for all regions.

We used a deterministic method to produce the gridded population projections, which means that the level of uncertainty in the created dataset originates from uncertainty in the input data. We would like to point out the potential over-influence of roads in the created dataset. This is due to the fact that WorldPop uses distance to roads and we further add the inverse distance to roads in order to create a unique population dataset as a starting point. However, since we rescale the distance to road to be between $1.0 \cdot 10^{-5}$ and $1.1 \cdot 10^{-5}$ we argue that this will only have an effect for pixels that were equal in the initial WorldPop dataset. Pixels (30 arc-seconds) with unequal population values in the initial dataset will have a very low probability of being affected by this small addition based on the distance to roads.

Table 2: Summary of gridded data

Select countries were aggregated to administrative region level 1 and 2 for year 2005 and compared with GPWv4. **n** indicates number of regions within each administrative level. **R²** is the coefficient of determination and **RMSE** is the root mean square error between GPWv4 and gridded population, aggregated to administrative level one or two.

		n	R ²	RMSE	GPWv4 average population	Gridded average population	GPWv4 country totals (‘000)	SSP country totals (‘000)
Benin							8 203	7 630
	<i>Adm1</i>	12	0.89	104 369	674 354	631 009		
	<i>Adm2</i>	76	0.81	38 391	106 477	99 633		
Madagascar							18 200	17 900
	<i>Adm1</i>	6	0.91	635 232	3 028 272	2 976 479		
	<i>Adm2</i>	22	0.86	407 449	825 892	811 767		
Morocco							29 920	30 400
	<i>Adm1</i>	15	0.79	587 860	1 988 823	2 015 600		
	<i>Adm2</i>	54	0.91	312 416	552 451	559 889		
Botswana							1 860	1 880
	<i>Adm1</i>	9	0.98	26 917	205 694	208 228		
	<i>Adm2</i>	25	0.52	47 608	74 050	74 962		
Ethiopia							76 536	74 300
	<i>Adm1</i>	11	0.99	1 162 510	6 953 130	6 749 082		
	<i>Adm2</i>	72	0.94	229 176	1 062 284	1 031 110		
Tunisia							9 757	10 000
	<i>Adm1</i>	24	0.83	174 471	404 435	414 169		
	<i>Adm2</i>	268	0.48	26 375	36 218	37 090		

3.4 Water controls on Sahelian GPP (Paper IV)

Hydrological processes generally control vegetation dynamics at multiple spatial and temporal scales. Apart from highly humid environments, all plants undergo photosynthesis at the expense of losing moisture to the atmosphere. This moisture loss is particularly an issue for dryland vegetation where an imbalance could occur between the amount of water plants require and the limited amount that is available in the ecosystem. In this study, we found that the two main moisture related biophysical limitations, plant available water (PAW) and vapor pressure deficit (VPD), are both critical factors that limit plant CO₂ uptake by influencing the greening and browning phases of vegetation phenology. With the start of the dry season in November, low PAW is present in the drying soils of the Sahel, which leads to decreased availability of water for uptake by plant roots (Figure 12). This in turn reduces evapotranspiration (latent heat) due to drier soils and the closure of the stomata commences to prevent moisture loss.

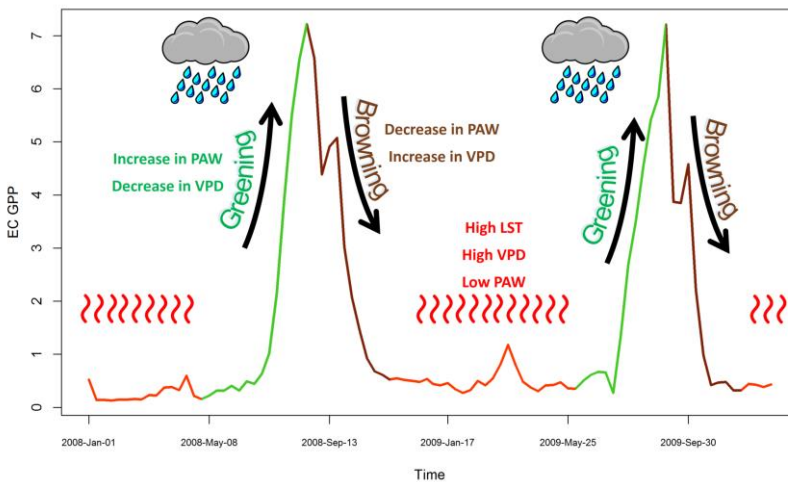


Figure 12: Illustrating water controls on GPP using data from the site in Demokeya, Sudan.

The start of the rainy season results in the replenishment of soil moisture and rapid growth of the herbaceous vegetation. The availability of PAW increases root water uptake and evapotranspiration along with reduction in VPD brought on by increase in humidity. An overview of the relationship between eddy covariance GPP (EC GPP), VPD and PAW across all sites is shown in Figure 13. The dry season is characterized by consistently high VPD (> 2 kPa), which is linked to the reduction

in evapotranspiration due to low PAW and the increase in land surface temperature (LST). Cross-site relationships of PAW and VPD with EC GPP were fairly moderate ($R^2 = 0.36$ and 0.43 , respectively). The relationships at the individual sites were varied with R^2 values of VPD ranging between 0.59 and 0.75 and those of PAW between 0.59 and 0.76 . The combination of PAW and VPD explained the largest variance across all three sites ($R^2 = 0.47$, $RMSE = 2.06 \text{ g C m}^{-2} \text{ d}^{-1}$), with the highest R^2 and lowest $RMSE$ at Wankama Fallow ($R^2 = 0.83$, $RMSE = 0.77 \text{ g C m}^{-2} \text{ d}^{-1}$). With the reduction/closure of stomatal conductance, plants deactivate metabolic activity in the shoots to reduce consumption of water (and subsequent transpiration) while simultaneously enhancing uptake of water and nutrients by the roots to mitigate the effect of the dry season (Gargallo-Garriga et al., 2014).

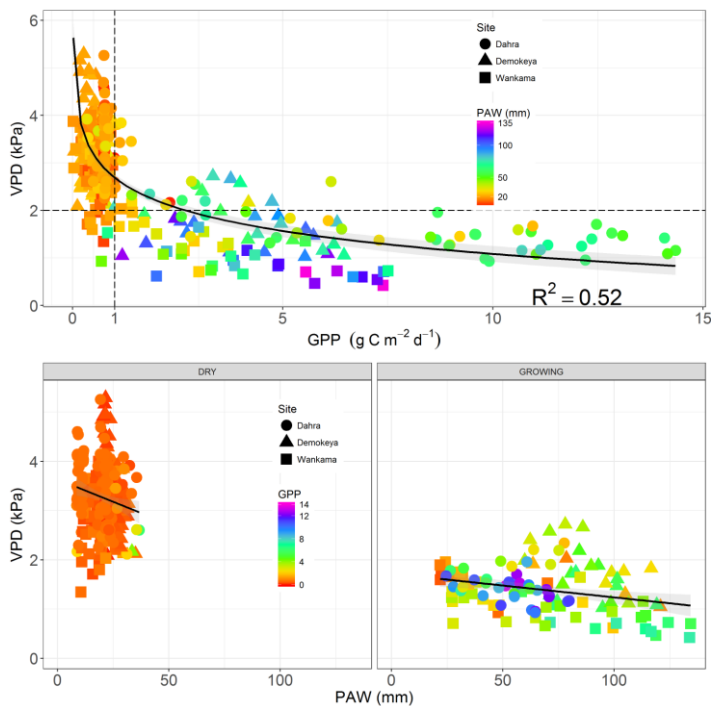


Figure 13: Drought stress metrics and eddy covariance gross primary productivity.

Top: Comparison of VPD and EC GPP with coloring that indicates corresponding values of PAW for each site. Values to the left of the vertical dotted line ($GPP < 1 \text{ g C m}^{-2} \text{ d}^{-1}$) and above the horizontal dotted line ($VPD > 2 \text{ kPa}$) represent the dry season. Bottom: Relationship between the VPD and PAW per corresponding GPP values during the dry and growing seasons. The solid black line is the regression line with 95% confidence interval in light gray.

3.5 Potential of PPI to estimate GPP (Paper V)

The calibration and evaluation output produced by the PPI GPP model were comparable with GPP modeled using other methods (Figure 14). The calibration and evaluation R^2 results of the G-R model (Gitelson et al., 2006) underperformed in comparison to the PPI GPP model (Figure 14 b), leading to a lower overall performance of that model. Additionally, the slopes of the regression lines in Figure 14, show that the PPI GPP model displayed the closest value to the 1:1 line. This indicates that PPI GPP model exhibits a relatively strong ability to estimate the magnitude of EC GPP compared to the G-R model. The PPI GPP model also outperformed the T-G model in both the calibration and evaluation datasets (Figure 14 c). The sites classified as “drought sites” in Sims et al. (2008) are considerably cooler than Sahelian sites (12°C vs 30°C), so the LST scaling factor in the T-G model cannot account for the environmental conditions in this warm region. However, the T-G model performed well at Skukuza ($R^2 = 0.74$), which is probably because it has a lower mean LST (29°C) that is within the optimal threshold set in the T-G model (Sims et al., 2008). The full PPI GPP model is show below:

$$GPP_{PPI} = 0.12 + 2.93 \times (PPI \times VPD_{Scaled})^{0.70}$$

The PPI GPP model tracked the seasonal and inter-annual development of EC GPP well. Furthermore, it managed to capture the amplitude of EC GPP reasonable well, which is further confirmed by the slope close to the 1:1 line in Figure 14 a. At Demokeya, the PPI model over-estimated GPP during the dry season, but captured the start and end of the growing season for all sites in-line with EC GPP except at Mongu. The MOD17 model underestimated GPP at all sites but was able to follow the greening and browning phases of Skukuza (30% canopy cover) and Mongu (65% canopy cover), suggesting that this model does better in tree-dominated areas than savanna. The T-G model either underestimated or overestimated peak GPP at most sites.

The Plant Phenology Index (PPI) was originally designed for boreal coniferous forests as a solution to suppressing the influence of snow in phenology metrics. In this study, we evaluated the performance of a PPI-based model in predicting the GPP at four semi-arid sites in sub-Saharan Africa with a wide canopy cover range (3 – 65%). We found that PPI is able to capture green canopy foliage reasonably well ($R^2 = 0.75$, $RMSE = 1.39 \text{ g C m}^{-2} \text{ d}^{-1}$) due to its sensitivity to green LAI. It

further managed to capture the magnitude of EC GPP relatively well compared to the other tested models. However, the performance of PPI can be further improved through the inclusion of total chlorophyll content as it is a principal factor influencing carbon assimilation. Canopy foliage remains green during the growing season despite considerable variability in total chlorophyll content between the beginning and end of the season. Accounting for total chlorophyll content, perhaps through the inclusion of chlorophyll-sensitive vegetation indices, could further enhance the ability of PPI to estimate GPP in semi-arid systems.

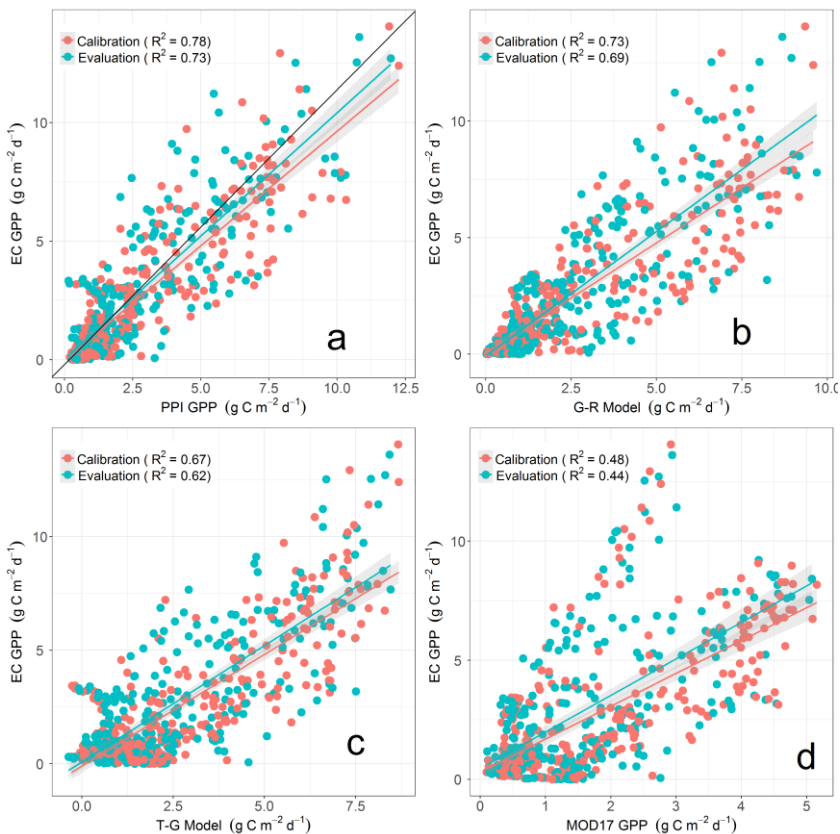


Figure 14: Results of the calibration and evaluation datasets.

Cross-site relationships between EC GPP and each of the four GPP models (a – d, see Table 4). The calibration and evaluation dataset each has the same quantity of data points ($n = 297$). The red and green lines are the regression line for calibration and evaluation, respectively, with 95% confidence interval in light gray shading.

4. Conclusions and Broader Impacts

Humans rely directly on the supply of NPP through the consumption of crops and use of wood for fuel and construction, and indirectly through animal products. This reliance creates demand that drives many of the ecological changes occurring in sub-Saharan drylands. The integrated analysis of the supply and demand of NPP allows the identification of areas at risk of consuming more resources than are available, either presently or in future scenarios. Evaluating socio-ecological impacts through isolated disciplinary analysis provides monocular views of a complex system that requires an integrated approach. That being said, such an approach needs to be reasonably accurate to represent reality. But it also needs to follow Occam's razor by being simple enough to be widely applicable and easily understood. It is a difficult balancing act.

This dissertation adds to a series of studies on sub-Saharan vegetation dynamics with a focus on the relationship between anthropogenic demand and ecosystem supply of NPP. The demand-supply balance of NPP was $86\% \pm 9$ across the drylands of sub-Saharan Africa during the first decade of the 21st century (Abdi et al., 2016). This balance was high in some regions. For example, in the Sahel, a climatically sensitive region with high anthropogenic activity, average demand-supply balance of NPP was $96\% \pm 7$. Additionally, the annual increase in NPP demand in the Sahel was 2.2% over the same period (Abdi et al., 2014). This rapidly increasing demand for food, fuel and feed driven by population growth makes this sub-Saharan region in particular vulnerable to climatic variability that may alter the per capita availability of NPP. There is risk that ecosystems may not be able to provide for the region's humans and livestock without a corresponding increase in NPP supply. In southern Africa, variability associated with the El Niño – Southern Oscillation causes a mean change in the NPP supply of $-6.6 \text{ g C m}^{-2} \text{ yr}^{-1}$ between 2000 and 2013 (Abdi et al., 2016). Couple this sensitivity to El Niño with an increasing trend in of NPP demand of $1.3 \text{ g C m}^{-2} \text{ yr}^{-1}$ indicates that demand for NPP has the potential to surpass supply during extreme El Niño events (Abdi et al., 2016). This underscores the importance of accounting for the balance between supply and demand of NPP because neither quantity provides a complete picture by itself. Overall, the combination of fluctuations in NPP supply and upsurges in

demand led to an average increase of 7.2% in the demand for NPP relative to its supply between 2000 and 2011.

Understanding the environmental constraints on primary production in drylands is an important step to improve estimates of NPP supply and better assess the demand-supply balance. The supply of primary production in sub-Saharan drylands is primarily controlled by water availability. This important factor is regulated by two processes, plant available water and vapor pressure deficit, that work in unison (increase in one, decrease in the other) during the greening and browning phases (Abdi et al., 2017b). In this dissertation, GPP in Sahelian drylands was found to increase when the vapor pressure deficit is under 2 kPa and plant available water is above 50 mm. Furthermore, the inclusion of dry season dynamics of these two variables helped better explain the variance in observed GPP and outperformed MOD17 GPP. A similar improvement was observed using Earth observation data that served as surrogates for vapor pressure deficit and soil moisture variability. Although there is barely any carbon assimilation in drylands during periods of drought, recent research points to the ability of these ecosystems to retain “memory” of past rainfall (Schwinning et al., 2004). The applicability of the Plant Phenology Index (PPI) at four sub-Saharan sites was explored in Abdi et al. (2017a). PPI was designed to capture green leaf area index (LAI), as opposed to total LAI (Jin and Eklundh, 2014) and could potentially improve GPP estimates. It was found that a PPI-based GPP model is able to follow the seasonal phenology of eddy covariance reasonably well ($R^2 = 0.75$, $RMSE = 1.39 \text{ g C m}^{-2} \text{ d}^{-1}$). It further managed to capture the magnitude of EC GPP relatively well compared to the other tested models. However, the performance of PPI can be further improved through the inclusion of total chlorophyll content as it is a principal factor influencing carbon assimilation. Vegetation indices such as EVI are primarily sensitive to chlorophyll content. Thus, for the same LAI, plants with different amount of chlorophyll would exhibit different values of EVI. Nevertheless, there is potential in obtaining better estimates of GPP in sub-Saharan drylands by combining green LAI-sensitive PPI with chlorophyll-sensitive vegetation indices.

The lack of annual spatial data on Africa population is a critical deficiency that hinders the estimation of NPP demand. Several of the large-scale gridded population data suffer from two fundamental problems: they are either too coarse (e.g. ~25 – 50 km pixel size) or they are provided as snapshots in time (e.g. 2000, 2005, 2010, etc.). Both Abdi et al. (2014) and Abdi et al. (2016) used 1-km gridded population data that were available in 5-year time slices, which had to be interpolated into annual intervals using United Nations data. In this dissertation, Boke-Olén et al. (2017) addresses this issue by creating a 1-km gridded population dataset for Africa that is (1) annual, to allow for temporal analysis, and (2)

accounts for radiative forcing and socioeconomic scenarios. The availability of gridded population data at annual time steps allows for monitoring inter-annual changes in the human landscape such as the expansion of settlements, prediction of fuelwood supply routes, access to markets etc.

The NPP-based framework presented in this dissertation should not be construed as a famine early warning system. This is because the dynamics of famines invariably depend upon institutional involvement (or lack thereof). Instead, the demand-supply balance of NPP should be considered as a “long-term warning system” as it integrates processes that affect human well-being across longer time scales. For example, one of the factors that could lead to a famine is the lack of infrastructure which prevents food from flowing from areas of surplus to areas of deficit (Olsson, 1993). Thus, an important utility of the demand-supply balance lies in helping identify areas where, in the long-term, demand can surpass supply and which could require better investments, for instance, in infrastructure, transportation, assistance in land rehabilitation, etc. A second practicality of the demand-supply balance is its linkage to population-driven resource-use. An increasing human population is not necessarily something negative. Indeed, for some countries, particularly those with developed economies, a certain rate of positive population growth is essential for economic growth (Harper, 2014). However, when this growth is assessed from the perspective of resource-use and the demands exerted by humans on ecosystem supply, a different picture emerges that is linked to, among other things, the rate of increase in demand.

An important limitation of the demand-supply balance of NPP is that it assumes NPP flows are constrained by the local population distribution and does not take into consideration NPP flows connected to international trade. This constraint is indeed applicable to several, if not most, rural communities in sub-Saharan Africa, however, the paradigm is shifting and human-environment systems on the continent are becoming increasingly telecoupled over large distances (Liu et al., 2013). Thus, a comprehensive, integrated approach is essential to further assess the factors driving this complex balance, particularly in the wake of climate change. Only through transdisciplinary analysis involving enhanced synthesis of biophysical, socio-ecological and socioeconomic data can improved assessments of the impacts of humans on ecosystems be made.

5. Outlook

Sociological data, such as surveys at the household (or even individual) level, which provide valuable information about fine-scale patterns of human-ecosystem interaction, are seldom integrated with biophysical datasets. An important factor that influences the balance between supply and demand is caloric requirement. In this sense, gridded population data, such as the one presented in this dissertation, will prove to be even more useful. High resolution gridded population data that accounts for different radiative forcing and socioeconomic scenarios will allow the linking the caloric requirement of a population with landscape availability. Data on average dietary energy requirement, e.g. 2,090 kcal per person per day in Southern Africa, could be further fine-tuned to local levels using census and survey data. Then, applied to time series gridded population data to get a better estimate of caloric demand across space and time. There are signs that the scientific community maybe heading in the direction of estimating caloric value of a landscape. For example, Cassidy et al. (2013) has shown that it is possible to spatialize the proportion of global agricultural yield that is used for food or feed on a per calorie basis. This allows for a direct comparison of how many people could be sustained in a particular area. Additionally, there is a need for spatially explicit network analysis, such as the type used in geographic information systems, to map NPP flows from producing areas to consuming areas through road networks. This is necessary to allow for flexible limits in the demand-supply framework so that factors such as market access and rural-urban flows could be taken into account.

The importance of global drylands in the terrestrial carbon cycle has recently been identified (Poulter et al., 2014; Ahlström et al., 2015). However, knowledge about their magnitude, spatial, temporal variability and seasonal process (e.g. during dry season) is incomplete (D. Stock, 2017). This is a crucial knowledge gap, particularly in the wake of rising atmospheric CO₂ concentrations and recurrent droughts (Dai, 2013). The quantification environmental controls on carbon assimilation is of particular importance because of a lack of gridded, high resolution time series of such data. Recently, Jägermeyr et al. (2014) found that MODIS land surface temperature the Enhanced Vegetation Index were able to explain 62% of the variability in ecosystem respiration across most global biomes.

In that sense, land surface temperature data, such as the 1-km daily MOD11A1/MYD11A1 product from MODIS holds considerable potential.

Africa accounts for roughly 20% of global NPP (Williams et al., 2007). It is widely recognized that there is a chronic lack of field data on carbon fluxes to validate satellite-based models because Africa has the least number of eddy covariance flux towers relative to its size (Mu et al., 2011a). One potential solution to this problem lies in capacity building, which produces three favorable outcomes. First, it eliminates the need for scientists to only rely on data that was collected in the past as their sole sources of validation because of the availability of skilled local labor. Second, it allows for increased scientific understanding of the principles and processes involved in ecosystem ecology, and, in combination with local knowledge, sets the foundation for locally-led projects. Third, it creates a mutually beneficial ecosystem based on an exchange of ideas, and that fosters collaboration and innovation.

Acknowledgements

This dissertation was supported by the Swedish National Space Board (*Rymdstyrelsen*), contract no. 100/11.

The first order of thanks goes to my main supervisor, Jonas Ardö, for taking me on this journey. Thank you for your mentoring and your valuable advice, you've been a colleague and a friend. I have arrived at the shore, on to the mountain!

My co-supervisor Jonathan Seaquist: thank you for making me see the big picture when I got entangled in the nitty-gritty of work. Our discussions have always helped me stay focused.

My co-supervisor Lars Eklundh: thank you for providing me with so much insight about vegetation remote sensing and for all the encouragement.

My co-supervisor David Tenenbaum: thank you for constantly showing me the light at the end of the tunnel. You have an impeccable ability of providing guidance that restores my sanity.

Since my life in Sweden revolved around the PhD, I feel that I should thank everyone who has been involved in making this a rewarding experience.

Paul Caplat: you're literally the first friend I made in Sweden when you dropped by my office to welcome me into the department on my first day (October 16, 2012). Thanks for the good times and I wish you all the best in your new adventure in Ireland.

Lina Eklund: *'shukran jazeelan'* for the multitude of discussions over the last 4+ years, and the ideas and insights that have sparked from them. I feel this tradition will surely continue into the future.

Niklas Boke-Olén: I'm not quite sure how my experience in the department would have been without all the stimulating troubleshooting discussions we've had, and your readiness to help with any and all Sweden-related matters. Thank you.

Mubarik Abdirahman: I am truly grateful for your friendship. You're the biggest Malmö advocate I've met, and you've opened my eyes to this wonderful city that I now call home.

Amina Jama: I am grateful to have met you, and thank you for your friendship. You're truly an inspiration and a role model.

Cecilia Olsson, Ehsan Abdolmajidi, Jing Tang, Laurie Charrieau, Ana Soares, Christian Stiegler, Finn Hedefalk, Min Wang, Zhazhang Cai: We hung out more times than I can remember :-). Thank you for every-single-second.

Jan Blanke and Finja Hansen: I sincerely appreciate the numerous times we spent together and the friendship our young families have. Thank you.

Michao Wu, Min Wang, and Wenxin Zhang: I'll never forget the time I've had in China with you. It was my first trip there, and I still tell the stories of how I got my eye glasses in Nanjing.

Florian Sallaba, Emma Li Johannson, Altaaf Mechiche-Alami, Oskar Lofgren, Wille Dubber, Enass Said, Pearl Mzobe, Norbert Pirk, Tomas Karlsson, Zhendong Wu, Patrik Vestin, Olive Niyomubyeyi, Jeppe Kristensen, Ylva Persson, Geert Hensgens, Hongxiao Jin, Fabien Rizinjirabake, Adrian Gustafson, Yanzi Yan, Tetiana Svystun: the phrase "PhD community" would be meaningless without you. Thanks for the good times.

Special thanks to those colleagues who graduated and are now in greener pastures: Bakhtiyor Pulatov, Balathandayuthabani Panneer Selvam, Kerstin Engström, Anders Ahlström, David Wårlind, Per-Ola Olsson, Julia Bosjö, Yengoh Genesis Tambang, Sadegh Jamali, Elin Sundqvist. You've all been part of the journey.

Natalie Nyman, Ekaterina Volkova, Rafael Przybyszewski, Ricardo Guillén, Eva Andersson, Karin Hall, Eva Kovacs: you're the engine that makes the department function, thank you for all your help.

A warm expression of gratitude goes to my colleagues in Sudan, particularly Hatim El Khidr and Abdelrahman El Khatir, and the residents of the various Sudanese villages I visited for their unwavering hospitality and good will.
Mashkureen ya ahl al khair

I want to sincerely thank Dr. Ranga Myneni for hosting me at the Department of Earth and Environment of Boston University, it was an amazing experience.

Special mention goes to Maria Taubman, my host when I first moved to Sweden. It is hard enough finding student accommodation in Europe from another continent, let alone trying to find it as a Black man. I am sincerely thankful to you for offering me a home during my first year in Lund.

My loving family, especially my parents, Fadumo Hussein and Mohamed Abdi, my brothers and my grandmother. I cannot thank you enough for your firm support, countless prayers and wishes for my success.

Last, but not least, from the bottom of my heart, I want to thank my partner, my lover, my friend, and the mother of our daughter: Martina, mein schatz, words cannot express the love and appreciation I have for you. Thank you for everything from your input on the various drafts and ideas, to your patience and perseverance, particularly leading up to the submission of this dissertation <3

References

- Abdi AM, Boke-Olén N, Jin H, et al. (2017a) Exploring the potential of the plant phenology index for estimating gross primary productivity in semi-arid Africa *Manuscript*.
- Abdi AM, Boke-Olén N, Tenenbaum DE, et al. (2017b) Evaluating water controls on vegetation growth in the semi-arid Sahel using field and Earth observation data. *Submitted to Remote Sensing*.
- Abdi AM, Seaquist J, Tenenbaum DE, et al. (2014) The supply and demand of net primary production in the Sahel. *Environmental Research Letters* 9: 094003.
- Abdi AM, Vrieling A, Yengoh GT, et al. (2016) The El Niño – La Niña cycle and recent trends in supply and demand of net primary productivity in African drylands. *Climatic Change* 138: 111-125.
- Abdissa F and Degefa T. (2011) Urbanization and Changing Livelihoods: The Case of Farmers' Displacement in the Expansion of Addis Ababa. In: Teller C (ed) *The Demographic Transition and Development in Africa: The Unique Case of Ethiopia*. Dordrecht: Springer Netherlands, 215-235.
- Adugna A and Hailemariam A. (2011) Rural–Urban Linkages in Ethiopia: Insuring Rural Livelihoods and Development of Urban Centers. In: Teller C (ed) *The Demographic Transition and Development in Africa*. Springer Netherlands, 167-186.
- Ahlström A, Raupach MR, Schurgers G, et al. (2015) The dominant role of semi-arid ecosystems in the trend and variability of the land CO₂ sink. *Science* 348: 895-899.
- Ahmed II and Green RH. (1999) The Heritage of War and State Collapse in Somalia and Somaliland: Local-Level Effects, External Interventions and Reconstruction. *Third World Quarterly* 20: 113-127.
- Andela N and van der Werf GR. (2014) Recent trends in African fires driven by cropland expansion and El Nino to La Nina transition. *Nature Clim. Change* 4: 791-795.
- Anderson DB. (1936) Relative Humidity or Vapor Pressure Deficit. *Ecology* 17: 277-282.
- Arino O, Ramos Perez JJ, Kalogirou V, et al. (2012) Global Land Cover Map for 2009 (GlobCover 2009). PANGAEA.
- Bailis R, Drigo R, Ghilardi A, et al. (2015) The carbon footprint of traditional woodfuels. *Nature Climate Change* 5: 266-272.
- Baldocchi DD, Hincks BB and Meyers TP. (1988) Measuring Biosphere-Atmosphere Exchanges of Biologically Related Gases with Micrometeorological Methods. *Ecology* 69: 1331-1340.
- Balogun O, Yusuf S and Ayantoye K. (2013) The Threats of Climate Change: Implication for Food Crisis in Sub-Sahara Africa. In: Behnassi M,

- Pollmann O and Kissinger G (eds) *Sustainable Food Security in the Era of Local and Global Environmental Change*. Springer Netherlands, 85-98.
- Barrett CB and Upton JB. (2013) Food Security and Sociopolitical Stability in Sub-Saharan Africa. *Food Security and Sociopolitical Stability*. New York, NY: Oxford University Press.
- Batterbury S. (2001) Landscapes of Diversity: A Local Political Ecology of Livelihood Diversification in South-Western Niger. *Ecumene* 8: 437-464.
- Battisti DS and Naylor RL. (2009) Historical Warnings of Future Food Insecurity with Unprecedented Seasonal Heat. *Science* 323: 240-244.
- Blench R. (1994) The Expansion and Adaptation of Fulbe Pastoralism to Subhumid and Humid Conditions in Nigeria (L'expansion et l'adaptation du pastoralisme peul aux conditions climatiques humides et subhumides du Nigeria). *Cahiers d'Études africaines* 34: 197-212.
- Boke-Olén N, Abdi AM, Hall O, et al. (2017) High-resolution African population projections from radiative forcing and socio-economic models, 2000 to 2100. *Scientific Data* 4: 160130.
- Breman H and Kessler J-J. (1995) The Distribution and Canopy Cover of Woody Species. *Woody Plants in Agro-Ecosystems of Semi-Arid Regions: with an Emphasis on the Sahelian Countries*. Berlin, Heidelberg: Springer Berlin Heidelberg, 4-53.
- Budyko MI. (1974) *Climate and life*, New York, NY: Academic Press.
- Caldwell JC. (1977) Demographic aspects of drought: An examination of the African drought of 1970-74. *African Environment Special Report* 6: 93-100.
- Campbell MM, Casterline J, Castillo F, et al. (2014) Population and climate change: who will the grand convergence leave behind? *The Lancet Global Health* 2: e253-e254.
- Cassidy ES, West PC, Gerber JS, et al. (2013) Redefining agricultural yields: from tonnes to people nourished per hectare. *Environmental Research Letters* 8: 034015.
- Ceccato P, Cressman K, Giannini A, et al. (2006) The desert locust upsurge in West Africa (2003 – 2005): Information on the desert locust early warning system and the prospects for seasonal climate forecasting. *International Journal of Pest Management* 53: 7-13.
- Cook KH. (1999) Generation of the African Easterly Jet and Its Role in Determining West African Precipitation. *Journal of Climate* 12: 1165-1184.
- D. Stock W. (2017) Plants anticipating rain – a challenge for modelling climate change impacts. *New Phytologist* 213: 475-477.
- Dai A. (2013) Increasing drought under global warming in observations and models. *Nature Clim. Change* 3: 52-58.
- de Haan A, Brock K and Coulibaly N. (2002) Migration, Livelihoods and Institutions: Contrasting Patterns of Migration in Mali. *The Journal of Development Studies* 38: 37-58.

- Degefu W. (1988) Some aspects of meteorological drought in Ethiopia. In: Glantz MH (ed) *Drought and Hunger in Africa*. Cambridge, UK: Cambridge University Press.
- Dingman SL. (2015) *Physical Hydrology: Third Edition*: Waveland Press.
- Dovie DBK. (2003) Rural economy and livelihoods from the non-timber forest products trade. Compromising sustainability in southern Africa? *International Journal of Sustainable Development & World Ecology* 10: 247-262.
- Doxsey-Whitfield E, MacManus K, Adamo SB, et al. (2015) Taking Advantage of the Improved Availability of Census Data: A First Look at the Gridded Population of the World, Version 4. *Papers in Applied Geography* 1: 226-234.
- Elbehri A, Kaminski J, Koroma S, et al. (2013) West Africa food systems: An overview of trends and indicators of demand, supply, and competitiveness of staple food value chains. In: Elbehri A (ed) *Rebuilding West Africa's Food Potential*. FAO/IFAD.
- Engström K, Olin S, Rounsevell MDA, et al. (2016) Assessing uncertainties in global cropland futures using a conditional probabilistic modelling framework. *Earth Syst. Dynam.* 7: 893-915.
- FAO. (2013) CountrySTAT Mali. Rome, Italy: Statistics Division, Food and Agriculture Organization of the United Nations
- FAOSTAT. (2015) FAO Statistical Databases. Rome, Italy.: Food and Agriculture Organization of the United Nations.
- Fetzel T, Niedertscheider M, Haberl H, et al. (2015) Patterns and changes of land use and land-use efficiency in Africa 1980–2005: an analysis based on the human appropriation of net primary production framework. *Regional Environmental Change*: 1-14.
- FEWSNET. (2016) Southern Africa: Illustrating the extent and severity of the 2015-16 drought. Famine Early Warning Systems Network/USAID.
- Fox L. (2015) Are African Households Heterogeneous Agents? . *IMF Working Paper*. Washington, DC: International Monetary Fund.
- Funk C, Peterson P, Landsfeld M, et al. (2015) The climate hazards infrared precipitation with stations—a new environmental record for monitoring extremes. *Scientific Data* 2: 150066.
- Gargallo-Garriga A, Sardans J, Pérez-Trujillo M, et al. (2014) Opposite metabolic responses of shoots and roots to drought. *Scientific Reports* 4: 6829.
- Gitelson AA, Viña A, Verma SB, et al. (2006) Relationship between gross primary production and chlorophyll content in crops: Implications for the synoptic monitoring of vegetation productivity. *Journal of Geophysical Research: Atmospheres* 111: n/a-n/a.
- Halweil B. (2002) Home Grown: The Case For Local Food In A Global Market. Worldwatch Institute.
- Harper S. (2014) Economic and social implications of aging societies. *Science* 346: 587.

- Hashimoto H, Dungan JL, White MA, et al. (2008) Satellite-based estimation of surface vapor pressure deficits using MODIS land surface temperature data. *Remote Sensing of Environment* 112: 142-155.
- Hassan R, Hertzler G and Benhin JKA. (2009) Depletion of forest resources in Sudan: Intervention options for optimal control. *Energy Policy* 37: 1195-1203.
- Heinsch FA, Reeves M, Bowker C, et al. (2003) GPP and NPP (MOD17A2/A3) Products NASA MODIS Land Algorithm. *MOD17 User's Guide*: 1-57.
- Hickler T, Eklundh L, Seaquist JW, et al. (2005) Precipitation controls Sahel greening trend. *Geophysical Research Letters* 32: L21415.
- Hiemstra-van der Horst G and Hovorka AJ. (2009) Fuelwood: The “other” renewable energy source for Africa? *Biomass and bioenergy* 33: 1605-1616.
- Hurt GC, Chini LP, Frohling S, et al. (2011) Harmonization of land-use scenarios for the period 1500–2100: 600 years of global gridded annual land-use transitions, wood harvest, and resulting secondary lands. *Climatic Change* 109: 117.
- Hurt GC, Frohling S, Fearon MG, et al. (2006) The underpinnings of land-use history: three centuries of global gridded land-use transitions, wood-harvest activity, and resulting secondary lands. *Global Change Biology* 12: 1208-1229.
- Ickowicz A, Ancey V, Corniaux C, et al. (2012) Crop–livestock production systems in the Sahel – increasing resilience for adaptation to climate change and preserving food security. In: Meybeck A, Lankoski J, Redfern S, et al. (eds) *Building resilience for adaptation to climate change in the agriculture sector*. Rome, Italy: Food and Agriculture Organization of the United Nations (FAO), 261-294.
- IPCC. (2014) *Climate Change 2014: Impacts, Adaptation, and Vulnerability. Part B: Regional Aspects. Contribution of Working Group II to the Fifth Assessment Report of the Intergovernmental Panel on Climate Change*. Cambridge, United Kingdom and New York, NY, USA.
- Itannam F and Olsson M. (2004) Land Degradation in Addis Ababa Due to Industrial and Urban Development. *Ethiopian Journal of Development Research* 26: 77-100.
- Jägermeyr J, Gerten D, Lucht W, et al. (2014) A high-resolution approach to estimating ecosystem respiration at continental scales using operational satellite data. *Global Change Biology* 20: 1191-1210.
- Jin H and Eklundh L. (2014) A physically based vegetation index for improved monitoring of plant phenology. *Remote Sensing of Environment* 152: 512-525.
- Johnson PL and Kelley JJ. (1970) Dynamics of Carbon Dioxide and Productivity in an Arctic Biosphere. *Ecology* 51: 73-80.
- Jones PG and Thornton PK. (2003) The potential impacts of climate change on maize production in Africa and Latin America in 2055. *Global Environmental Change* 13: 51-59.

- Jones PG and Thornton PK. (2009) Croppers to livestock keepers: livelihood transitions to 2050 in Africa due to climate change. *Environmental Science & Policy* 12: 427-437.
- Jönsson P and Eklundh L. (2004) TIMESAT—a program for analyzing time-series of satellite sensor data. *Computers & Geosciences* 30: 833-845.
- Kaboré D and Reij C. (2004) The emergence and spreading of an improved traditional soil and water conservation practice in Burkina Faso. Washington, DC: International Food Policy Research Institute.
- Knips V. (2004) Review of the livestock sector in the Horn of Africa (IGAD countries). *Livestock Sector Report*. Rome, Italy: Food and Agriculture Organization of the United Nations.
- Knox J, Hess T, Daccache A, et al. (2012) Climate change impacts on crop productivity in Africa and South Asia. *Environmental Research Letters* 7: 034032.
- Lees SH and Bates DG. (1974) The Origins of Specialized Nomadic Pastoralism: A Systemic Model. *American Antiquity* 39: 187-193.
- Lieth H. (1964) Versuch einer kartographischen Darstellung der Produktivität der Pflanzendecke auf der Erde. *Geographisches Taschenbuch* 65: 72-80.
- Lieth H. (1972) Über die Primärproduktion der pflanzendecke der Erde. *Angewandte Botanik* 46: 1-37.
- Lieth H. (1973) Primary Production: Terrestrial Ecosystems. *Human Ecology* 1: 303-332.
- Lieth H and Whittaker RH. (1975) *Primary Productivity of the Biosphere*, Berlin: Springer.
- Linard C, Gilbert M, Snow RW, et al. (2012) Population Distribution, Settlement Patterns and Accessibility across Africa in 2010. *PLoS ONE* 7: e31743.
- Liu J, Hull V, Batistella M, et al. (2013) Framing Sustainability in a Telecoupled World. *Ecology and Society* 18.
- Maiga A, Chen G, Wang Q, et al. (2008) Renewable energy options for a Sahel country: Mali. *Renewable and Sustainable Energy Reviews* 12: 564-574.
- Maroco J, atilde, P. o, et al. (1997) Stomatal Responses to Leaf-to-Air Vapour Pressure Deficit in Sahelian Species. *Functional Plant Biology* 24: 381-387.
- Masih I, Maskey S, Mussá FEF, et al. (2014) A review of droughts on the African continent: a geospatial and long-term perspective. *Hydrol. Earth Syst. Sci.* 18: 3635-3649.
- Merbold L, Ardö J, Arneth A, et al. (2009) Precipitation as driver of carbon fluxes in 11 African ecosystems. *Biogeosciences* 6: 1027-1041.
- Moller LC. (2012) The Ethiopian urban migration study 2008: the characteristics, motives and outcomes to immigrants to Addis Ababa. Washington, DC: The World Bank.
- Moncrieff JB, Monteny B, Verhoef A, et al. (1997) Spatial and temporal variations in net carbon flux during HAPEX-Sahel. *Journal of Hydrology* 188: 563-588.

- Monteith J. (1981) Does light limit crop production? In: Johnson C (ed) *Physiological Processes Limiting Plant Productivity*. London: Butterworth, 23-38.
- Monteith JL. (1972) Solar radiation and productivity in tropical ecosystems. *Journal of Applied Ecology* 9: 747-766.
- Monteith JL and Moss CJ. (1977) Climate and the efficiency of crop production in Britain. *Philosophical Transactions of the Royal Society of London. B, Biological Sciences* 281: 277-294.
- Mu Q, Zhao M and Running S. (2011a) Remote Sensing and Modeling of Global Evapotranspiration. *Multiscale Hydrologic Remote Sensing*. CRC Press, 443-480.
- Mu Q, Zhao M and Running SW. (2011b) Improvements to a MODIS global terrestrial evapotranspiration algorithm. *Remote Sensing of Environment* 115: 1781-1800.
- Nicholson SE. (2011) *Dryland Climatology*: Cambridge University Press.
- Nicholson SE, Tucker CJ and Ba M. (1998) Desertification, drought, and surface vegetation: An example from the West African Sahel. *Bulletin of the American Meteorological Society* 79: 815-830.
- O'Neill BC, Kriegler E, Riahi K, et al. (2014) A new scenario framework for climate change research: the concept of shared socioeconomic pathways. *Climatic Change* 122: 387-400.
- Obayelu AE. (2011) Assessment of Food Reserves, Markets, Trade, and Regional Integration Systems in Sub-Saharan Africa: Are these effective pathways to food security? In: Asenso-Okyere K and Jemaneh S (eds) *Increasing agricultural productivity and enhancing food security in Africa*. Addis Ababa, Ethiopia: International Food Policy Research Institute, 34.
- Olsson L. (1985) An Integrated Study of Desertification. *Department of Physical Geography and Ecosystem Science*. Lund, Sweden: Lund University, 170.
- Olsson L. (1993) On the Causes of Famine: Drought, Desertification and Market Failure in the Sudan. *Ambio* 22: 395-403.
- Pappas C, Fatichi S, Leuzinger S, et al. (2013) Sensitivity analysis of a process-based ecosystem model: Pinpointing parameterization and structural issues. *Journal of Geophysical Research: Biogeosciences* 118: 505-528.
- Philippon N, Martiny N, Camberlin P, et al. (2014) Timing and Patterns of the ENSO Signal in Africa over the Last 30 Years: Insights from Normalized Difference Vegetation Index Data. *Journal of Climate* 27: 2509-2532.
- Pires M. (2003) The Spatial Polarization of Woodfuel Supply and Demand in Senegal. *African Geographical Review* 22: 29-47.
- Poulter B, Frank D, Ciais P, et al. (2014) Contribution of semi-arid ecosystems to interannual variability of the global carbon cycle. *Nature* 509: 600-603.
- Prince SD. (1991) Satellite remote sensing of primary production: comparison of results for Sahelian grasslands 1981-1988. *International Journal of Remote Sensing* 12: 1301-1311.
- Rouse JW, Haas RH, Deering DW, et al. (1973) Monitoring the vernal advancement and retrogradation (green wave effect) of natural vegetation.

- College Station, Texas: Remote Sensing Center, Texas A&M University, 44-47.
- Running SW. (1986) Global primary production from terrestrial vegetation: Estimates integrating satellite remote sensing and computer simulation technology. *Science of The Total Environment* 56: 233-242.
- Running SW. (2012) A Measurable Planetary Boundary for the Biosphere. *Science* 337: 1458-1459.
- Running SW, Baldocchi DD, Turner DP, et al. (1999) A Global Terrestrial Monitoring Network Integrating Tower Fluxes, Flask Sampling, Ecosystem Modeling and EOS Satellite Data. *Remote Sensing of Environment* 70: 108-127.
- Running SW, Justice CO, Salomonson V, et al. (1994) Terrestrial remote sensing science and algorithms planned for EOS/MODIS. *International Journal of Remote Sensing* 15: 3587-3620.
- Running SW, Nemani RR, Heinsch FA, et al. (2004) A Continuous Satellite-Derived Measure of Global Terrestrial Primary Production. *BioScience* 54: 547-560.
- Running SW, Thornton PE, Nemani RR, et al. (2000) Global terrestrial gross and net primary productivity from the Earth Observing System. In: Sala OE, Mooney HA and Howarth RW (eds) *Methods in Ecosystem Science*. Springer-Verlag, New York, 44-57.
- Running SW and Zhao M. (2015) User's Guide ver. 3.0: Daily GPP and Annual NPP (MOD17A2/A3) Products. NASA Earth Observing System MODIS Land Algorithm. Missoula, Montana: Numerical Terradynamics Simulation Group.
- Samatar AI. (1989) *The State and Rural Transformation in Northern Somalia, 1884-1986*, Madison, Wisconsin: University of Wisconsin Press.
- Savitzky A and Golay MJE. (1964) Smoothing and Differentiation of Data by Simplified Least Squares Procedures. *Analytical Chemistry* 36: 1627-1639.
- Schlenker W and Lobell DB. (2010) Robust negative impacts of climate change on African agriculture. *Environmental Research Letters* 5: 014010.
- Schlesinger WH. (1997) *Biogeochemistry: an analysis of global change*: Academic press.
- Schwinning S, Sala OE, Loik ME, et al. (2004) Thresholds, memory, and seasonality: understanding pulse dynamics in arid/semi-arid ecosystems. *Oecologia* 141: 191-193.
- Seaman J. (1993) Famine Mortality in Africa. *IDS Bulletin* 24: 27-32.
- Sen A. (1999) *Development as Freedom*, New York, NY: Anchor Books.
- Shapouri S and Rosen SL. (1999) Food Security Assessment: Why Countries Are at Risk. Washington, DC: U.S. Department of Agriculture.
- Sims DA, Rahman AF, Cordova VD, et al. (2008) A new model of gross primary productivity for North American ecosystems based solely on the enhanced vegetation index and land surface temperature from MODIS. *Remote Sensing of Environment* 112: 1633-1646.

- Sjöström M, Ardö J, Arneth A, et al. (2011) Exploring the potential of MODIS EVI for modeling gross primary production across African ecosystems. *Remote Sensing of Environment* 115: 1081-1089.
- Sjöström M, Zhao M, Archibald S, et al. (2013) Evaluation of MODIS gross primary productivity for Africa using eddy covariance data. *Remote Sensing of Environment* 131: 275-286.
- Smith A. (1776) *An Inquiry into the Nature and Causes of the Wealth of Nations*, London: W. Strahan and T. Cadell.
- Sperling L. (1987) The adoption of camels by Samburu cattle herders. *Nomadic Peoples*: 1-17.
- Stige LC, Stave J, Chan K-S, et al. (2006) The effect of climate variation on agropastoral production in Africa. *Proceedings of the National Academy of Sciences of the United States of America* 103: 3049-3053.
- Szarek SR and Woodhouse RM. (1977) Ecophysiological studies of Sonoran Desert plants. *Oecologia* 28: 365-375.
- Templeton A. (2002) Out of Africa again and again. *Nature* 416: 45-51.
- Thornton PK, Jones PG, Ericksen PJ, et al. (2011) *Agriculture and food systems in sub-Saharan Africa in a 4°C+ world*.
- Tschakert P, Sagoe R, Ofori-Darko G, et al. (2010) Floods in the Sahel: an analysis of anomalies, memory, and anticipatory learning. *Climatic Change* 103: 471-502.
- Tucker CJ, Holben BN, Elgin JH, et al. (1981) Remote sensing of total dry-matter accumulation in winter wheat. *Remote Sensing of Environment* 11: 171-189.
- Tucker CJ, Vanpraet C, Boerwinkel E, et al. (1983) Satellite remote sensing of total dry matter production in the Senegalese Sahel. *Remote Sensing of Environment* 13: 461-474.
- Turner DP, Ritts WD, Cohen WB, et al. (2006) Evaluation of MODIS NPP and GPP products across multiple biomes. *Remote Sensing of Environment* 102: 282-292.
- van der Plas RJ and Abdel-Hamid MA. (2005) Can the woodfuel supply in sub-Saharan Africa be sustainable? The case of N'Djaména, Chad. *Energy Policy* 33: 297-306.
- van Vuuren DP, Edmonds J, Kainuma M, et al. (2011) The representative concentration pathways: an overview. *Climatic Change* 109: 5-31.
- Verhoef A, Allen SJ, Bruin HAR, et al. (1996) Fluxes of carbon dioxide and water vapour from a Sahelian savanna. *Agric For Meteorol.* 80.
- Ward AD, Trimble SW, Burckhard SR, et al. (2015) *Environmental Hydrology, Third Edition*: CRC Press.
- Williams CA, Hanan NP, Neff JC, et al. (2007) Africa and the global carbon cycle. *Carbon Balance and Management* 2: 1-13.
- Wu C, Chen JM and Huang N. (2011) Predicting gross primary production from the enhanced vegetation index and photosynthetically active radiation: Evaluation and calibration. *Remote Sensing of Environment* 115: 3424-3435.

- Wu C, Munger JW, Niu Z, et al. (2010) Comparison of multiple models for estimating gross primary production using MODIS and eddy covariance data in Harvard Forest. *Remote Sensing of Environment* 114: 2925-2939.
- Zhao M, Running S, Heinsch FA, et al. (2011) MODIS-derived terrestrial primary production. In: Ramachandran B, Justice CO and Abrams MJ (eds) *Land Remote Sensing and Global Environmental Change*. New York: Springer, 635-660.
- Zulu LC. (2010) The forbidden fuel: Charcoal, urban woodfuel demand and supply dynamics, community forest management and woodfuel policy in Malawi. *Energy Policy* 38: 3717-3730.

Paper I

The supply and demand of net primary production in the Sahel

A M Abdi, J Seaquist, D E Tenenbaum, L Eklundh and J Ardö

Department of Physical Geography and Ecosystem Science, Lund University, Sölvegatan 12, SE-223 62, Sweden

E-mail: hakim.abdi@nateko.lu.se


Received 5 June 2014, revised 25 July 2014

Accepted for publication 5 August 2014

Published 9 September 2014

Abstract

Net primary production (NPP) is the principal source of energy for ecosystems and, by extension, human populations that depend on them. The relationship between the supply and demand of NPP is important for the assessment of socio-ecological vulnerability. We present an analysis of the supply and demand of NPP in the Sahel using NPP estimates from the MODIS sensor and agri-environmental data from FAOSTAT. This synergistic approach allows for a spatially explicit estimation of human impact on ecosystems. We estimated the annual amount of NPP required to derive food, fuel and feed between 2000 and 2010 for 22 countries in sub-Saharan Africa. When comparing annual estimates of supply and demand of NPP, we found that demand increased from 0.44 PgC to 1.13 PgC, representing 19% and 41%, respectively, of available supply due to a 31% increase in the human population between 2000 and 2010. The demand for NPP has been increasing at an annual rate of 2.2% but NPP supply was near-constant with an inter-annual variability of approximately 1.7%. Overall, there were statistically significant ($p < 0.05$) increases in the NPP of cropland (+6.0%), woodland (+6.1%) and grassland/savanna (+9.4%), and a decrease in the NPP of forests (−0.7%). On the demand side, the largest increase was for food (20.4%) followed by feed (16.7%) and fuel (5.5%). The supply-demand balance of NPP is a potentially important tool from the standpoint of sustainable development, and as an indicator of stresses on the environment stemming from increased consumption of biomass.

 Online supplementary data available from stacks.iop.org/ERL/9/094003/mmedia

Keywords: Drylands, sustainability, NPP, Sahel, climate change, vulnerability

1. Introduction

Net primary production (NPP) represents the amount of atmospheric carbon that is fixed by vegetation during photosynthesis and accumulates as biomass. It represents the availability of carbon in the form of plant material for consumption as food, fuel and feed. NPP has been linked to crop yield (Tao *et al* 2005), biomass energy potential (Field *et al* 2008), forest production (Baisden 2006), and grazing resources (Leriche *et al* 2001). In sub-Saharan Africa NPP

resulting from extensive agriculture and dry woodlands plays an important role in maintaining food security and providing household energy. However, these resources are under pressure from high population growth, which increases demand for NPP, and climate change, which impacts supply (IPCC 2014). The ‘supply’ of NPP is defined here as the annual amount of carbon stored in the ecosystem as plant tissue.

Semi-arid regions are particularly vulnerable to fluctuations in the supply of NPP due to its natural scarcity. In these regions, increased human activities are often driven by the demand for food, fuel and feed, which brings about changes that alter the spatial patterns of NPP such as cropland expansion, pasture creation, and fuelwood extraction. For example, large increases in demand for NPP lead to increased



Content from this work may be used under the terms of the [Creative Commons Attribution 3.0 licence](http://creativecommons.org/licenses/by/3.0/). Any further distribution of this work must maintain attribution to the author(s) and the title of the work, journal citation and DOI.

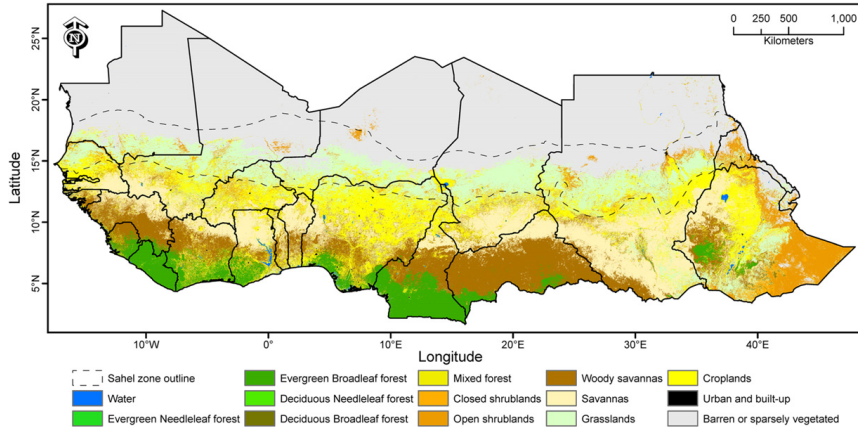


Figure 1. IGBP classification of the study area according to the MODIS Land Cover Type Product (MCD12Q1). The dashed line represents rainfall isohyets between 100 and 600 mm that delineate the Sahelian zone.

pasture stocking rates (Vargas *et al* 2009) resulting in soil compaction and vegetation defoliation (Hiemaux *et al* 1999). Additionally, crop yields, particularly in parts of sub-Saharan Africa, have been declining (Aune *et al* 2005, Chianu *et al* 2006) due to, among other things, reduction in soil fertility caused by continuous cropping to meet demand (Samaké *et al* 2005).

We use the terms ‘demand’ and ‘consumption’ to denote two different, but closely related, things. Demand for NPP is defined as the annual amount of carbon required to derive the food, fuel and feed necessary for human survival, and which also includes carbon lost during harvest and handling. The term ‘consumption’ refers to the actual amount of NPP that is extracted from the ecosystem as reported in the statistical database of the Food and Agriculture Organization of the United Nations (FAOSTAT).

Field estimation of NPP involves harvesting vegetation and calculating the annual growth of wood, the mass of foliage at peak leaf display, and the difference in the mass of tissue harvested at the beginning and end of the growing season (Schlesinger 1997). NPP varies spatially due to both environmental and anthropogenic factors and, because fieldwork is both labor and cost intensive, it would be exorbitantly expensive to conduct measurements over large extents. In this regard, data from satellite remote sensing platforms provide useful tools for quantifying the availability of NPP at regional scales.

We chose the Sahel region of Africa as an example of a complex, semi-arid, human-environment system where the supply-demand balance of NPP is in a constant flux. The Sahel has been subject to numerous droughts in the late 20th and early 21st centuries. Severe, region-wide, drought-induced famines occurred in 1972–1973 and 1984–1985 (Sen 1983, Ibrahim 1988), and there were localized food shortages in 1990, 2002 and 2004. Recently, food production

deficits were reported by several Sahelian countries in 2011/2012 and it is presently estimated that over 11 million people across the region are food insecure (United Nations 2013). A combination of unfavorable climatic conditions (Gonzalez *et al* 2012) and anthropogenic pressure (Sop and Oldeland 2011, Hassan *et al* 2009) have caused declines in crop yield (Thornton *et al* 2008) and the diversity of Sahelian woody plant species (Wezel 2005).

The objectives of this paper are to quantify for the period 2000–2010: (1) the amount of NPP required to derive food, fuel and feed, (2) the fluctuations in the supply NPP, and (3) the percent of NPP demand relative to supply across the region. The chosen study period coincides with the availability of two open-access datasets (1) a continuous, high-resolution, satellite-derived NPP dataset, and (2) a high resolution population distribution dataset covering three time slices: 2000, 2005, and 2010.

2. Materials and methods

2.1. Study area

The study area covers the portion of the African continent between 5° and 25° north latitude with a focus on the Sahel, which is bounded by the 100 mm and 600 mm rainfall isohyets (figure 1). Northern parts of the area that border the Sahara Desert have a mean annual rainfall of less than 100 mm. To south of the Sahel are the humid savannas of the Sudano-Guinean zone that receive ample rainfall, between 600–1000 mm, enabling high vegetation productivity. Most of the region has one growing season, the start and length of which varies with latitude. The growing season in northern parts of the of the study area begins in July and ends in October; in the southern parts (<10°N) the season starts around April and lasts until November (Vrieling *et al* 2013).

2.2. NPP supply

We obtained the latest Collection 5.1 annual MODIS NPP data from 2000 to 2010 from the NASA Earth Observation System repository at the University of Montana (www.nsg.umt.edu/). The MOD17 light use efficiency model (Heinsch *et al* 2003) calculates NPP as the difference between gross primary production (parameters within parentheses in equation (1)) and autotrophic respiration including growth and maintenance components:

$$\text{NPP}_{\text{Supply}} = (\text{PAR} * \text{FPAR} * \epsilon_{\text{max}} * \text{VPD} * T_{\text{min}}) - \text{Ra} \quad (1)$$

where $\text{NPP}_{\text{Supply}}$ is the NPP available in the ecosystem regardless of land use type; PAR is incoming photo-synthetically active radiation; FPAR is the fraction of incident PAR absorbed by the vegetation canopy; ϵ_{max} represents maximum light use efficiency under hypothetical biome-specific ideal conditions according to Monteith (1972); VPD and T_{min} are environmental scalars that constrain light use efficiency and stand for vapor pressure deficit and minimum temperature, respectively; Ra (autotrophic respiration) represents maintenance and growth respiration of leaves, fine roots and woody tissue. Further descriptions of the MOD17 model are detailed in Running *et al* (2004), Zhao *et al* (2005) and Zhao and Running (2010).

In order to delineate the land cover classes that source NPP for food, fuel, and feed, we obtained the latest Collection 5.1 of the MODIS Land Cover Type Product (MCD12C1) (Friedl *et al* 2010) from NASA's Land Processes Distributed Active Archive (LPDAAC) (<https://lpdaac.usgs.gov>). We used the International Geosphere Biosphere Program (IGBP) classification system and aggregated the 14 land cover classes within the study area into four land cover groupings (table 1S, supplementary information) based on ecophysiological similarities and their shared NPP sourcing capacity. For example, grasslands (<10% tree cover) and savannas (10–30% tree cover) were grouped together because both categories are predominantly composed of herbaceous cover that serve as grazing habitat for the region's livestock population. Similarly croplands and cropland/natural vegetation mosaics were grouped together into one category. We calculated $\text{NPP}_{\text{Supply}}$ trends for the region based on regression slopes resulting from ordinary least squares versus time. We then isolated areas that displayed significance ($p < 0.05$) and intersected them with reclassified grids of the land cover groupings. This procedure resulted in grids of statistically significant $\text{NPP}_{\text{Supply}}$ change for each land cover grouping. We also calculated annual $\text{NPP}_{\text{Supply}}$ anomalies for the 2000–2010 time period by subtracting the decadal average from each yearly total.

2.3. Population density

Gridded population data for the years 2000, 2005 and 2010 were downloaded from the WorldPop Project (<http://worldpop.org.uk/>). The dataset is derived by using high resolution census data as a dependent variable in a Random Forest model along with a suite of independent variables that

include land use and land cover, digital elevation, night-time lights, mean annual precipitation and mean annual temperature. Detailed descriptions of the population model are presented in Tatem *et al* (2007) and Linard *et al* (2011). We interpolated between 2000–2005 and 2005–2010 using annual population growth data from United Nations Statistical Database (UNSTAT 2014) to obtain continuous annual coverage between 2000 and 2010.

2.4. NPP demand

The Sahelian growing season coincides with the summer rains; crops are generally planted between May and July and harvested from October to November (USDA 1994). The NPP of croplands during the growing season represents the annual provision crops that are produced in the region. Sorghum, millet and maize, which together constitute 50% of Sahelian crop distribution (Leff *et al* 2004) are important both for human consumption and as fodder for livestock. Sahelian pastoralists depend on grassland and savanna productivity as forage for their livestock herds. Presently, 80% of the crop calories produced in the region are used for food, 10% for animal feed, and the remaining 10% for other uses (Cassidy *et al* 2013). In most parts of the Sahel, energy demand is met by woodfuels, and NPP provides biomass for energy in the form of fuelwood and charcoal.

We calculate demand for NPP ($\text{NPP}_{\text{Demand}}$) as the annual amount (in grams of carbon) of terrestrial carbon necessary to derive food, fuel and feed requirement in each country and account for carbon lost due to burning and harvest losses. Approximately 90% of the food produced in the region is consumed domestically (Gollin 2009, Barrett 2013), leaving 10% for other use. Therefore we constrained $\text{NPP}_{\text{Demand}}$ within each country in the region by using domestic production data from FAOSTAT (<http://faostat3.fao.org/>) (FAOSTAT 2013).

$$\text{NPP}_{\text{Demand}} = \text{NPP}_{\text{food}} + \text{NPP}_{\text{fuel}} + \text{NPP}_{\text{feed}} + \text{NPP}_{\text{burned}} + \text{NPP}_{\text{residues}} \quad (2)$$

where NPP_{food} is the NPP required to produce domestically consumed food items which includes meats sourced from six types of domestic animals (cattle, goats, sheep, pigs, camels, chickens) and two non-meat animal products (eggs and milk) (table 2S, supplementary information). Also included were 27 types of regionally important primary crops (table 3S, supplementary information). These crops represent 95% of all those that are domestically consumed by most of the countries in the study area (FAOSTAT 2013). A conceptual flowchart of the demand module is depicted in figure 1S in the supplementary information.

NPP_{fuel} represents fuelwood and charcoal extracted from the region's dry woodlands. Woodfuel requirement ranges from 55% in Senegal (Pires 2003) to over 90% in Chad (van der Plas and Abdel-Hamid 2005), but on average it is around 80% across the study area. NPP_{feed} is the total amount of feed required to sustain the region's livestock population. This was calculated by converting the total number of heads of the six Sahelian domestic animal species to their equivalent Tropical

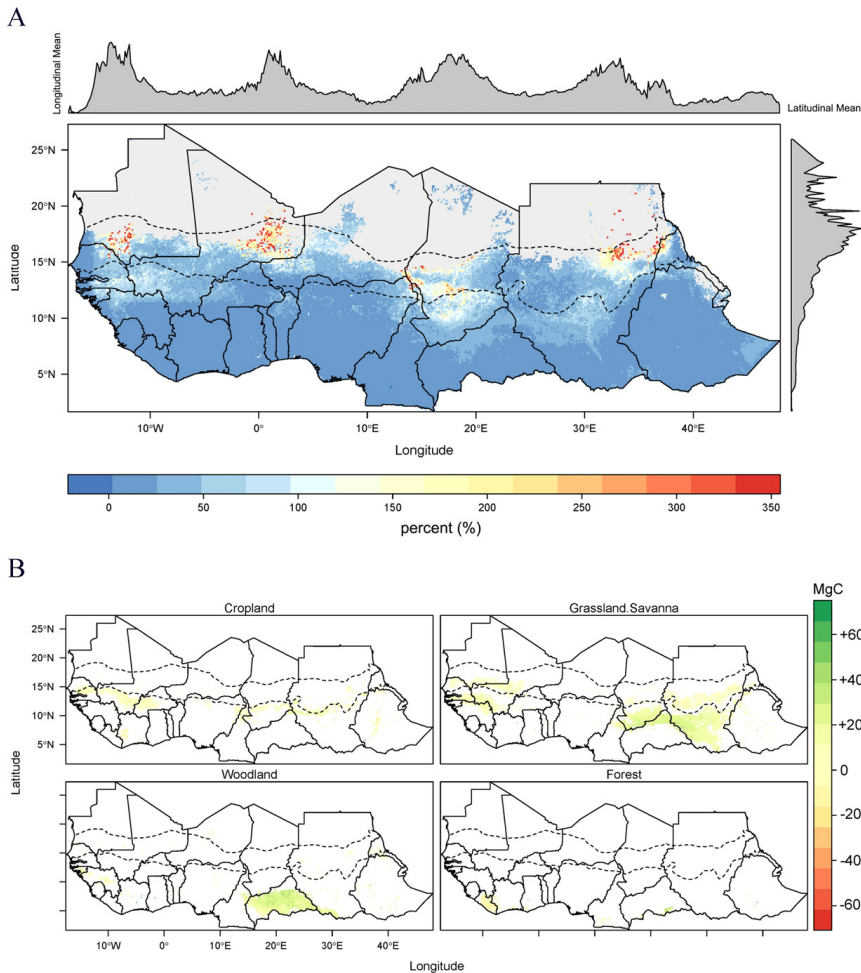


Figure 2. (A) Coefficient of variation of NPP 2000–2010. The dashed line represents rainfall isohyets between 100 and 600 mm that delineate the Sahelian zone. There are well-defined clusters of high NPP variability (>100%) in the Sahelian zone notably in southern Mauritania, northeast Mali, central and eastern Chad and northeastern Sudan. The gray coloration within each countries national borders signify areas with no data. (B) Significant trends ($p < 0.05$) in NPP_{Supply} for the four land cover groupings in the study area between 2000 and 2010.

Livestock Units (TLU), then multiplying by the annual feed requirement for each TLU (table 4S, supplementary information). Domestic human-driven NPP loss resulting from biomass burning of forest resources for land clearing is represented by NPP_{burned}. Agricultural byproducts are represented by NPP_{residues} and were calculated by applying harvest factors provided in literature (table 5S, supplementary information).

Urban and rural consumption ratios vary due to differences in diet, lifestyle and wealth (Popkin 1999). We separated urban and rural areas by masking the urban extent of the

WorldPop grids using data from the Global Rural-Urban Mapping Project (CIESIN *et al* 2011). We derived per capita NPP_{Demand} by dividing total consumption with each country’s population, and used the WorldPop data as a spatial surrogate to apply the per capita NPP_{Demand} to grid cells. Consumption patterns of NPP in sub-Saharan Africa can differ considerably and depend on several factors such as income and product availability. We applied ratio factors for urban and rural consumption to national sums of each component of NPP_{Demand} based on figures from the literature (Reardon 1993, Teklu 1996, Marufu *et al* 1997, Hartter and

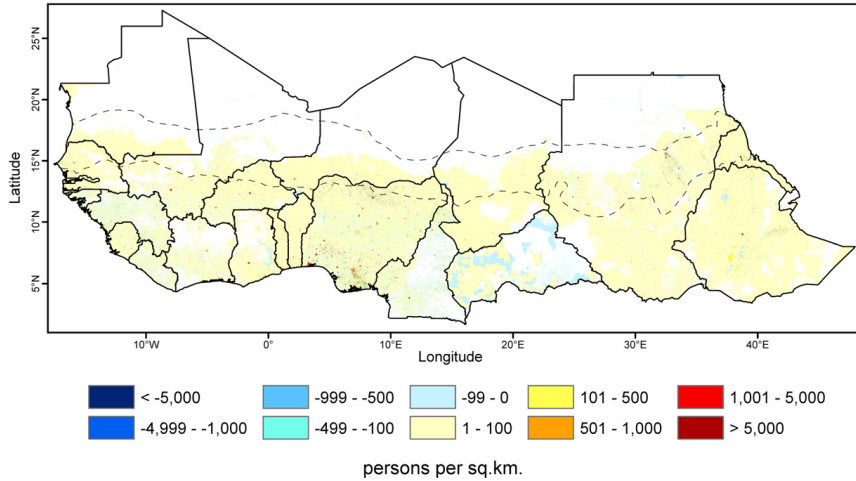


Figure 3. Difference in population density (persons per km²) between 2000 and 2010 according to WorldPop data. There is a general increase of 1–100 persons per sq. km across much of the region with large increases of up to, and greater than, 5,000 persons per sq. km in and around the major urban centers. Several countries exhibit large patches of decrease in population density, most notably in the Central African Republic. Areas with difference values of less than 1 were masked out.

Table 1. Statistically significant ($p < 0.05$) NPP_{Supply} trends based on regression slopes of ordinary least squares regression versus time (2000 and 2010).

Country	Cropland NPP	Woodland NPP	Forest NPP	Grassland/Savanna NPP	Total NPP
Benin	-0.37%	4.80%	—	8.09%	4.17%
Burkina Faso	8.68%	8.17%	—	8.47%	8.44%
Cameroon	7.57%	4.00%	-0.98%	6.86%	4.36%
Central African Republic	8.50%	5.45%	4.15%	9.87%	6.99%
Chad	14.86%	12.85%	—	17.87%	15.19%
Djibouti	—	—	—	10.78%	10.78%
Eritrea	16.14%	10.05%	—	10.69%	12.29%
Ethiopia	1.87%	5.13%	-1.28%	5.32%	2.76%
Gambia	9.47%	—	—	10.37%	9.92%
Ghana	1.17%	12.42%	-0.84%	8.27%	5.26%
Guinea	1.94%	3.48%	-2.00%	4.59%	2.00%
Guinea Bissau	4.35%	14.18%	—	19.87%	12.80%
Ivory Coast	-1.93%	1.17%	-1.80%	14.83%	3.07%
Liberia	-1.84%	—	-1.97%	—	-1.90%
Mali	12.53%	9.96%	—	9.05%	10.51%
Mauritania	17.54%	19.26%	—	12.39%	16.40%
Niger	-6.70%	-20.82%	—	-6.97%	-11.50%
Nigeria	3.36%	-5.08%	-0.16%	4.01	0.53%
Senegal	16.36%	17.84%	—	14.44%	16.21%
Sierra Leone	0.61%	2.62%	-1.47%	—	0.59%
Sudan	11.74%	5.36%	—	9.48%	8.86%
Togo	0.53%	5.46%	—	9.70%	5.23%

Boston 2008) and national household consumption surveys (ISTEEBU 2001, Maziya-Dixon *et al* 2004, Tafere and Worku 2012, GSS 2008, Food Security Technical Secretariat 2010, NSO 2012). Grids of urban and rural consumption were then merged to produce a single grid of NPP_{Demand} for each year.

3. Results

3.1. NPP supply

Mean total NPP_{Supply} based on 2000–2010 MODIS data is 2.41 PgC with an inter-annual variability of approximately 0.04 PgC (1.7%). The dry Sahelian zone exhibited high

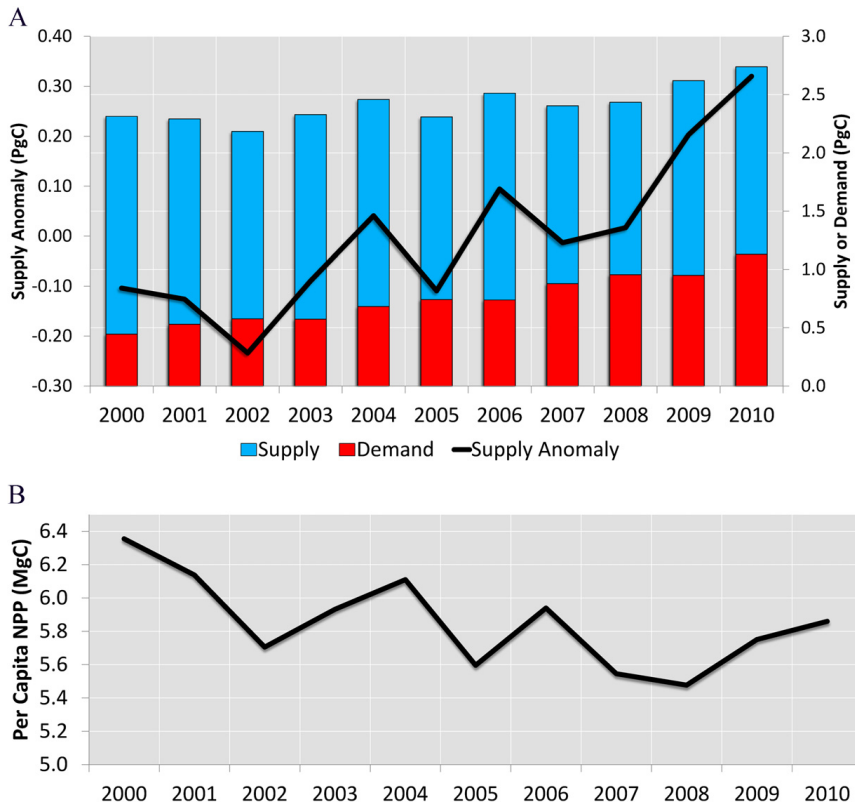


Figure 4. (A) Total NPP_{Supply} , NPP_{Demand} , and NPP_{Supply} anomalies in the study area between 2000 and 2010. NPP_{Supply} anomalies were computed as differences of NPP_{Supply} from annual mean using the 11-year record. (B) Per capita NPP from 2000 to 2010. The total amount of NPP that is available to the region's population experienced abrupt declines in 2002 and 2005 (see section 3.1).

coefficients of variation values in south-central Mauritania, northeast Mali, central Chad and around the Khartoum metropolitan area in Sudan (red colors in figure 2(A)). The years 2002 and 2005 had the lowest total regional NPP_{Supply} values with anomalies of -0.23 and -0.11 PgC, respectively (figure 4(A)). The trend in NPP_{Supply} between 2000 and 2010 for each of the 22 countries is given in table 1. There were significant ($p < 0.05$) region-wide increases in the NPP_{Supply} of cropland (+6.0%), woodland (+6.1%) and grassland/savanna (+9.4%) and a decrease in forest NPP_{Supply} (-0.7%). NPP_{Supply} in individual countries varied considerably; some such as Niger demonstrated large NPP_{Supply} decreases in cropland (-6.7%), woodland (-20.8%) and grassland/savanna (-6.9%), while others such as Senegal had relatively substantial increases in the NPP_{Supply} of cropland (+16.3%), woodland (+17.8%) and grassland/savanna (+14.4%) (figure 2(B)). In 2002, the total region-wide NPP_{Supply} dropped -9.7% below the decadal average due to droughts in

Ethiopia, Eritrea, parts of Sudan, Senegal, Mali and Mauritania.

3.2. Population density

Between 2000 and 2010 the population of the region grew from 367 million to 471 million at an average rate of 2.8% per year, and is projected to increase to nearly one billion by 2050 (United Nations 2011). The increase was highest in Eritrea (43.2%) and lowest in Central African Republic (18.9%). Most of the growth took place around and between existing settlements, creating networks that link different urban centers (figure 3).

3.3. NPP demand

The total regional NPP_{Demand} between 2000 and 2010 ranged from 0.44 PgC to 1.13 PgC, representing between 19% and 41%, respectively, of NPP_{Supply} (figure 4(A)). Overall,

Table 2. Variability in the demand for food, fuel, feed and total demand between 2000 and 2010. Food includes crop- and meat-derived products; fuel is the household energy requirement in the form of woodfuel and charcoal; feed is the amount of NPP required to sustain the region's livestock population. Total demand includes the above as well as crop residues and burnt biomass. Total population refers to the percent change in a country's aggregated population (i.e. total persons) between 2000 and 2010 according to the WorldPop data.

Country	Food	Fuel	Feed	Total demand	Total population
Benin	9.81%	2.68%	12.79%	8.61%	35.78%
Burkina Faso	34.43%	27.03%	22.03%	28.04%	33.96%
Cameroon	34.27%	12.32%	-2.63%	24.84%	25.01%
Central African Republic	13.92%	11.11%	21.85%	18.92%	18.88%
Chad	16.76%	13.62%	18.57%	19.88%	36.55%
Djibouti	-1.49%	5.92%	-3.63%	-1.24%	19.03%
Eritrea	19.62%	-23.16%	1.72%	1.37%	21.45%
Ethiopia	39.59%	9.67%	28.64%	27.22%	43.24%
Gambia	18.04%	9.06%	14.09%	18.19%	26.49%
Ghana	19.93%	19.42%	18.62%	20.57%	33.23%
Guinea	14.81%	5.06%	29.16%	17.70%	27.27%
Guinea Bissau	9.13%	4.66%	10.54%	9.66%	19.63%
Ivory Coast	2.14%	4.26%	13.32%	2.07%	22.08%
Liberia	2.65%	20.81%	23.18%	12.93%	40.29%
Mali	38.77%	7.45%	26.02%	31.34%	36.08%
Mauritania	13.52%	14.54%	5.03%	6.73%	30.91%
Niger	46.03%	-44.03%	22.37%	28.41%	42.03%
Nigeria	11.67%	6.68%	13.22%	11.42%	28.08%
Senegal	17.78%	4.76%	8.60%	12.30%	30.80%
Sierra Leone	54.34%	2.15%	48.50%	25.41%	41.64%
Sudan	18.35%	13.50%	14.44%	15.07%	27.39%
Togo	14.50%	-7.64%	21.14%	11.01%	25.74%

NPP_{Demand} increased 22% between 2000 and 2010 with the highest increase being for food (20.4%) followed by feed (16.7%) and fuel (5.5%) (table 2). We found large decreases in demand for woodfuel in the Sahelian countries of Eritrea (-23.1%) and Niger (-44%), which could be the result of initiatives promoting alternative fuels such as liquefied petroleum gas (LPG), provision of efficient cookstoves, and rural fuelwood markets aimed at sustainable forest management (Foley 1997, Habtetsion and Tsighe 2007, Rives *et al* 2013). Per capita NPP dropped in 2002 and 2005 (figure 4(B)) due to shortages in NPP_{Supply} caused by climatic variability (see section 4). The difference in NPP_{Demand} between 2000 and 2010 (figure 5(A)) generally followed the difference in population with the areas in and around urban centers displaying the highest values. However, significant trends in percent NPP_{Demand} relative to NPP_{Supply} (figure 5(B)) were confined mostly to the south of the Sahelian zone. Sizeable parts of the study area have experienced large increases (>200%) of percent NPP_{Demand}.

4. Discussion

At the present time around 41% of Sahelian NPP_{Supply} is consumed by humans. The low regional inter-annual variability of NPP, at 1.7%, is representative of the global trend over the past 35 years (Running 2012) suggesting that the supply of NPP is at a near constant level. On the other hand, both population and NPP_{Demand} are increasing at

similar annual rates of 2.8% and 2.2%, respectively. This supply-demand relationship is sensitive to systemic shocks such as droughts or pest invasions that might lower the regional NPP_{Supply}. For example, there were two years, 2002 and 2005, that exhibited large negative NPP_{Supply} anomalies. The year 2002 was marked with a severe drought in Ethiopia and parts of Sudan that caused food and water deficit to over 12 million people (Balogun *et al* 2013) as well as localized food shortages in West Africa. In 2004, the largest desert locust (*Schistocerca gregaria*) invasion in 17 years, resulting from heavy rains the preceding year that created ideal breeding conditions, reduced the regional NPP_{Supply} until the 2005 growing season (Ceccato *et al* 2006). These incidents illustrate the vulnerability of the regional NPP_{Supply} to fluctuations in climate that can lead to declines in the availability of NPP for human consumption.

The spatial pattern of significant trends in the NPP_{Supply} of the four land cover groupings that source food, fuel and feed to the region exhibited non-uniform patterns (figure 2(B)): cropland exhibited modest increases just south of the 600 mm rainfall isohyet; woodland exhibited increases that were mostly confined to the Central African Republic (CAR); grassland/savanna displayed no change in the Sahelian zone but increases south of the 600 mm rainfall isohyet, particularly in CAR, southern Chad and Sudan; forest displayed decreases everywhere except in CAR.

The overall increase in the demand for NPP_{Fuel} (table 2) generally triggers more fuelwood extraction unless there is a

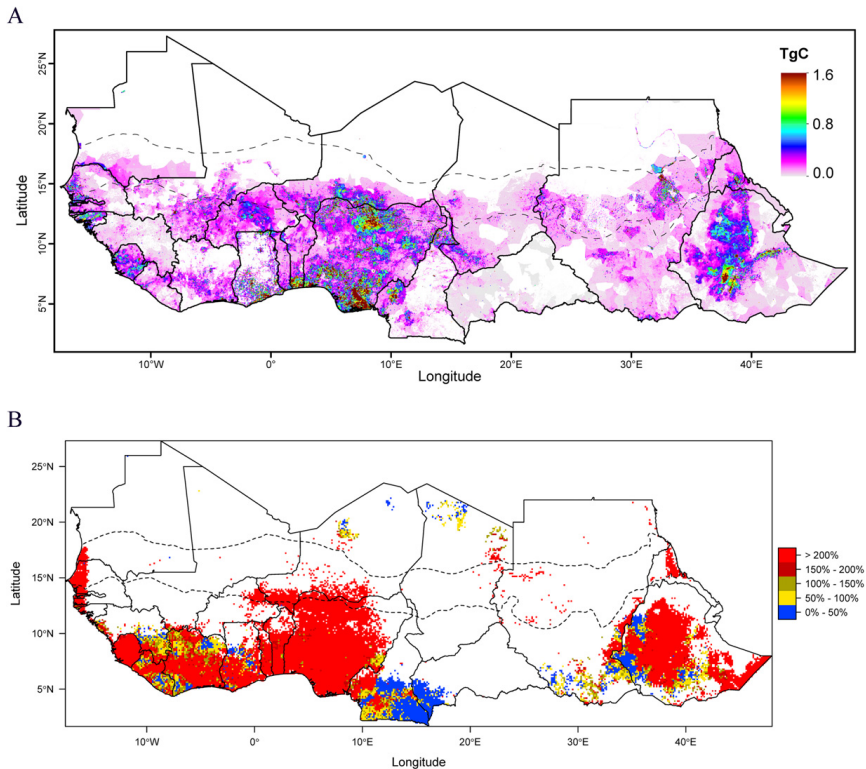


Figure 5. (A) Difference in NPP_{Demand} over the region between 2000 and 2010 in areas that exhibited changes in population density of greater than one person per km^2 during the same time frame. (B) Percent of NPP_{Demand} relative to NPP_{Supply} between 2000–2010. Only areas with a statistical significance of $p < 0.05$ are shown here. Large areas, most notably in West Africa and Ethiopia, experience NPP_{Demand} that is much larger than available supply.

major shift towards efficient cooking stoves or alternative household fuels such as LPG. For example, in Eritrea, a combination of factors, all taking place during the study period, may have contributed to the decrease in the demand for woodfuel. By the end of 2004, the country's Ministry of Energy and Mines had installed 27 000 efficient stoves in rural households through its Improved Stove Dissemination Program (Habtetsion and Tsighe 2007). An additional 10 120 stoves were planned for 2005 and 5000 stoves every year thereafter (Bode 2005, Habtetsion and Tsighe 2007), though statistics about the implementation of those plans are not available. Additionally, the Eritrean government had invested heavily in promotion of LPG as an alternative household energy source to the extent that LPG became cheaper than woodfuels for the purposes of cooking (Habtetsion and Tsighe 2007).

This paper revealed that the Sahelian NPP supply and demand nexus is driven by the geographic distribution of population density and climatic variability, and projections

for the future are alarming. A combination of increasing temperatures and changes in the precipitation regime will likely decrease the NPP_{Supply} of important crops in the region as well as increase the prevalence of pest infestations (IPCC 2014). Forecasts of Sahelian rainfall for the next four decades are inconsistent (Ben Mohamed 2011), and the best-case scenarios predict that the region will receive more rainfall, which should cause an increase in NPP_{Supply} . However, the impact of higher temperatures may counteract this effect, producing a net reduction in NPP_{Supply} across the region (Delire *et al* 2008). Similarly, forecasts of reduced crop yields of up to -41% due to increased temperature have been consistent across various studies despite projected increases in rainfall (Jones and Thornton 2003, Wolfram and David 2010, Sultan *et al* 2013). These factors point to a complex system in a delicate balance between human requirement on the one hand, and the ecosystem's capacity to satisfy it on the other.

4.1. Uncertainties and limitations

Uncertainties in the estimates of NPP_{Supply} stem from MOD17's implementation of water stress control through atmospheric VPD. Mu et al (2007) demonstrated that VPD underestimates water stress and overestimates NPP_{Supply} in Sahelian conditions. Pan et al (2006) have shown that correcting for soil water content improves MOD17 NPP estimates. Another source of uncertainty in NPP_{Supply} stems from the static biome-specific values of the maximum light use efficiency (ϵ_{max} , see section 2.2) that MODIS implements, which have been found to be considerably lower than field estimated values (Sjöström et al 2013).

We acknowledge the limitations presented by using data from FAOSTAT, which is sometimes challenged either due to shortage of resources to perform meticulous surveys or over-/under-reporting of national statistics by certain countries (Krausmann et al 2008). Despite these shortcomings, FAOSTAT represents the only available, widely used, resource that compiles, cross-checks and standardizes global agricultural data (Goudriaan et al 2001, Ciaia et al 2005, Ramankutty et al 2008, Ma et al 2012). We, therefore, consider it acceptable for the purposes of this study.

A drawback to employing annual land cover groupings to represent exploitable resources is the complete dependence on the MODIS Land Cover Type Product. Although the latest version of the product (Collection 5.1) has undergone several refinements and possesses an overall accuracy of 75% (Friedl et al 2010), the amount of training data from the Sahel that the algorithm employs is considerably small ($n=58$) and for one class (woody savanna) it is as low as a single site.

5. Conclusion

In this paper, we quantified the spatiotemporal variation of supply of NPP in relation to anthropogenic demand for a portion of sub-Saharan Africa using a combination of satellite remote sensing and socioeconomic data. We identified region-wide spatial patterns of annual NPP extraction to derive food, fuel and feed from the available supply.

This research adds to a series of studies on Sahelian vegetation dynamics with a focus on the relationship between anthropogenic exploitation and supply of NPP. The combination of rapidly increasing demand for food, fuel and feed driven by population growth makes the region vulnerable to climatic changes that may alter the per capita availability of NPP. Additionally, the region's location in a geographic transition zone between the arid Sahara desert and the high NPP Sudano-Guinean zone increases its sensitivity to fluctuations in rainfall. Investigating inter-annual variations of NPP supply and demand could help explain patterns of ecosystem change by identifying areas under anthropogenic pressure. Considering the current 2.2% annual increase in NPP_{Demand} , there is a risk that ecosystems may not be able to provide food, fuel and feed for the region's humans and livestock without a corresponding increase in NPP_{Supply} . If future droughts occur at similar climatic magnitudes as the

ones that took place in the 1970s and 1980s the Sahel will be at risk of mega famines.

The integrated analysis of the supply and demand of NPP allows the identification of areas where demand for carbon exceeds available supply, either presently or in future scenarios. Hence, the methodology presented in this paper can be applied to other human-environment systems where the supply-demand balance of NPP approaches critical levels.

Acknowledgments

Funding for this study was provided by the Swedish National Space Board (Rymdstyrelsen), contract no. 100/11. The authors sincerely thank the anonymous referees for their helpful comments that have improved the paper.

References

- Aune J B, Berthe A and Doumbia M 2005 Conservation agriculture as an approach to agricultural development in dryland areas of Mali *Sustainable Agriculture Systems for the Drylands* ed G Omanyia and D Pasternak (Niamey, Niger: International Crops Research Institute for the Semi-Arid Tropics) p 239
- Baisden WT 2006 Agricultural and forest productivity for modelling policy scenarios: Evaluating approaches for New Zealand greenhouse gas mitigation *J. R. Soc. N. Z.* **36** 1–15
- Balogun O, Yusuf S and Ayantoye K 2013 The threats of climate change: implication for food crisis in sub-sahara Africa *Sustainable Food Security in the Era of Local and Global Environmental Change* ed M Behnassi, O Pollmann and G Kissinger (Dordrecht: Springer) pp 85–98
- Barrett CB 2013 *Food Security and Sociopolitical Stability* (New York: Oxford University Press)
- Ben Mohamed A. 2011 Climate change risks in Sahelian Africa *Reg. Environ. Change* **11** 109–17
- Bode S 2005 Tenders: an option for developing countries to support renewable energies under the CDM *Clim. Policy* **5** 221–8
- Cassidy ES et al 2013 Redefining agricultural yields: from tonnes to people nourished per hectare *Environ. Res. Lett.* **8** 034015
- Ceccato P et al 2006 The desert locust upsurge in West Africa (2003–2005): information on the desert locust early warning system and the prospects for seasonal climate forecasting *Int. J. Pest Manage.* **53** 7–13
- Chianu J N, Tsujii H and Awange J 2006 Environmental impact of agricultural production practices in the savannas of northern Nigeria *J. Food Agric. Environ.* **4** 255–60
- Ciaia P et al 2005 Europe-wide reduction in primary productivity caused by the heat and drought in 2003 *Nature* **437** 529–33
- CIESIN et al 2011 *Global Rural-Urban Mapping Project, Version 1 (GRUMPv1): Urban Extents Grid, Palisades* (New York: NASA Socioeconomic Data and Applications Center (SEDAC))
- Delire C, Ngomanda A and Jolly D. 2008 Possible impacts of 21st century climate on vegetation in central and West Africa *Glob. Planet. Change* **64** 3–15
- FAOSTAT 2013 *FAO Statistical Databases* (Rome: FAO)
- Field C B, Campbell J E and Lobell D B 2008 Biomass energy: the scale of the potential resource *Trends Ecol. Evol.* **23** 65–72
- Foley G 1997 *The Niger Household Energy Project: Promoting Rural Fuelwood Markets and Village Management of Natural Woodlands* (Washington, DC: World Bank)

- Food Security Technical Secretariat 2010 *Food and Nutrition Security Assessment in Sudan: Analysis of the 2009 Baseline Household Survey* (Khartoum, Sudan: Ministry of Agriculture)
- Friedl MA et al 2010 MODIS Collection 5 global land cover: algorithm refinements and characterization of new datasets *Remote Sens. Environ.* **114** 168–82
- Gollin D 2009 Agriculture as an engine of growth and poverty reduction: what we know and what we need to know *A Framework paper for the African Economic Research Consortium Project on 'Understanding Links between Growth and Poverty Reduction in Africa'* (Nairobi, Kenya: African Economic Research Consortium)
- Gonzalez P, Tucker C and Sy H 2012 Tree density and species decline in the African Sahel attributable to climate *J. Arid Environ.* **78** 55–64
- Goudriaan J, Groot J J R and Uithol P W J 2001 Productivity of Agro-ecosystems ed J Roy, B Saugier and H A mooney *Terrestrial Global Productivity* (San Diego, CA: Academic) pp 301–13
- GSS 2008 Report of the fifth round *Ghana Living Standards Survey* (Accra, Ghana: Ghana Statistical Service)
- Habtetsion S and Tsighe Z 2007 Energy sector reform in eritrea: initiatives and implications *J. Cleaner Prod.* **15** 178–89
- Hartter J and Boston K 2008 Consuming fuel and fuelling consumption: modelling human calorific demands and fuelwood use *Small-scale Forestry* **7** 1–15
- Hassan R, Hertzler G and Benhin J K A 2009 Depletion of forest resources in Sudan: intervention options for optimal control *Energy Policy* **37** 1195–203
- Heinsch FA et al 2003 GPP and NPP (MOD17A2/A3) products NASA MODIS land algorithm *MOD17 User's Guide* 1–57
- Hiernaux P et al 1999 Effects of livestock grazing on physical and chemical properties of sandy soils in Sahelian rangelands *J. Arid Environ.* **41** 231–45
- Ibrahim F N 1988 Causes of the famine among the rural population of the Sahelian zone of the Sudan *GeoJournal* **17** 133–41
- IPCC 2014 *Final draft on impacts, adaptation and vulnerability. contribution of working group II to the fifth assessment report of the intergovernmental panel on climate change* (Cambridge: Cambridge University Press)
- ISTEEBU 2001 Enquête prioritaire 1998 *Etude Nationale sur les Conditions de Vie des Populations* (Bujumbura, Burundi: Institut de la Statistique et des Etudes Economiques)
- Jones P G and Thornton P K 2003 The potential impacts of climate change on maize production in Africa and Latin America in 2055 *Glob. Environ. Change* **13** 51–9
- Krausmann F et al 2008 Global patterns of socioeconomic biomass flows in the year 2000: a comprehensive assessment of supply, consumption and constraints *Ecol. Econ.* **65** 471–87
- Leff B, Ramankutty N and Foley J A 2004 Geographic distribution of major crops across the world *Glob. Biogeochem. Cycles* **18** GB1009
- Leriche H et al 2001 Which functional processes control the short-term effect of grazing on net primary production in grasslands? *Oecologia* **129** 114–24
- Linard C, Gilbert M and Tatem A 2011 Assessing the use of global land cover data for guiding large area population distribution modelling *GeoJournal* **76** 525–38
- Ma T, Zhou C and Pei T 2012 Simulating and estimating temporal patterns in global human appropriation of net primary production (HANPP): a consumption-based approach *Ecol. Indicators* **23** 660–7
- Marufu L et al 1997 Domestic biomass burning in rural and urban Zimbabwe—part A *Biomass Bioenergy* **12** 53–68
- Maziya-Dixon B et al 2004 *Nigeria food Consumption and Nutrition Survey, 2001–2003: Summary* (Ibadan, Nigeria: International Institute of Tropical Agriculture)
- Monteith J L 1972 Solar radiation and productivity in tropical ecosystems *J. Appl. Ecol.* **9** 747–66
- Mu Q et al 2007 Evaluating water stress controls on primary production in biogeochemical and remote sensing based models *J. Geophys. Res.* **112** G01012
- NSO 2012 Malawi integrated household survey *Household Socioeconomic Characteristics Report* (Zomba, Malawi: National Statistical Office)
- Pan Y et al 2006 Improved estimates of net primary productivity from MODIS satellite data at regional and local scales *Ecol. Appl.* **16** 125–32
- Pires M 2003 The spatial polarization of woodfuel supply and demand in senegal *Afr. Geogr. Rev.* **22** 29–47
- Popkin B M 1999 Urbanization, lifestyle changes and the nutrition transition *World Dev.* **27** 1905–16
- Ramankutty N et al 2008 Farming the planet: 1. geographic distribution of global agricultural lands in the year 2000 *Glob. Biogeochem. Cycles* **22** GB1003
- Reardon T 1993 Cereals demand in the Sahel and potential impacts of regional cereals protection *World Dev.* **21** 17–35
- Rives F, Peltier R and Montagne P 2013 Fifteen years of forest community management in niger: from a technician's dream to social reality *Small-scale Forestry* **12** 87–105
- Running S W 2012 A measurable planetary boundary for the biosphere *Science* **337** 1458–9
- Running S W et al 2004 A continuous satellite-derived measure of global terrestrial primary production *BioScience* **54** 547–60
- Samaké O et al 2005 Effects of cultivation practices on spatial variation of soil fertility and millet yields in the Sahel of Mali *Agric. Ecosyst. Environ.* **109** 335–45
- Schlesinger W H 1997 *Biogeochemistry: An Analysis of Global Change* (New York: Academic)
- Sen A 1983 *Poverty and Famines: An Essay on Entitlement and Deprivation* (Oxford: Oxford University Press)
- Sjöström M et al 2013 Evaluation of MODIS gross primary productivity for Africa using eddy covariance data *Remote Sens. Environ.* **131** 275–86
- Sop T K and Oldeland J 2011 Local perceptions of woody vegetation dynamics in the context of a 'greening Sahel': a case study from Burkina Faso *Land Degradation Dev.* **24** 511–27
- Sultan B et al 2013 Assessing climate change impacts on sorghum and millet yields in the Sudanian and Sahelian savannas of West Africa *Environ. Res. Lett.* **8** 014040
- Tafere K and Worku I 2012 *Consumption Patterns of Livestock Products in Ethiopia: Elasticity Estimates Using HICES (2004/05) Data* (Washington, DC: International Food Policy Research Institute)
- Tao F et al 2005 Remote sensing of crop production in China by production efficiency models: models comparisons, estimates and uncertainties *Ecol. Modelling* **183** 385–96
- Tatem A J et al 2007 High resolution population maps for low income nations: combining land cover and census in East Africa *PLoS ONE* **2** e1298
- Teklu T 1996 Food demand studies in sub-saharan Africa: a survey of empirical evidence *Food Policy* **21** 479–96
- Thornton PK et al 2008 Climate change and poverty in Africa: mapping hotspots of vulnerability *Afr. J. Agric. Resour. Econ.* **2** 24–44
- United Nations 2011 World population prospects: the 2010 revision *Highlights and Advanced Tables. Working paper No. ESA/P/WP.220* (Department of Economic and Social Affairs) (New York: United Nations)
- United Nations 2013 *Sahel Regional Strategy Mid-Year Review 2013* (Office for the Coordination of Humanitarian Affairs)
- UNSTAT 2014 *Population and Vital Statistics Report* (New York: United Nations)
- USDA 1994 *Major World Crop Areas and Climatic Profiles* (Washington, DC: United States Department of Agriculture)
- van der Plas R J and Abdel-Hamid M A 2005 Can the woodfuel supply in sub-saharan Africa be sustainable? The case of N'Djaména, Chad *Energy Policy* **33** 297–306

- Vargas RR *et al* 2009 Land degradation assessment and recommendation for a monitoring framework in Somaliland *FAO-SWALIM Technical Report L-14* (Nairobi, Kenya)
- Vrieling A, de Leeuw J and Said M. 2013 Length of growing period over Africa: variability and trends from 30 years of NDVI time series *Remote Sens.* **5** 982–1000
- Wezel A. 2005 Decline of woody species in the Sahel *African Biodiversity* (New York: Springer) pp 415–21
- Wolfram S and David B L 2010 Robust negative impacts of climate change on african agriculture *Environ. Res. Lett.* **5** 014010
- Zhao M *et al* 2005 Improvements of the MODIS terrestrial gross and net primary production global data set *Remote Sens. Environ.* **95** 164–76
- Zhao M and Running S W 2010 Drought-induced reduction in global terrestrial net primary production from 2000 through 2009 *Science* **329** 940–3

SUPPLEMENTARY INFORMATION

Table 1S: Original IGBP classification and land cover groupings.

Class	IGBP Class	Merged Class
1	Evergreen Needleleaf forest	Forest
2	Evergreen Broadleaf forest	
3	Deciduous Needleleaf forest	
4	Deciduous Broadleaf forest	
5	Mixed forest	
6	Closed shrublands	Woodland
7	Open shrublands	
8	Woody savannas	
9	Savannas	Grassland/Savanna
10	Grasslands	
11	Permanent wetlands	Not Included
12	Croplands	Cropland
14	Cropland/Natural vegetation mosaic	
13	Urban and built-up	Not Included
15	Snow and ice	
16	Barren or sparsely vegetated	
255	Fill Value/Unclassified	

Table 2S: Conversion rates of products derived from food-producing animals.

Type	Dry Matter Intake (Kg)	Reference
Beef	6.5	Bradford (1999)
Camel	12	Eltahir et al. (2011)
Eggs	4	Haberl et al. (2007)
Milk, whole	1.5	Hutjens (2005)
Mutton/Goat	6.3	Karim et al. (2002)
Pigmeat	8.5	Wirsenius (2000)
Chicken	5.5	"

Table 3S: Dry matter and carbon content of the 27 types of crops selected for inclusion into the consumption module.

Crop	Dry Matter Content (%)	Carbon Content (%)	Reference
Bananas	35	45	IIASA/FAO (2012)
Barley	88	47	Pradhan et al. (2013)
Beans, dry	90	47	“
Cassava	38	44	“
Cereals, other	85	47	“
Dates	15	45	“
Fruits	15	45	Goudriaan et al. (2001)
Grapes	15	45	Pradhan et al. (2013)
Groundnuts	95	60	IIASA/FAO (2012)
Maize	85	49	Goudriaan et al. (2001)
Millet	88	48	“
Onions, dry	15	45	Pradhan et al. (2013)
Oranges	15	45	“
Plantains	35	45	“
Potatoes	25	44	Goudriaan et al. (2001)
Pulses	90	47	“
Rice	88	48	“
Roots and tubers	30	44	Pradhan et al. (2013)
Sorghum	88	48	Goudriaan et al. (2001)
Soybeans	92	52	“
Sugar beet	21	44	“
Sugar cane	27	48	“
Sweet potatoes	30	44	IIASA/FAO (2012)
Tomatoes	15	45	Pradhan et al. (2013)
Vegetables	13	46	Goudriaan et al. (2001)
Wheat	87	47	IIASA/FAO (2012)
Yams	35	44	Pradhan et al. (2013)

Table 4S: Conversion factors for each livestock type to its equivalent tropical livestock unit and the annual amount of dry matter feed each type requires for maintenance.

Animal Type	Tropical Livestock Unit Equivalent	Annual Dry Matter Requirement (Kg)	Reference
Camels	1.0	2372	Houerou and Hoste (1977); Jahnke (1982); FAOSTAT (2013)
Cattle	0.70	1660	“
Chickens	0.01	23.72	“
Goats	0.10	237	“
Pigs	0.20	474	“
Sheep	0.10	237	“

Table 5S: Harvest factors for the selected crops.

Crop	Harvest Factor	Reference
Bananas	2.50	Wirsenius (2000); Haberl et al. (2007)
Barley	1.20	“
Cassava	0.80	“
Cereals, other	2.30	“
Dates	2.50	“
Fruits	2.50	“
Grapes	2.50	“
Groundnuts	1.50	“
Maize	3.50	“
Millet	3.50	“
Oranges	2.50	“
Plantains	2.50	“
Potatoes	1.00	“
Pulses	0.40	“
Rice	1.50	“
Roots and tubers	1.00	“
Sorghum	3.50	“
Soybeans	1.50	“
Sugar beet	0.70	“
Sugar cane	0.50	“
Sweet potatoes	1.00	“
Wheat	2.30	“
Yams	1.00	“

REFERENCES

- Bradford GE. (1999) Contributions of animal agriculture to meeting global human food demand. *Livestock Production Science* 59: 95-112.
- Eltahir IE, Mohamed AM, El Khidir OA, et al. (2011) Feedlot performance and carcass characteristics of Sudan dromedary camels (*Camelus dromedarius*) fed on molasses and sorghum grain based diets. *Journal of Camelid Science* 4: 70-78.
- FAOSTAT. (2013) FAO Statistical Databases. Rome: Food and Agriculture Organization of the United Nations
- Goudriaan J, Groot JJR and Uithol PWJ. (2001) Productivity of Agro-ecosystems. In: Roy J, Saugier B and Mooney HA (eds) *Terrestrial Global Productivity*. San Diego: Academic Press, 301-313.
- Haberl H, Erb KH, Krausmann F, et al. (2007) Quantifying and mapping the human appropriation of net primary production in earth's terrestrial ecosystems. *Proceedings of the National Academy of Sciences* 104: 12942-12947.
- Houerou HNL and Hoste CH. (1977) Rangeland Production and Annual Rainfall Relations in the Mediterranean Basin and in the African Sahelo-Sudanian Zone. *Journal of Range Management* 30: 181-189.
- Hutjens MF. (2005) Dairy Efficiency and Dry Matter Intake. *Proceedings of the 7th Western Dairy Management Conference*. Reno, Nevada. .
- IIASA/FAO. (2012) Global Agro-ecological Zones (GAEZ v3.0). IIASA, Laxenburg, Austria and FAO, Rome, Italy. .
- Jahnke HE. (1982) *Livestock production systems and livestock development in tropical Africa*, Kiel, Germany: Kieler Wissenschaftsverlag Vauk Kiel.
- Karim SA, Santra A and Verma DL. (2002) Growth, feed conversion efficiency and carcass characteristics of Malpura and Malpura× Awassi crossbred lambs in a hot semi arid environment. *Asian-australasian journal of animal sciences* 15: 377-381.
- Pradhan P, K. B. Lüdeke M, E. Reusser D, et al. (2013) Embodied crop calories in animal products. *Environmental Research Letters* 8: 044044.
- Wirsenius S. (2000) Human use of land and organic materials: modeling the turnover of biomass in the global food system. *Department of Physical Resource Theory*. Göteborg, Sweden: Chalmers University of Technology.

Paper II

The El Niño – La Niña cycle and recent trends in supply and demand of net primary productivity in African drylands

A. M. Abdi¹ · A. Vrieling² · G. T. Yengoh³ ·
A. Anyamba⁴ · J. W. Seaquist¹ · C. C. Ummenhofer⁵ ·
J. Ardö¹

Received: 1 January 2016 / Accepted: 21 June 2016
© Springer Science+Business Media Dordrecht 2016

Abstract Inter-annual climatic variability over a large portion of sub-Saharan Africa is under the influence of the El Niño-Southern Oscillation (ENSO). Extreme variability in climate is a threat to rural livelihoods in sub-Saharan Africa, yet the role of ENSO in the balance between supply and demand of net primary productivity (NPP) over this region is unclear. Here, we analyze the impact of ENSO on this balance in a spatially explicit framework using gridded population data from the WorldPop project, satellite-derived data on NPP supply, and statistical data from the United Nations. Our analyses demonstrate that between 2000 and 2013 fluctuations in the supply of NPP associated with moderate ENSO events average $\pm 2.8 \text{ g C m}^{-2} \text{ yr}^{-1}$ across sub-Saharan drylands. The greatest sensitivity is in arid Southern Africa where a $+1 \text{ }^\circ\text{C}$ change in the Niño-3.4 sea surface temperature index is associated with a mean change in NPP supply of $-6.6 \text{ g C m}^{-2} \text{ yr}^{-1}$. Concurrently, the population-driven trend in NPP demand averages $3.5 \text{ g C m}^{-2} \text{ yr}^{-1}$ over the entire region with densely populated urban areas exhibiting the highest mean demand for NPP. Our findings highlight the importance of accounting for the role ENSO

Electronic supplementary material The online version of this article (doi:10.1007/s10584-016-1730-1) contains supplementary material, which is available to authorized users.

✉ A. M. Abdi
hakim.abdi@gmail.com

- ¹ Department of Physical Geography and Ecosystem Science, Lund University, Sölvegatan 12, 22362 Lund, Sweden
- ² Faculty of Geo-information Science and Earth Observation, University of Twente, P.O. Box 217, 7500 AE Enschede, The Netherlands
- ³ Lund University Center for Sustainability Studies, 22362 Lund, Sweden
- ⁴ Goddard Space Flight Center, Biospheric Sciences Laboratory, National Aeronautics and Space Administration, Greenbelt, MD, USA
- ⁵ Department of Physical Oceanography, Woods Hole Oceanographic Institution, Woods Hole, MA, USA

plays in modulating the balance between supply and demand of NPP in sub-Saharan drylands. An important implication of these findings is that increase in NPP demand for socio-economic metabolism must be taken into account within the context of climate-modulated supply.

Keywords Sub-Saharan Africa · Drylands · El Niño-southern oscillation · Net primary productivity · Climate variability

1 Introduction

Drylands cover more than half of sub-Saharan Africa and are characterized by a combination of low rainfall and high potential evapotranspiration that leads to low levels of soil moisture and net primary productivity (NPP) (Nicholson 2011). In these regions, climatic variability is one of the most acute and widespread threats to the agro-pastoral systems that are inhabited by 60 % of the population (IPCC 2014). Most of sub-Saharan Africa has one rainy season (East Africa has two) that is modulated by large-scale ocean-atmosphere teleconnections. The largest of these, the El Niño-Southern Oscillation (ENSO), has been identified as a dominant factor that regulates inter-annual photosynthetic activity in global drylands (Ahlström et al. 2015). The two extreme phases of ENSO, El Niño and La Niña, represent positive and negative departures, respectively, from long term mean sea surface temperatures in the central and eastern equatorial Pacific Ocean. El Niño generally brings dry conditions to parts of the Sahel and most of Southern Africa, and wet conditions to Eastern Africa, while La Niña is associated with approximately opposite conditions (Giannini et al. 2008). These dry or wet conditions are exacerbated in severe El Niño or La Niña events, causing droughts or floods that reduce the amount of NPP in a given area. The most recent example of the impact of a severe El Niño is the 2015/16 drought in Southern Africa, where the October 2015 – March 2016 rainfall was 75 % below the 1982–2011 average (FEWSNET 2016). The 2011/12 famine in the Horn of Africa exemplifies a confluence of risk factors, such as political instability, armed conflict and inaccessibility, exacerbated by La Niña. The strong La Niña of 2010/11 (Supplementary Fig. 2) induced the failure of both the short rains in late 2010 and the long rains in mid-2011, causing collapses in both agricultural production and the associated labor market in Somalia (Maxwell and Fitzpatrick 2012).

NPP supplies the annual provision of crops, animal feed and pasture, and adds to annual increments of woody biomass (Running 2012). The societal implications of reduced NPP can be severe and could lead to crop failure and eventual food insecurity (Battisti and Naylor 2009). Sub-Saharan Africa has experienced a steep increase in demand for NPP in the twentieth century, which is likely to continue rising as a function of population growth and per capita consumption (Fetzel et al. 2016). Furthermore, recent studies predict an 11.7 % decrease in the productivity of major sub-Saharan crops (wheat, maize, sorghum and millet) by the 2050s (Knox et al. 2012), expansion of drylands, particularly in the Sahel, East and Southern Africa (Greve et al. 2014), and an increased frequency of severe ENSO events (Cai et al. 2015). Thus, the effects of extreme climatic variability could have drastic impacts on NPP supply and intensified by the need to keep pace with an increasing population (Campbell et al. 2014).

Here, we adopt the concepts of “supply” and “demand” to demonstrate the linkage between ecosystem productivity, human livelihood, and inter-annual climatic variability in sub-Saharan drylands. As demand for food, feed and fuel drives land use change, the proportion of NPP

required by humans relative to its supply (demand-supply ratio, DSR) could serve as an integrative benchmark of human dependence on ecosystems. We focus on ENSO and investigate its role in the balance between supply and demand of NPP in sub-Saharan drylands using a spatially explicit framework. We focus on the time period between 2000 and 2013 for NPP supply and 2000–2011 for NPP demand and DSR. The shorter time period for NPP demand and DSR is due to the fact that data on domestic supply quantities for several items, such as crops and woodfuel, were limited to 2011 at the time of writing. Our specific aims are to (1) quantify trends in NPP supply and demand in sub-Saharan drylands for 2000–2011; (2) map the spatial variability of NPP and DSR anomalies during ENSO years for 2000–2011; (3) assess the relationship between ENSO and NPP supply for 2000–2013.

2 Data and methods

2.1 Derivation of NPP supply

The estimation of NPP supply was performed using the light use efficiency approach as defined in Monteith (1972) and applied in the MOD17 algorithm of the moderate-resolution imaging spectroradiometer (MODIS) sensor on board the Terra and Aqua satellites:

$$NPP_{\text{Supply}} = (PAR * FPAR * \varepsilon_{\text{max}} * VPD * T_{\text{min}}) - Ra \quad (1)$$

where NPP_{Supply} is the NPP available in the ecosystem regardless of land use type in grams of carbon per meter square per year ($\text{g C m}^{-2} \text{ yr}^{-1}$); PAR is incoming photosynthetically active radiation in megajoules per meter square per year ($\text{MJ m}^{-2} \text{ yr}^{-1}$); FPAR is the fraction of incident PAR absorbed by the vegetation canopy; ε_{max} represents maximum light use efficiency, in grams of carbon per megajoule of PAR (g C MJ^{-1}), under hypothetical biome-specific ideal conditions; VPD and T_{min} are simple linear ramp functions of vapor pressure deficit and minimum temperature, respectively, which constrain maximum light use efficiency; Ra (autotrophic respiration) represents the amount of carbon respired, in $\text{g C m}^{-2} \text{ yr}^{-1}$, during maintenance and growth respiration of leaves, fine roots and woody tissue. Further descriptions of the MOD17 algorithm are detailed in Zhao et al. (2011) and the dataset is available from the NASA Earth Observation System repository at the University of Montana (<http://www.ntsg.umt.edu/project/mod17>). NPP supply estimates were restricted to sub-Saharan Africa's arid, semi-arid and dry sub-humid areas (Supplementary Fig. 1).

2.2 Niño-3.4 index and standardized anomalies

We used the Niño-3.4 sea surface temperature index as a representation of ENSO. To differentiate between positive, negative and neutral ENSO years, we applied the threshold set by the National Oceanic and Atmospheric Administration. Accordingly, an ENSO year is characterized by a minimum of five consecutive 3-month running mean of the Extended Reconstructed Sea Surface Temperature version 3b (ERSST.v3b) anomalies in the Niño 3.4 region based on a threshold of ± 0.5 °C (Supplementary Fig. 2). The base period for computing the anomalies in ERSST.v3b is 1971–2000. To visualize differences in NPP between the three ENSO phases (El Niño, La Niña, Neutral), standardized anomalies (Z-scores) were calculated for

NPP supply and DSR using Eqs. 2–4. The ENSO cycle begins around July, peaks in December – February (of the following year), starts to decay in March – April, and enters the post-phase in May – June (Philippon et al. 2014). The monthly NPP supply anomalies reflect this July to June cycle and were summed to annual values spanning two calendar years (1999/00, 2000/01, 2001/02, etc.). However, the data used to compute NPP demand are provided in single calendar years (2000, 2001, 2002, etc.). Therefore, DSR anomalies correspond to the years in the second half of the ENSO cycle to account for the lagged effect of the peak and decay phases of ENSO.

$$Z_{El_Ni\ o} = \sum_{t=1999/00}^{2010/11} \frac{OBS_{NPP,t} - MN_{NPP,t}}{SD_{NPP,t}}, \text{ if } Nino3.4_t \geq +0.5 \tag{2}$$

$$Z_{La_Nia} = \sum_{t=1999/00}^{2010/11} \frac{OBS_{NPP,t} - MN_{NPP,t}}{SD_{NPP,t}}, \text{ if } Nino3.4_t \leq -0.5 \tag{3}$$

$$Z_{Neutral} = \sum_{t=1999/00}^{2010/11} \frac{OBS_{NPP,t} - MN_{NPP,t}}{SD_{NPP,t}}, \text{ if } -0.5 < Nino3.4_t < +0.5 \tag{4}$$

where, $OBS_{NPP,t}$, $MN_{NPP,t}$, $SD_{NPP,t}$ are the observed, mean, and standard deviation, respectively, of NPP supply, demand or DSR at time t .

2.3 Derivation of NPP demand

We define the term “consumption” as the actual amount of NPP extracted from the ecosystem as reported in the statistical database of the Food and Agriculture Organization of the United Nations (FAOSTAT, <http://faostat3.fao.org/>). The term “demand” is defined as the annual amount of NPP required by the sub-Saharan dryland population. Building on earlier work (Abdi et al. 2014), we developed a framework based on FAOSTAT to calculate demand for NPP (Supplementary Fig. 3). We downloaded data from 2000 to 2011 for the components of NPP demand for each country from the food balance sheets provided by FAOSTAT. However, contrary to Abdi et al. (2014), who used the total primary crop production of each country, we used domestic supply quantities to account NPP supply for domestic utilization.

The first component of NPP demand is domestically consumed food (NPP_{food}). This category includes twenty-seven types of regionally important primary crops, which represent 95 % of all those that are domestically consumed by most of the countries in the study area (Supplementary Table 2) (FAOSTAT 2015). Additionally, meats sourced from six types of domestic animals (cattle, goats, sheep, pigs, camels, poultry) and two non-meat animal products (eggs and milk) (Supplementary Table 1) were also included.

$$NPP_{food} = \left[\left(\sum_{p=1}^{27} P_{p,y} + I_{p,y} - E_{p,y} + S_{p,y} \right) \times D_{p,y} \times C_{p,y} \right] + \left[\left(\sum_{a=1}^7 M_{a,y} \right) \times K_{a,y} \times 0.45 \right] \tag{5}$$

where, P , I and E are produced, imported and exported quantities of crop type p , in year y ; S is the variation (positive or negative) in the stocks of crop type p , in year y ; D and C are the crop-

specific dry matter and carbon conversion coefficients, respectively; M is the wet carcass weight (i.e. without internal organs) of animal type a , in year y , and K is the dry matter intake required to produce that weight, in year y . We converted crop tonnage to carbon units using the conversion factors provided in Supplementary Tables 1 and 2.

Livestock are assets in sub-Saharan Africa. Pastoralists and agro-pastoralists depend on livestock for nutritional value and economic growth. NPP_{feed} represents the total amount of animal feed required to sustain the livestock population of the region.

$$NPP_{feed} = \left(\sum_{a=1}^6 T_{a,y} \right) \times R_{a,y} \times 0.45 \tag{6}$$

where, T is the Tropical Livestock Unit (TLU) for livestock type a , in year y ; R is the annual dry matter requirement as provided in Supplementary Table 3. A ratio of 0.45 was used to convert dry matter into carbon.

Crop residues ($NPP_{residues}$) refer to the parts of the crop that are left over in a field after harvest. Thus, they are not part of the crop yield (i.e. edible seeds, roots, fruits, leaves, or stalks) and vary according to crop type.

$$NPP_{residues} = \sum_{p=1}^{23} H_{p,y} \times 0.45 \tag{7}$$

where, H is the residue factor (proportion of non-yield contributing crop phytomass) of crop type p , in year y . The residue factors applied in Eq. 7 are detailed in Supplementary Table 4.

In most parts of the sub-Saharan Africa household energy demand is met by woodfuels comprising fuel wood and wood charcoal (NPP_{fuel}) extracted from the region’s dry woodlands. The demand for woodfuels across sub-Saharan Africa is variable and ranges from 55 % in Senegal (Pires 2003) to over 91 % in Malawi (Zulu 2010), but on average it is approximately 80 % across the study area.

$$NPP_{fuel} = \left(\sum W_{NC,y} \times 0.58 \times 0.45 \right) + \left(\sum W_{CN,y} \times 0.43 \times 0.45 \right) + \left(\sum W_{CH,y} \times 0.75 \right) \tag{8}$$

where, NC , CN and CH represent non-coniferous, coniferous and wood charcoal. Dry matter conversion ratios of 0.58 and 0.43 were applied to the non-coniferous and coniferous fuel wood, respectively, and a ratio of 0.45 to convert dry matter into carbon (Supplementary Table 5). Wood charcoal was directly converted to carbon content by applying a ratio of 0.75 (Supplementary Table 5).

Landscape fires, both natural and anthropogenic, play an important role in sub-Saharan dryland ecosystems. One of the anthropogenic applications of burning in sub-Saharan Africa is to expand cropland area (Andela and van der Werf 2014). Consequently, the amount of NPP lost to support human demand for food is taken into account. NPP_{burned} represents domestic human-driven NPP loss resulting from burning of both forest and savanna resources.

$$NPP_{burned} = \sum B_y \times 0.45 \tag{9}$$

where, B is the total amount of dry matter burnt in year y . The data are presented as dry matter content, therefore a ratio of 0.45 was used to convert dry matter into carbon.

We did not assume a homogeneous per capita consumption within each country due to variations in diet, lifestyle and wealth between urban and rural populations in sub-Saharan Africa. Rather, we applied ratio factors for urban and rural consumption to national sums of each group of products based on statistics from peer-reviewed literature and national household consumption surveys (Supplementary Table 6).

$$NPP_{demand_urban} = \overbrace{NPP_{food} + NPP_{feed} + NPP_{residues} + NPP_{fuel} + NPP_{burned}}^{Urban} \quad (10)$$

$$NPP_{demand_rural} = \overbrace{NPP_{food} + NPP_{feed} + NPP_{residues} + NPP_{fuel} + NPP_{burned}}^{Rural} \quad (11)$$

$$NPP_{demand} = NPP_{demand_urban} + NPP_{demand_rural} \quad (12)$$

We derived per capita NPP consumption by dividing rural and urban consumption values by each country's rural and urban population. Grids of urban and rural consumption were then merged to produce a single map of total per capita consumption. We used gridded population data from the WorldPop project (<http://www.worldpop.org.uk/>) (Linard et al. 2012), which came in three time slices: 2000, 2005, 2010. We interpolated between these time slices using growth rates from the United Nations Population Division (<http://esa.un.org/unpd/wpp/>) and added an extra year, 2011, to coincide with the FAOSTAT data. We then used the gridded population data as a spatial surrogate to disaggregate per capita demand to grid cells for each year between 2000 and 2011. The years 2012 and 2013 were not included because domestic supply data on food, feed and fuel from FAOSTAT were limited to 2011 at the time of writing. We distinguished urban and rural areas by masking urban extent on the WorldPop grids based on the "Artificial Areas" category in the European Space Agency's GlobCover 2009 land cover map (<https://doi.pangaea.de/10.1594/PANGAEA.787668>).

2.4 Statistical analysis

We tested the data (NPP supply, NPP demand) for temporal autocorrelation before identifying the presence or absence of trends because significant first order autocorrelation can inflate trend significance, leading to a Type I error. A two-sided Mann-Kendall trend test was then applied to evaluate the significance of monotonic trends in the supply and demand of NPP (Mann 1945). The null hypothesis is that our supply or demand data are independent and randomly ordered; the alternative hypothesis is that the data possess a monotonic trend in one or more years in the time series. To account for non-normal distributions of the supply and demand of NPP, the nonparametric Theil-Sen estimate of slope was used to measure the magnitude of the linear trend (Wilcox 2012). The null hypothesis is rejected if the test statistic is different from zero at the 5 % level. Mean (μ) trends in supply and demand of NPP were calculated to facilitate comparison between different areas across the continent. To quantify the lagged response of NPP to ENSO forcing, we applied a lagged ordinary least squares regression to monthly NPP and Niño 3.4 index time series. This was done by shifting the time series one month at each lag to a maximum of 12 months over the July – June ENSO lifecycle. For the resultant monthly lags, we combined all significant pixels ($P < 0.05$) using

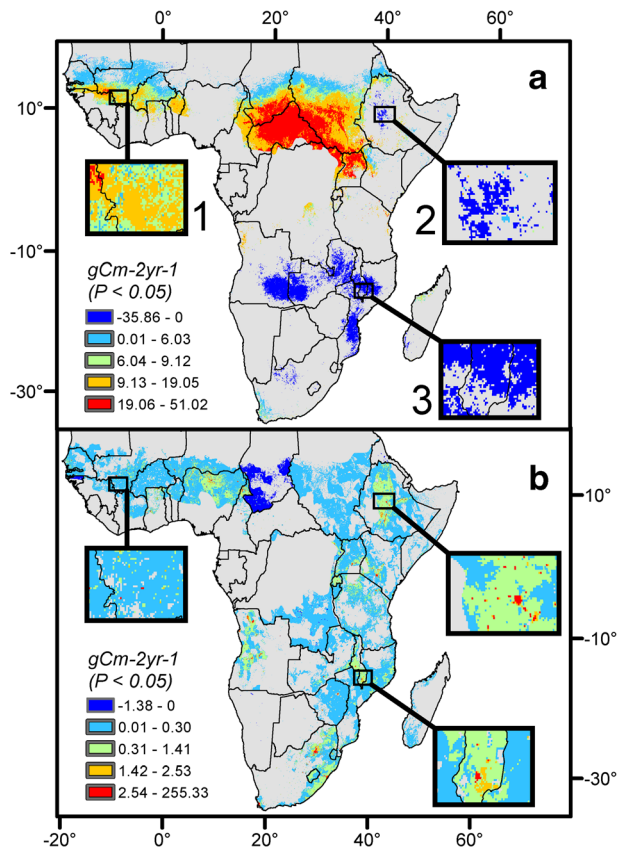
absolute maximum value compositing (i.e. the highest absolute value is retained for each pixel location). We then partitioned the final image according to the GlobCover 2009 land cover types. Pearson's product-moment correlation was used to quantify the strength of the linear relationship between cropland NPP and FAOSTAT crop production data between 2000 and 2013.

3 Results and discussion

3.1 Trends of NPP supply and demand

The linear trends of NPP supply and demand are presented in Fig. 1. NPP supply trends over 2000–2013 are significant in 32 % of the area (4.7 million km²). However, the trends are concentrated in three distinct areas: the western Sahel ($\mu = 2 \text{ g C m}^{-2} \text{ yr}^{-1}$, $P < 0.05$), central Africa ($\mu = 30 \text{ g C m}^{-2} \text{ yr}^{-1}$, $P < 0.05$) and parts of Zambia, Malawi and Mozambique ($\mu = -25 \text{ g C m}^{-2} \text{ yr}^{-1}$, $P < 0.05$) (Fig. 1a). By contrast, trends of NPP demand over 2000–2011 are significant in 48 % of the area and roughly evenly distributed (Fig. 1b). The mean overall trend of NPP demand is $3.5 \text{ g C m}^{-2} \text{ yr}^{-1}$, though in urban areas it averages approximately $50 \text{ g C m}^{-2} \text{ yr}^{-1}$. The tradeoffs between NPP supply and demand trends (i.e. change in one quantity relative to another) are locally constrained and linked to the

Fig. 1 Linear trends in NPP supply (2000–2013) and demand (2000–2011). NPP supply (a) and NPP demand (b). Detail showing pixel-level supply and demand trends for different urban and rural areas in sub-Saharan Africa: (1) the agricultural region of Sikasso in southern Mali, (2) the Addis Ababa metropolitan area, and (3) southern Malawi within the vicinity of the city of Blantyre. Since the units of NPP supply are generally denoted as quantity per unit area per unit time, and demand generally represents NPP required by the inhabitants in each pixel, we divided each NPP demand pixel in **b** by its area to facilitate comparability. Grey areas indicate both statistically insignificant ($P > 0.05$) and areas outside the study region



prevailing climate, population growth and net migration. For instance, in the region of Sikasso in southern Mali, the trend of NPP supply averages $10 \text{ g C m}^{-2} \text{ yr}^{-1}$ (Fig. 1a-1) and that of demand is $1 \text{ g C m}^{-2} \text{ yr}^{-1}$ (Fig. 1b-1). This region is agriculturally productive and exhibits positive NPP supply anomalies during La Niña (Fig. 2b). The low trend in NPP demand is surprising because the population of Sikasso grew 3.9 % a year between 2000 and 2011 (FAO 2013). This paradox of high land productivity, rapid population growth and low demand for NPP could be a sign that the population is not consuming adequate amounts of food, feed and fuel. Indeed, Eozenou et al. (2013) found that 45 % of the population of Sikasso is classified as “food poor” (i.e. per capita consumption is below the food poverty line) and 19 % are chronically malnourished. Therefore, it is apparent that, despite favorable climatic conditions, agricultural revenues from cotton, the main export crop grown in Sikasso, are insufficient to remove a majority of the region’s population out of poverty.

In recent years, major urban areas in sub-Saharan Africa have experienced influxes of economic migrants due to increased investment in infrastructure development (Cheung et al. 2012). Perhaps the best example of this phenomenon is Addis Ababa, Ethiopia. Here, population grew by 40 % between 2000 and 2010 driven by economic migration from other parts of the country (Adugna and Hailemariam 2011; Moller 2012). Consequently, the observed average trend in demand for NPP in the Addis Ababa metropolitan area was $153 \text{ g C m}^{-2} \text{ yr}^{-1}$ for 2000–2011 (Fig. 1b-2), the highest in sub-Saharan Africa. The observed decrease in NPP supply in the vicinity of Addis Ababa over 2000–2013 (Fig. 1a-2) could be linked to the rapid growth of the city. Itannam and Olsson (2004) found that urbanization and industrialization resulting from Addis Ababa’s rapid expansion contributed to land degradation in surrounding agricultural areas. This adversely affects the livelihoods of farmers prompting further economic migration into the city (Abdissa and Degefa 2011). Several La Niña events in the latter half of the analysis period (2007/08, 2008/09, 2010/11) could have further contributed to the observed decrease in NPP supply around Addis Ababa. The impact of ENSO on seasonal rainfall in Ethiopia, and natural hazards associated with strong ENSO, particularly La Niña events, are well documented (Korecha and Sorteberg 2013). La Niña years are correlated with decreased rainfall during the February – May rainy season, potentially extending the November – January dry season through to June (Korecha and Sorteberg 2013; Reda et al. 2015). Furthermore, strong La Niña events induce intense rainfall during the main June – September rainy season, causing floods and subsequent loss in agricultural productivity (Korecha and Barnston 2007; Wolde-Georgis 2002).

In Malawi, approximately 45 % of the population lives in the southern part of the country (van Vuuren et al. 2011), where the vicinity of the country’s second-largest city, Blantyre, has experienced an overall decrease in NPP supply ($-11 \text{ g C m}^{-2} \text{ yr}^{-1}$, Fig. 1a-3) over 2000–2013 and an increase of NPP demand ($0.80 \text{ g C m}^{-2} \text{ yr}^{-1}$, Fig. 1b-3). The supply of NPP in this region is highly sensitive to ENSO events (Fig. 2a, b) with a net negative impact. This means that the negative correlation the region has with El Niño outweighs its positive correlation with La Niña (Supplementary Fig. 4). The strong El Niño of 2015/16 reduced the October 2015 – February 2016 rainy season to its lowest level since 1981 (FEWSNET 2016). This severe drought condition caused below average crop production leading to low earnings from agricultural labor and high food prices (FEWSNET 2016).

3.2 ENSO in relation to NPP supply and DSR

The standardized anomalies of NPP supply and DSR in El Niño (2002/03, 2004/05, 2006/07, 2009/10), La Niña (1999/00, 2000/01, 2005/06, 2007/08, 2008/09, 2010/11) and neutral

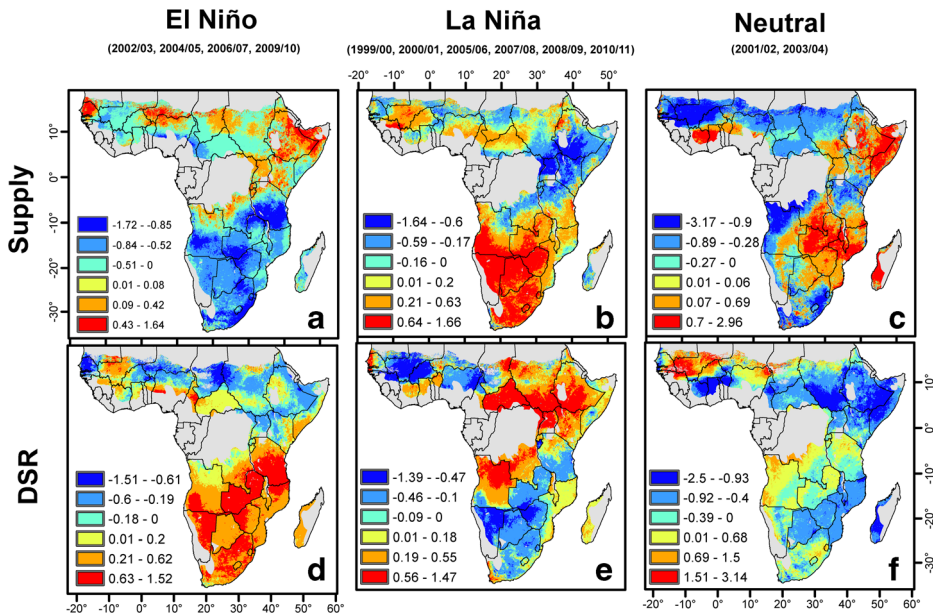


Fig. 2 Standardized anomalies (2000–2011). Standardized anomalies for NPP supply (**a, b, c**) and demand-supply ratio (**d, e, f**). Means were calculated for El Niño (**a, d**), La Niña (**b, e**) and neutral years (**c, f**). For each panel, the anomaly indicates the number of standard deviations an observation is above or below the mean. The ENSO cycle typically straddles two calendar years, beginning around July, with a peak in December – February, and begins to decay in March – April of the following year. The monthly NPP supply anomalies reflect this cycle and were summed to annual values. Since the FAOSTAT data is provided in calendar years, the DSR data reflects that nomenclature. Accordingly, DSR anomalies shown here represent the latter half of the ENSO cycle, e.g. for the ENSO-neutral years of 2001/02 and 2003/04, the corresponding DSR anomalies are the years 2002 and 2003. Grey areas are outside the study region

(2001/02, 2003/04) phases are presented in Fig. 2. Southern Africa shows the largest contiguous region of negative NPP supply anomalies during El Niño (Fig 2a), and consequently also shows the largest positive DSR anomalies (Fig 2d). Demand for NPP is coupled to population growth and consumption patterns, but it is not linked to, nor does it change with, ENSO phases. Consequently, when NPP supply is reduced by El Niño, NPP demand increases relative to it, causing positive DSR anomalies. The opposite effect can be seen during La Niña, when NPP supply anomalies in southern Africa are positive and DSR anomalies are negative. Negative NPP supply anomalies during La Niña are concentrated around equatorial East Africa resulting in positive DSR anomalies (Fig. 2b, e).

The response of NPP supply to ENSO in the Sahel, East and Southern Africa is shown in Fig. 3. The greatest sensitivity occurs in the mainly arid region of Southern Africa (Supplementary Fig. 1). Here, a + 1 °C shift in the Niño 3.4 index causes a mean change in the NPP supply of $-6.6 \text{ g C m}^{-2} \text{ yr}^{-1}$. El Niño events in Southern Africa are associated with dry conditions, while La Niña events are associated with wet conditions. Most land cover types in Southern Africa exhibit negative NPP supply values relative to changes in the Niño 3.4 index (Fig. 3). The exceptions, with either the median value or a large number of positive outliers, are the region’s forests and woodlands that are adapted to prolonged dry seasons or droughts, and possess physiological mechanisms such as extensive roots allowing efficient deep water access or are drought deciduous (i.e. the trees lose leaves to conserve water)

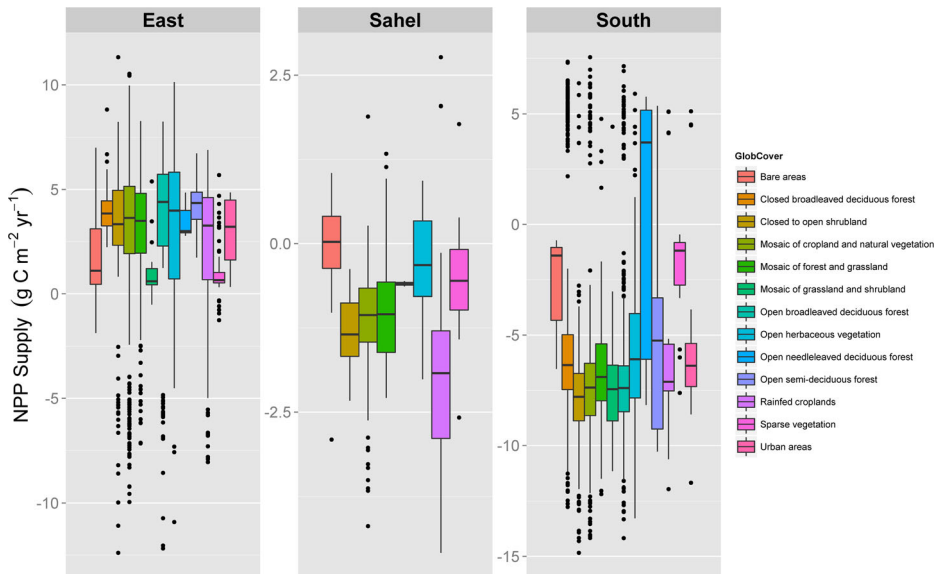


Fig. 3 Relationship between ENSO and NPP supply (2000–2013). Change in NPP supply per GlobCover land cover class relative to a +1 °C change in the Niño 3.4 index anomaly for 2000–2013 ($n = 7927$). Despite the general response of each region to change in the Niño 3.4 anomaly, the presence of a large number of outliers in certain land cover classes could mean that there are underlying physiological adaptations (e.g. water-storing and/or deep roots systems, drought deciduous, etc.) that surmount the impact of climate

(Nicholson 2011). Despite the fact that there were more La Niña events than El Niño events between 2000 and 2011, the negative impact of El Niño on Southern Africa is strong enough to tip the balance toward the negative (Supplementary Fig. 4). This sensitivity, coupled with a $1.3 \text{ g C m}^{-2} \text{ yr}^{-1}$ trend in NPP demand, increases demand relative to available supply (Fig. 4a and b). This is troubling because the difference in NPP supply in Southern Africa between El Niño and La Niña years corresponds to what is required to feed approximately 15 million people for one year (Stige et al. 2006).

3.3 Demand-supply balance of NPP in food producing regions

Food production in sub-Saharan drylands is almost entirely dependent on rain-fed agriculture (You et al. 2011). The median response of NPP supply in rain-fed croplands to a +1 °C change in the Niño 3.4 region is $-2 \text{ g C m}^{-2} \text{ yr}^{-1}$ in the Sahel, $3 \text{ g C m}^{-2} \text{ yr}^{-1}$ in East Africa, and $-7 \text{ g C m}^{-2} \text{ yr}^{-1}$ in Southern Africa (Fig. 3). Average DSR within rain-fed croplands is high ($\mu = 0.9 \pm 0.1$), with a large spatial variability (Fig. 5a). In Sahel, East and Southern Africa NPP, demand in croplands, which also includes associated villages and settlements, has been increasing at a rate of 1.35 % per year ($P < 0.001$), while supply has been marginally decreasing at a rate of 0.2 % per year ($P = 0.65$) (Fig. 5b).

These observations reinforce reports of persistent undernourishment in sub-Saharan Africa as approximately 90 % of consumption comes from domestic production (Barrett and Upton 2013). Rain-fed croplands occupy most of the agricultural landscape in sub-Saharan drylands and domestic crop production is strongly linked to cropland NPP (Supplementary Fig. 5). In sub-Saharan drylands, increases in crop production are generally achieved by expanding agricultural land through savanna burning, the spatial patterns of which are determined by the

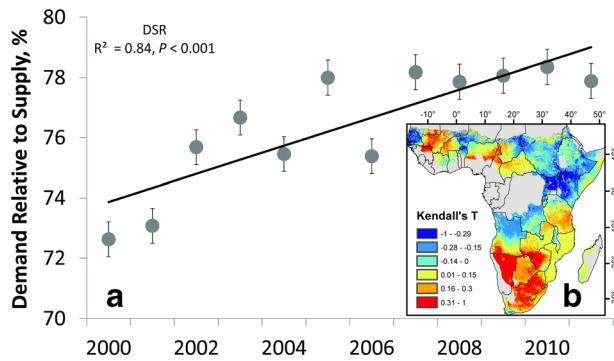


Fig. 4 Trend in DSR and its correlation with ENSO (2000–2011). **a** Annual trend of the demand-supply ratio expressed as percent across sub-Saharan drylands; **(b)** Spatial pattern of the correlation between DSR and the Niño-3.4 sea surface temperature index. A positive DSR–Niño 3.4 index correlation signifies decreasing NPP supply relative to demand as Niño 3.4 index values increase (i.e. anomalously warm conditions in the central equatorial Pacific). Negative DSR–Niño 3.4 index correlation means increasing NPP supply relative to demand as Niño 3.4 index values increase. Demand for NPP is always increasing and parallels the rate of population growth. The *error bars* represent standard error of the mean

ENSO-controlled rainfall regime (Andela and van der Werf 2014). However, despite observed increases in cropland extent in several parts of the continent, yields per unit area for major food crops remain low (Bekunda et al. 2010). Additionally, variability of crop yields in several parts of sub-Saharan Africa can be attributed to ENSO. For example, 64 % of the yield variability of maize in Zimbabwe could be accounted for by ENSO with yield predictions up to a full year before harvest (Cane et al. 1994). Considering these challenges, increasing crop yield means increasing resilience of croplands to the impact of ENSO and other stressors through accurate forecasting and improved land and water management strategies. Water management in particular is vital for crop production and is one of the most important factors required to improve livelihoods in sub-Saharan dryland agro-ecosystems (Sissoko et al. 2011).

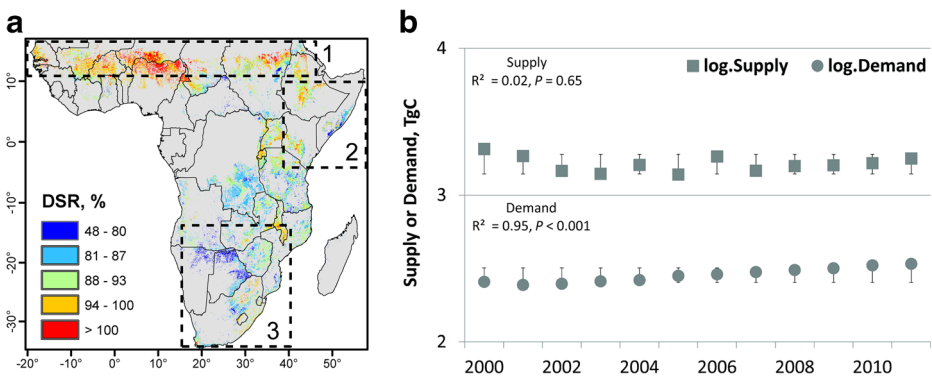


Fig. 5 NPP supply and demand trends in food-producing areas (2000–2011). **a** Spatial pattern of cropland demand-supply ratio expressed as percent. The *dashed boxes* denote the high aridity regions of the Sahel (a1), East Africa (a2) and Southern Africa (a3). See Supplementary Fig. 1 for the regional aridity map; **(b)** Mean annual trend in NPP supply and demand over cropland areas in the Sahel, East and Southern Africa. The *error bars* represent standard error of the mean

NPP supply deficiency is exacerbated in sub-Saharan drylands by large-scale, trans-national land acquisitions, whereby investors from countries rich in financial capital purchase or lease land from developing countries for the production of goods (Seaquist et al. 2014). These deals often involve projects that maximize crop yield in purchased land using expensive technologies providing crops, biofuel feedstock and wood charcoal to markets outside the region of production (Seaquist et al. 2014). The 1.3 million km² of reported deals deplete household income from agricultural production and lead to the displacement of communities (Zetland and Möller-Gulland 2013). Consequently, DSR increases as the consumable supply of NPP is reduced and local resources are depleted to satisfy demand elsewhere (Yengoh and Armah 2015). This external demand for productive land is also an important driver of land degradation and deforestation. Land is acquired to provide maximum return on investment, and thus it is often intensively managed through year-round planting, and excessive use of pesticides and inorganic fertilizers, all factors that contribute to land degradation (Robertson and Pinstrup-Andersen 2010). The negative effects of deforestation are particularly pronounced in East Africa, where 91 % of the region exhibits an increasing DSR trend ($\mu = 0.12 \pm 0.10$). Rural household energy in East Africa is largely satisfied by wood fuels with around 90 million people living in areas where demand is high and wood harvest unsustainable (Bailis et al. 2015). In countries where there is little or no government regulation the exploitation of local NPP supply to meet external demand is unrestricted. For example, demand for wood charcoal in the Persian Gulf countries drives a 1.4 % annual loss of tree cover in Somalia (Bolognesi et al. 2015).

3.4 Limitations

Although DSR provides an indicator of pressures exerted on ecosystem services at large scales, it must be used in combination with other data. This is particularly important at local scales where coarse resolution data cannot capture critical biophysical and socio-ecological processes that occur at higher resolutions. A possible limitation in our approach is the reliance on FAOSTAT data to estimate NPP demand. FAO has traditionally relied on the quality of data provided by national statistical institutions with minimal quality control. However, in recent years the agency has been taking steps through its regional offices to intensify data control and harmonize collection, processing and dissemination with various national partner agencies (FAO 2011). The quantification of human vulnerability to food insecurity is complex and metrics such as those provided by FAOSTAT have been criticized for being poor predictors (Barrett 2010). We addressed this critique by: (1) using household consumption surveys to apply appropriate ratios distinguishing between per capita urban and rural consumption for each component of NPP demand, and (2) spatially constraining these ratios to gridded population data.

4 Conclusions

In this paper we focused on the El Niño-Southern Oscillation (ENSO) and its impact on the balance between supply and demand of net primary productivity (NPP) in African drylands. Our analyses demonstrated that fluctuations in the supply of NPP associated with a + 1 °C change in the Niño 3.4 region average $-2.8 \text{ g C m}^{-2} \text{ yr}^{-1}$ and population and socioeconomic-driven trend in NPP demand averages $3.5 \text{ g C m}^{-2} \text{ yr}^{-1}$. The combination of reductions in

supply and increases in demand lead to a 7.2 % increase in the demand for NPP relative to its supply. Our findings highlight the role played by ENSO and population growth in modulating the balance between supply and demand of NPP in sub-Saharan drylands. Our findings also emphasize the importance of accounting for this balance, which has so far been overlooked in climate impact studies.

Humans rely directly on the supply of NPP through the consumption of crops and use of wood for fuel and construction, and indirectly through animal products. This reliance creates demand that drives many of the ecological changes occurring in sub-Saharan drylands. Evaluating the socio-ecological impact of ENSO and other large-scale ocean-atmosphere teleconnections through isolated disciplinary analysis provides monocular views of a complex system that requires an integrated approach. Moreover, several of the factors that influence the balance between supply and demand, such as population density and consumption patterns, are dependent on scale. Sociological data, such as surveys at the household (or even individual) level, which provide valuable information about fine-scale patterns of human-ecosystem interaction, are seldom integrated with biophysical datasets. Thus, a comprehensive, interdisciplinary approach is required to further assess the factors driving this complex balance in the wake of climate change. Only through interdisciplinary analysis involving enhanced synthesis of both biophysical and socio-ecological data can we make improved assessments of the impacts of climatic variability on human livelihood and wellbeing.

Acknowledgments We thank Dan Metcalfe, Lina Eklund, A.J. (Han) Dolman, and Katharina Waha for their insight and comments during early stages of the manuscript. We also thank the programming assistance provided by the volunteers at the *Stack Overflow* and *Cross Validated* online communities. Funding for this project was provided by the Swedish National Space Board (contract no. 100/11 to J.A.). A.M.A. received support from the Royal Physiographic Society in Lund and the Lund University Center for Studies of Carbon Cycle and Climate Interactions (LUCCI). C.C.U. was supported by NSF grant OCE-1203892.

References

- Abdi AM, Seaquist J, Tenenbaum DE, Eklundh L, Ardo J (2014) The supply and demand of net primary production in the Sahel. *Environ Res Lett* 9:094003
- Abdissa F, Degefa T (2011) Urbanization and changing livelihoods: the case of farmers' displacement in the expansion of Addis Ababa. In: Teller C (ed) *The demographic transition and development in Africa: the unique case of Ethiopia*. Springer Netherlands, Dordrecht, pp. 215–235
- Adugna A, Hailemariam A (2011) Rural–urban linkages in Ethiopia: insuring rural livelihoods and development of urban centers. In: Teller C (ed) *The demographic transition and development in Africa*. Springer, Netherlands, pp. 167–186
- Ahlström A, Raupach MR, Schurgers G, Smith B, Arnett A, Jung M, Reichstein M, Canadell JG, Friedlingstein P, Jain AK, Kato E, Poulter B, Sitch S, Stocker BD, Viouy N, Wang YP, Wiltshire A, Zaehle S, Zeng N (2015) The dominant role of semi-arid ecosystems in the trend and variability of the land CO₂ sink. *Science* 348:895–899
- Andela N, van der Werf GR (2014) Recent trends in African fires driven by cropland expansion and el Niño to La Niña transition. *Nat Clim Chang* 4:791–795
- Bailis R, Drigo R, Ghilardi A, Masera O (2015) The carbon footprint of traditional woodfuels. *Nat Clim Chang* 5:266–272
- Barrett CB (2010) Measuring food insecurity. *Science* 327:825–828
- Barrett CB, Upton JB (2013) *Food security and sociopolitical stability in sub-Saharan Africa*. Food security and sociopolitical stability. Oxford University Press, New York
- Battisti DS, Naylor RL (2009) Historical warnings of future food insecurity with unprecedented seasonal heat. *Science* 323:240–244
- Bekunda M, Sangina N, Woomeer PL (2010) Restoring soil fertility in sub-Saharan Africa. In: Donald LS (ed.) *Advances in agronomy*. Academic Press, pp. 183–236

- Bolognesi M, Vrieling A, Rembold F, Gadain H (2015) Rapid mapping and impact estimation of illegal charcoal production in southern Somalia based on WorldView-1 imagery. *Energy Sustain Dev* 25:40–49
- Cai W, Santoso A, Wang G, Yeh S-W, An S-I, Cobb KM, Collins M, Guilyardi E, Jin F-F, Kug J-S, Lengaigne M, McPhaden MJ, Takahashi K, Timmermann A, Vecchi G, Watanabe M, Wu L (2015) ENSO and greenhouse warming. *Nat Clim Chang* 5:849–859
- Campbell MM, Casterline J, Castillo F, Graves A, Hall TL, May JF, Perlman D, Potts M, Speidel JJ, Walsh J, Wehner MF, Zulu EM (2014) Population and climate change: who will the grand convergence leave behind? *The Lancet Global Health* 2:e253–e254
- Cane MA, Eshel G, Buckland RW (1994) Forecasting Zimbabwean maize yield using eastern equatorial Pacific Sea surface temperature. *Nature* 370:204–205
- Cheung Y-W, de Haan J, Qian X, Yu S (2012) China's outward direct investment in Africa. *Rev Int Econ* 20:201–220
- Eozenou PH-V, Madani D, Swinkels R (2013) Poverty, malnutrition and vulnerability in Mali. World Bank Policy Research Working Paper No. 6561. The World Bank, Washington, DC
- FAO (2011) Review of the availability and quality of official data from African commission on agricultural statistics member countries. Food and agriculture Organization of the United Nations, Addis Ababa, Ethiopia
- FAO (2013) CountrySTAT Mali. Statistics Division, Food and Agriculture Organization of the United Nations Rome, Italy
- FAOSTAT (2015) FAO statistical databases. Food and agriculture Organization of the United Nations, Rome, Italy
- Fetzel T, Niedertscheider M, Haberl H, Krausmann F, Erb K-H (2016) Patterns and changes of land use and land-use efficiency in Africa 1980–2005: an analysis based on the human appropriation of net primary production framework. *Reg Environ Change* 16:1507–1520
- FEWSNET (2016) Southern Africa: illustrating the extent and severity of the 2015–16 drought. Famine Early Warning Systems Network/USAID
- Giannini A, Biasutti M, Held IM, Sobel AH (2008) A global perspective on African climate. *Clim Chang* 90:359–383
- Greve P, Orłowski B, Mueller B, Sheffield J, Reichstein M, Seneviratne SI (2014) Global assessment of trends in wetting and drying over land. *Nat Geosci* 7:716–721
- IPCC (2014) Climate Change 2014: Impacts, Adaptation, and Vulnerability. Part B: Regional Aspects. Contribution of Working Group II to the Fifth Assessment Report of the Intergovernmental Panel on Climate Change. Cambridge, United Kingdom and New York, NY, USA
- Itannam F, Olsson M (2004) Land degradation in Addis Ababa due to industrial and urban development. *Ethiopian J Dev Res* 26:77–100
- Knox J, Hess T, Daccache A, Wheeler T (2012) Climate change impacts on crop productivity in Africa and South Asia. *Environ Res Lett* 7:034032
- Korecha D, Barnston AG (2007) Predictability of June–September rainfall in Ethiopia. *Mon Weather Rev* 135:628–650
- Korecha D, Sorteberg A (2013) Validation of operational seasonal rainfall forecast in Ethiopia. *Water Resour Res* 49:7681–7697
- Linard C, Gilbert M, Snow RW, Noor AM, Tatem AJ (2012) Population distribution, settlement patterns and accessibility across Africa in 2010. *PLoS One* 7:e31743
- Mann HB (1945) Nonparametric tests against trend. *Econometrica: Journal of the Econometric Society*:245–259
- Maxwell D, Fitzpatrick M (2012) The 2011 Somalia famine: context, causes, and complications. *Global Food Security* 1:5–12
- Moller LC (2012) The Ethiopian urban migration study 2008: the characteristics, motives and outcomes to immigrants to Addis Ababa. The World Bank, Washington, DC
- Monteith JL (1972) Solar radiation and productivity in tropical ecosystems. *J Appl Ecol* 9:747–766
- Nicholson SE (2011) Dryland climatology. Cambridge University Press
- Philippon N, Martiny N, Camberlin P, Hoffman MT, Gond V (2014) Timing and patterns of the ENSO signal in Africa over the last 30 Years: insights from normalized difference vegetation index data. *J Clim* 27:2509–2532
- Pires M (2003) The spatial polarization of woodfuel supply and demand in Senegal. *African Geographical Review* 22:29–47
- Reda DT, Engida AN, Asfaw DH, Hamdi R (2015) Analysis of precipitation based on ensembles of regional climate model simulations and observational databases over Ethiopia for the period 1989–2008. *Int J Climatol* 35:948–971
- Robertson B, Pinstrup-Andersen P (2010) Global land acquisition: neo-colonialism or development opportunity? *Food Sec* 2:271–283
- Running SW (2012) A measurable planetary boundary for the biosphere. *Science* 337:1458–1459

- Seaquist JW, Johansson EL, Nicholas KA (2014) Architecture of the global land acquisition system: applying the tools of network science to identify key vulnerabilities. *Environ Res Lett* 9:114006
- Sissoko K, van Keulen H, Verhagen J, Tekken V, Battaglini A (2011) Agriculture, livelihoods and climate change in the west African Sahel. *Reg Environ Chang* 11:119–125
- Stige LC, Stave J, Chan K-S, Ciannelli L, Pettoirelli N, Glantz M, Herren HR, Stenseth NC (2006) The effect of climate variation on agro-pastoral production in Africa. *Proc Natl Acad Sci U S A* 103:3049–3053
- van Vuuren DP, Edmonds J, Kainuma M, Riahi K, Thomson A, Hibbard K, Hurtt GC, Kram T, Krey V, Lamarque J-F, Masui T, Meinshausen M, Nakicenovic N, Smith SJ, Rose SK (2011) The representative concentration pathways: an overview. *Clim Chang* 109:5–31
- Wilcox R (2012) Chapter 10 - robust regression. *Introduction to robust estimation and hypothesis testing*, Third edn. Academic Press, Boston, pp. 471–532
- Wolde-Georgis T (ed) (2002) *The impact of cold events on Ethiopia*. United Nations University Press, New York, NY
- Yengoh G, Armah F (2015) Effects of large-scale acquisition on food insecurity in Sierra Leone. *Sustainability* 7: 9505
- You L, Ringler C, Wood-Sichra U, Robertson R, Wood S, Zhu T, Nelson G, Guo Z, Sun Y (2011) What is the irrigation potential for Africa? A combined biophysical and socioeconomic approach. *Food Policy* 36:770–782
- Zetland D, Möller-Gulland J (2013) The political economy of land and water grabs. In: Allan JA, Keulertz M, Sojamo S, Warner J (eds) *Handbook of land and water grabs in Africa: foreign direct investment and food and water security*. Routledge, New York, NY
- Zhao M, Running S, Heinsch FA, Nemani R (2011) MODIS-derived terrestrial primary production. In: Ramachandran B, Justice CO, Abrams MJ (eds) *Land remote sensing and global environmental change*. Springer, New York, pp. 635–660
- Zulu LC (2010) The forbidden fuel: charcoal, urban woodfuel demand and supply dynamics, community forest management and woodfuel policy in Malawi. *Energy Policy* 38:3717–3730

SUPPLEMENTARY INFORMATION

The El Niño – La Niña cycle and recent trends in supply and demand of net primary productivity in African drylands

A. M. Abdi ^{1,*}, A. Vrieling ², G. T. Yengoh ³, A. Anyamba ⁴, J. W. Seaquist ¹, C. C. Ummenhofer ⁵, J. Ardö ¹

¹ Department of Physical Geography and Ecosystem Science, Lund University, Sölvegatan 12, 22362 Lund, Sweden

² University of Twente, Faculty of Geo-information Science and Earth Observation, P.O. Box 217, 7500 AE Enschede, The Netherlands

³ Lund University Center for Sustainability Studies, 22362 Lund, Sweden

⁴ National Aeronautics and Space Administration, Goddard Space Flight Center, Biospheric Sciences Laboratory, Greenbelt, Maryland, United States of America

⁵ Department of Physical Oceanography, Woods Hole Oceanographic Institution, Woods Hole, Massachusetts, United States of America

* Corresponding author. E-mail: hakim.abdi@gmail.com. Tel: +46462223132. Fax: +46462220321

SUPPLEMENTARY INFORMATION

Derivation of the aridity index

For each year between 2000 and 2013 we calculated an aridity index (AI) from the ratio between annual rainfall data from the Climate Hazards Group InfraRed Precipitation with Station data (Funk et al., 2014) (<http://chg.geog.ucsb.edu/data/chirps/>) and satellite-derived potential evapotranspiration from the MOD16 project (Mu et al., 2011) (<http://www.ntsug.umt.edu/project/mod16>). Arid (ARD, $0.05 < AI < 0.20$), semi-arid (SARD, $0.20 < AI < 0.50$), and dry sub-humid (DSH, $0.50 < AI < 0.65$) areas were delineated. Altogether, drylands cover 14.7 million km² of Africa (Supplementary Fig. 1).

Disaggregation of annual NPP supply to monthly intervals

The MODIS data used are provided as monthly satellite-derived GPP (MOD17A2) and annual NPP (MOD17A3) at the same spatial resolution. We multiplied monthly GPP with the 14-year (2000 – 2013) mean NPP/GPP ratio to get an estimate of monthly NPP:

$$NPP_{monthly} = GPP_{monthly} \times \left[\frac{NPP}{GPP} \right]_{2000-2013} \quad (1)$$

To test whether our derived monthly NPP supply data were within reasonable values, we aggregated them into annual sums, and compared them against the MOD17A3 product using root mean square error (RMSE) and mean absolute error (MAE). The monthly NPP derived using this approach had mean RMSE and MAE of 32 gCm⁻²yr⁻¹ and 27 gCm⁻²yr⁻¹, respectively (Supplementary Fig. 6). Since the purpose of temporally disaggregating annual MOD17A3 data to monthly time steps was to compare it to the monthly Niño-3.4 index, we find these error estimates to be acceptable as they are lower than errors associated with other large-scale primary productivity estimates e.g. Jung et al. (2011) and Maselli et al. (2006).

SUPPLEMENTARY INFORMATION

Calculation of cropland NPP and crop production statistics

A detailed cropland mask (<ftp://mars.jrc.ec.europa.eu/Public/cropmask>) developed at the Joint Research Centre of the European Commission (Vancutsem et al., 2012) was used to quantify NPP anomalies within rain-fed croplands in sub-Saharan drylands. Compared to existing crop maps, this dataset has a larger agreement with a high-resolution validation sample in areas where cropland represents more than 30% of a pixel. Pearson's product-moment correlation exhibited a strong relationship between log-transformed cropland NPP and primary crop production between 2000 and 2013 (Pearson's $r = 0.54$, $P < 0.01$) (Supplementary Fig. 5). Only cropland found in the arid, semiarid and dry subhumid areas were considered (Supplementary Table 7).

SUPPLEMENTARY INFORMATION

Supplementary Table 1. Conversion rates of products derived from food-producing animals. A ratio of 0.45 was used to convert dry matter requirement into carbon.

Type	Dry Matter Requirement (Kg)	Reference
Beef	6.5	Bradford (1999)
Camel	12	Eltahir et al. (2011)
Eggs	4	Haberl et al. (2007)
Milk, whole	1.5	Hutjens (2005)
Mutton/Goat	6.3	Karim et al. (2002)
Pigmeat	8.5	Wirsenius (2000)
Poultry	5.5	"

SUPPLEMENTARY INFORMATION

Supplementary Table 2. Dry matter and carbon content of the 27 types of crops selected for inclusion into the consumption module.

Crop	Dry Matter Content (%)	Carbon Content (%)	Reference
Bananas	35	45	IIASA/FAO (2012)
Barley	88	47	Pradhan et al. (2013)
Beans, dry	90	47	“
Cassava	38	44	“
Cereals, other	85	47	“
Dates	15	45	“
Fruits	15	45	Goudriaan et al. (2001)
Grapes	15	45	Pradhan et al. (2013)
Groundnuts	95	60	IIASA/FAO (2012)
Maize	85	49	Goudriaan et al. (2001)
Millet	88	48	“
Onions, dry	15	45	Pradhan et al. (2013)
Oranges	15	45	“
Plantains	35	45	“
Potatoes	25	44	Goudriaan et al. (2001)
Pulses	90	47	“
Rice	88	48	“
Roots/tubers	30	44	Pradhan et al. (2013)
Sorghum	88	48	Goudriaan et al. (2001)
Soybeans	92	52	“
Sugar beet	21	44	“
Sugar cane	27	48	“
Sweet potatoes	30	44	IIASA/FAO (2012)
Tomatoes	15	45	Pradhan et al. (2013)
Vegetables	13	46	Goudriaan et al. (2001)
Wheat	87	47	IIASA/FAO (2012)
Yams	35	44	Pradhan et al. (2013)

SUPPLEMENTARY INFORMATION

Supplementary Table 3. Conversion factors derived from FAOSTAT (2015); Houerou and Hoste (1977); Jahnke (1982). For each livestock type to its equivalent tropical livestock unit and the annual amount of dry matter feed each type requires for maintenance.

Livestock Type	Tropical Livestock Unit Equivalent	Annual Dry Matter Requirement (Kg)
Camels	1.00	2372
Cattle	0.70	1660
Chickens	0.01	23.72
Goats	0.10	237
Pigs	0.20	474
Sheep	0.10	237

SUPPLEMENTARY INFORMATION

Supplementary Table 4. Residue factors for selected crops derived using data from Haberl et al. (2007) and Wirsenius (2000). Residue factors are the proportion of total crop phytomass that does not contribute to the crop yield. The inverse of the residue factor is the harvest index.

Crop	Residue Factor
Bananas	0.45
Barley	0.65
Cassava	0.80
Cereals, other	0.60
Dates	0.85
Fruits	0.85
Grapes	0.85
Groundnuts	0.60
Maize	0.78
Millet	0.80
Oranges	0.85
Plantains	0.45
Potatoes	0.50
Pulses	0.40
Rice	0.60
Roots and tubers	0.50
Sorghum	0.78
Soybeans	0.60
Sugar beet	0.70
Sugar cane	0.40
Sweet potatoes	0.50
Wheat	0.70
Yams	0.50

SUPPLEMENTARY INFORMATION

Supplementary Table 5. Conversion factors for different types of woodfuels. FAOSTAT provides non-coniferous and coniferous fuel wood in cubic meters, while wood charcoal is given in tonnes of dry matter.

Wood fuel Type	Conversion Type	Conversion Factor	Reference
Non-coniferous fuel wood	m ³ → dry matter	0.58	Brown (1997), Penman et al. (2003)
Coniferous fuel wood	m ³ → dry matter	0.43	Brown (1997), Penman et al. (2003)
Wood charcoal	dry matter → carbon	0.75	Girard (2002)

SUPPLEMENTARY INFORMATION

Supplementary Table 6. Sources of the ratio factors for urban and rural consumption of the components of NPP demand.

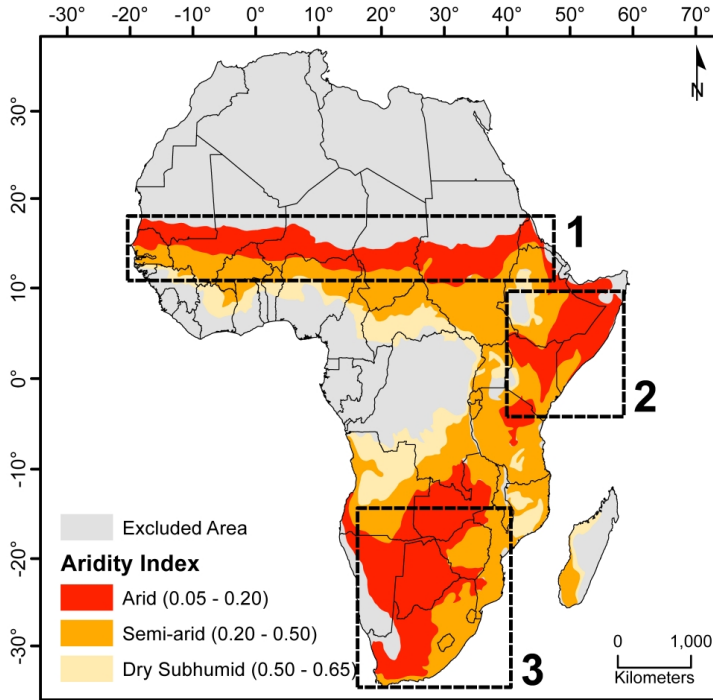
Urban/Rural Consumption	Reference
Peer-reviewed Literature	Hartter and Boston (2008), Marufu et al. (1997), Reardon (1993), Teklu (1996)
National Household Consumption Surveys	
Burundi	INSEE (2001)
Ethiopia	Tafere and Worku (2012)
Ghana	Ghana Statistical Service (2008)
Malawi	NSO (2012)
Nigeria	Maziya-Dixon et al. (2004)
Sudan	Food Security Technical Secretariat (2010)
Zambia	CSO (2012)

SUPPLEMENTARY INFORMATION

Supplementary Table 7. Annual dry cropland NPP and FAOSTAT crop production for 2000 – 2013 in the descending order of cropland area. Annual NPP was extracted from croplands within arid, semi-arid and dry subhumid zones.

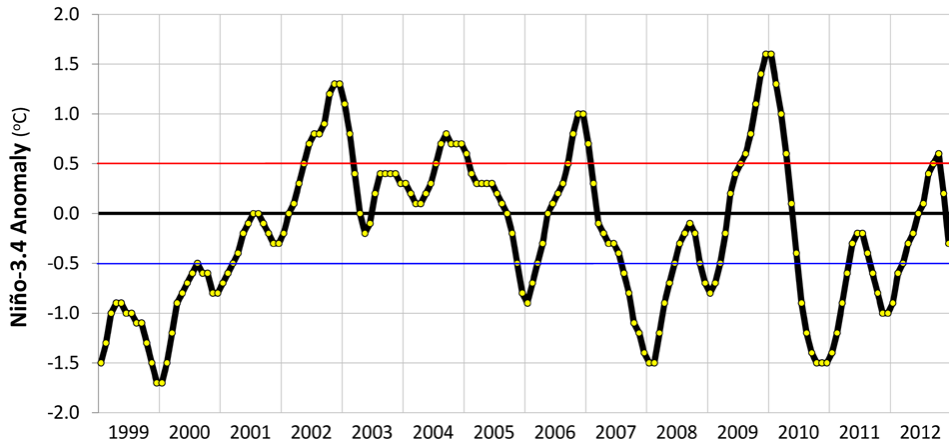
Country	Dry Cropland NPP, (TgC)	Crop Production, (Mt)	Dry Cropland area, (km²)
Congo, DRC	250	49	305,755
Tanzania	210	58	288,980
Sudan	44	45	286,990
Nigeria	28	340	190,815
Ethiopia	116	76	185,481
Zambia	115	14	161,100
South Africa	100	117	158,365
Mali	18	21	146,057
Niger	8	21	128,857
Chad	18	11	124,077
Mozambique	82	29	115,060
Burkina Faso	16	19	111,952
Zimbabwe	57	12	111,441
Botswana	39	0	105,597
Angola	64	31	90,359
Uganda	96	55	87,863
Kenya	63	39	85,870
Malawi	36	30	57,776
Somalia	11	3	56,633
Senegal	9	10	42,616
Namibia	16	1	39,378
Cameroon	7	36	37,942
Ghana	10	57	32,735
Ivory Coast	10	34	21,263
Burundi	18	10	19,580
Rwanda	17	17	17,312
Eritrea	1	1	16,559
Guinea	4	17	16,473
Central African Republic	7	4	14,818
Benin	3	19	14,685
Lesotho	3	1	7,037
Gambia	1	1	5,385
Togo	1	8	5,031
Swaziland	5	6	4,727
Guinea Bissau	1	2	4,506

SUPPLEMENTARY INFORMATION



Supplementary Fig. 1. Aridity zones delineated from the ratio between annual rainfall and potential evapotranspiration. The boxes represent the three main high-aridity regions of the Sahel (1), East Africa (2) and Southern Africa (3).

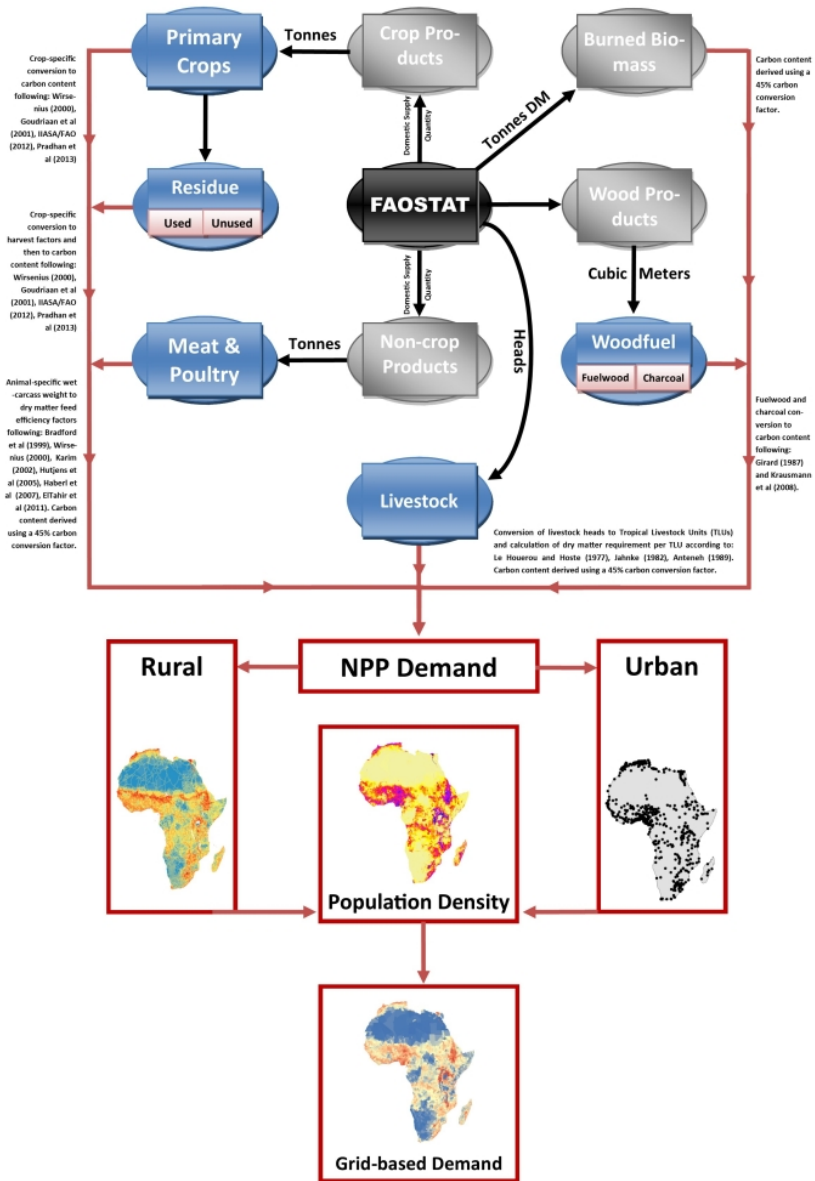
SUPPLEMENTARY INFORMATION



Supplementary Fig. 2. Classification of ENSO years according to the NOAA the specification of a minimum of five consecutive 3-month running mean of the Extended Reconstructed Sea Surface Temperature version 3b (ERSST.v3b) anomalies in the Niño 3.4 region based on a threshold of $\pm 0.5^{\circ}\text{C}$. Red and blue lines denote El Niño and La Niña thresholds, respectively. Each yellow dot symbolizes a 3-month running mean. Note that, though included in the analysis, the 2005-2006 and 2008-2009 La Niña events were comparatively weak and short-lived, thus some definitions may not characterize them as an ENSO events. In both years negative sea surface temperature (SST) anomalies across the central and east-central equatorial Pacific Ocean met the threshold of -0.5°C for exactly five consecutive 3-month periods (October-November-December to February-March-April).

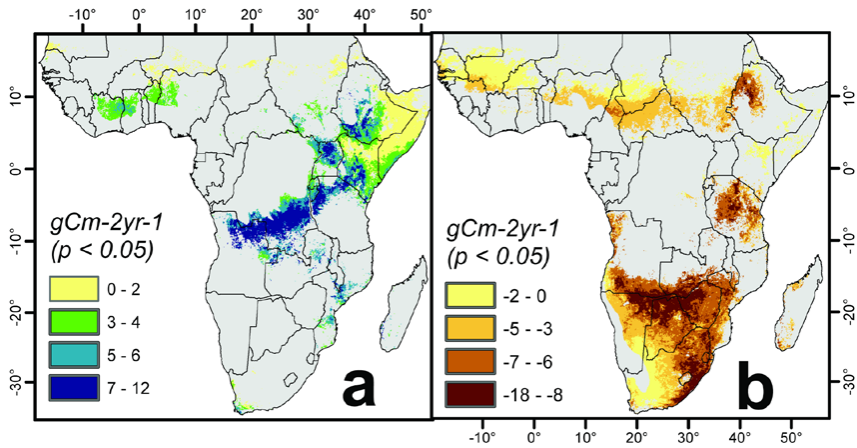
Data source: http://www.cpc.ncep.noaa.gov/products/analysis_monitoring/ensostuff/ensoyears_ERSSTv3b.shtml

SUPPLEMENTARY INFORMATION

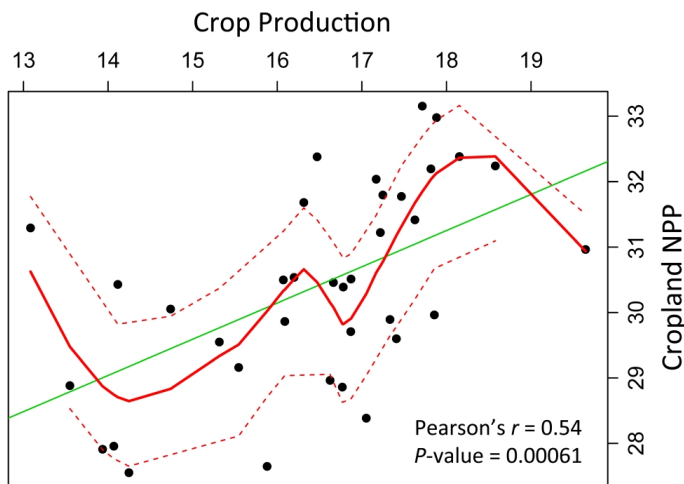


Supplementary Fig. 3. A visual representation of the framework for estimating demand for NPP.

SUPPLEMENTARY INFORMATION

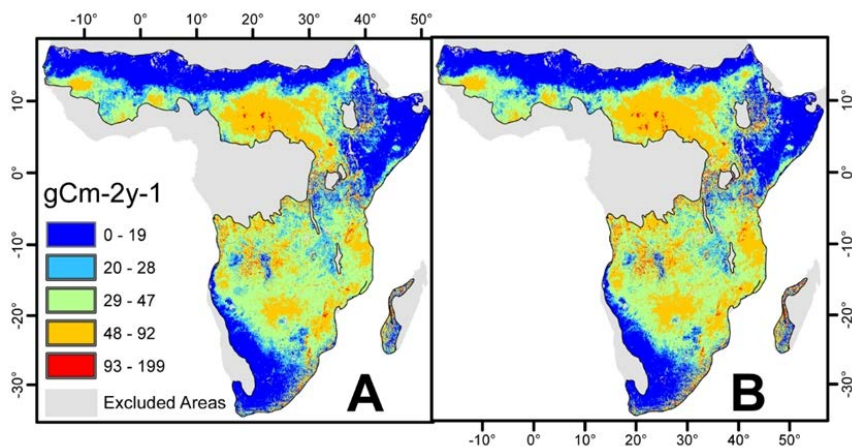


Supplementary Fig. 4. The output of maximum value compositing showing positive (a) and negative (b) correlations of ENSO and NPP supply. This represents change in NPP supply relative to a +1°C change in the Nino3.4 anomaly for 2000 – 2013.



Supplementary Fig. 5. Correlation between log-transformed dry cropland NPP and FAOSTAT annual crop production for 2000 – 2013. Each data point represents a country listed in Extended Table 2 and the crop data is an aggregate of the 27 crop types listed in Supplementary Table 1S.

SUPPLEMENTARY INFORMATION



Supplementary Fig. 6. Mean RMSE (a) and MAE (b) of annual aggregates of monthly NPP estimates compared to the MOD17A3 annual NPP product. The mean RMSE and MAE for all dryland regions were $32 \text{ gCm}^{-2}\text{yr}^{-1}$ and $27 \text{ gCm}^{-2}\text{yr}^{-1}$, respectively.

SUPPLEMENTARY INFORMATION

Supplementary References

1. Bradford GE (1999) Contributions of animal agriculture to meeting global human food demand. *Livestock Production Science* 59:95-112.
2. Brown S (1997) Estimating biomass and biomass change of tropical forests: a primer. Food and Agriculture Organization, Rome, Italy.
3. CSO (2012) Living conditions monitoring survey report (2006 - 2010). Central Statistical Office, Republic of Zambia, Lusaka, Zambia.
4. Eltahir IE, Mohamed AM, El Khidir OA, Atta M (2011) Feedlot performance and carcass characteristics of Sudan dromedary camels (*Camelus dromedarius*) fed on molasses and sorghum grain based diets. *Journal of Camelid Science* 4:70-78.
5. FAOSTAT (2015) FAO Statistical Databases. Food and Agriculture Organization of the United Nations, Rome, Italy.
6. Food Security Technical Secretariat (2010) Food and Nutrition Security Assessment in Sudan: Analysis of the 2009 Baseline Household Survey. Ministry of Agriculture, Khartoum, Sudan.
7. Funk CC, Peterson PJ, Landsfeld MF, Pedreros DH, Verdin JP, Rowland JD, Romero BE, Husak GJ, Michaelsen JC, Verdin AP (2014) A Quasi-Global Precipitation Time Series for Drought Monitoring. USGS Data Series 832. U.S. Geological Survey, Sioux Falls, South Dakota.
8. Ghana Statistical Service (2008) Report of the Fifth Round. Ghana Living Standards Survey. Ghana Statistical Service, Accra, Ghana.
9. Girard P (2002) Charcoal production and use in Africa: what future? *Unasylva* 53:30-35.
10. Goudriaan J, Groot JJR, Uithol PWJ (2001) Productivity of Agro-ecosystems. in Roy J, Saugier B, Mooney HA (eds.) *Terrestrial Global Productivity*. Academic Press, San Diego, pp. 301-313.
11. Haberl H, Erb KH, Krausmann F, Gaube V, Bondeau A, Plutzer C, Gingrich S, Lucht W, Fischer-Kowalski M (2007) Quantifying and mapping the human appropriation of net primary production in earth's terrestrial ecosystems. *Proceedings of the National Academy of Sciences* 104:12942-12947.
12. Hartter J, Boston K (2008) Consuming Fuel and Fuelling Consumption: Modelling Human Caloric Demands and Fuelwood Use. *Small-scale Forestry* 7:1-15.
13. Houerou HNL, Hoste CH (1977) Rangeland Production and Annual Rainfall Relations in the Mediterranean Basin and in the African Sahelo-Sudanian Zone. *Journal of Range Management* 30:181-189.
14. Hutjens MF Dairy Efficiency and Dry Matter Intake. in *Proceedings of the 7th Western Dairy Management Conference*, Reno, Nevada. .
15. IIASA/FAO (2012) Global Agro-ecological Zones (GAEZ v3.0). IIASA, Laxenburg, Austria and FAO, Rome, Italy. .
16. INSEE (2001) Enquête Prioritaire 1998. Etude Nationale sur les Conditions de Vie des Populations. Institut de la Statistique et des Etudes Economiques, Bujumbura, Burundi.
17. Jahnke HE (1982) Livestock production systems and livestock development in tropical Africa. Kieler Wissenschaftsverlag Vauk Kiel, Kiel, Germany.
18. Jung M, Reichstein M, Margolis HA, Cescatti A, Richardson AD, Arain MA, Arneth A, Bernhofer C, Bonal D, Chen J, Gianelle D, Gobron N, Kiely G, Kutsch W, Lasslop G, Law BE, Lindroth A, Merbold L, Montagnani L, Moors EJ, Papale D, Sottocornola M,

SUPPLEMENTARY INFORMATION

- Vaccari F, Williams C (2011) Global patterns of land-atmosphere fluxes of carbon dioxide, latent heat, and sensible heat derived from eddy covariance, satellite, and meteorological observations. *Journal of Geophysical Research: Biogeosciences* 116:G00J07.
19. Karim SA, Santra A, Verma DL (2002) Growth, feed conversion efficiency and carcass characteristics of Malpura and Malpura× Awassi crossbred lambs in a hot semi arid environment. *Asian-Australasian Journal of Animal Sciences* 15:377-381.
 20. Marufu L, Ludwig J, Andreae MO, Meixner FX, Helas G (1997) Domestic biomass burning in rural and urban Zimbabwe—Part A. *Biomass and Bioenergy* 12:53-68.
 21. Maselli F, Barbati A, Chiesi M, Chirici G, Corona P (2006) Use of remotely sensed and ancillary data for estimating forest gross primary productivity in Italy. *Remote Sensing of Environment* 100:563-575.
 22. Maziya-Dixon B, I.O. Akinyele, Oguntona EB, Nokoe S, Sanusi RA, Harris E (2004) Nigeria Food Consumption and Nutrition Survey, 2001-2003: Summary. International Institute of Tropical Agriculture, Ibadan, Nigeria.
 23. Mu Q, Zhao M, Running SW (2011) Improvements to a MODIS global terrestrial evapotranspiration algorithm. *Remote Sensing of Environment* 115:1781-1800.
 24. NSO (2012) Malawi Integrated Household Survey. Household Socioeconomic Characteristics Report National Statistical Office, Zomba, Malawi.
 25. Penman J, Gytarsky M, Hiraishi T, Krug T, Kruger D, Pipatti R, Buendia L, Miwa K, Ngara T, Tanabe K (2003) Good practice guidance for land use, land-use change and forestry. Institute for Global Environmental Strategies, Hayama, Japan.
 26. Pradhan P, K. B. Lüdeke M, E. Reusser D, P. Kropp J (2013) Embodied crop calories in animal products. *Environmental Research Letters* 8:044044.
 27. Reardon T (1993) Cereals demand in the Sahel and potential impacts of regional cereals protection. *World Development* 21:17-35.
 28. Tafere K, Worku I (2012) Consumption Patterns of Livestock Products in Ethiopia: Elasticity Estimates Using HICES (2004/05) Data. International Food Policy Research Institute, Washington, DC.
 29. Teklu T (1996) Food demand studies in Sub-Saharan Africa: a survey of empirical evidence. *Food Policy* 21:479-496.
 30. Vancutsem C, Marinho E, Kayitakire F, See L, Fritz S (2012) Harmonizing and combining existing land cover/land use datasets for cropland area monitoring at the African continental scale. *Remote Sensing* 5:19-41.
 31. Wirsenius S (2000) Human use of land and organic materials: modeling the turnover of biomass in the global food system, Chalmers University of Technology, Göteborg, Sweden.

Paper III

SCIENTIFIC DATA

OPEN Data Descriptor: High-resolution African population projections from radiative forcing and socio-economic models, 2000 to 2100

Received: 11 July 2016
Accepted: 25 November 2016
Published: 17 January 2017

Niklas Boke-Olén¹, Abdulhakim M. Abdi¹, Ola Hall² & Veiko Lehsten^{1,3}

For its fifth assessment report, the Intergovernmental Panel on Climate Change divided future scenario projections (2005–2100) into two groups: Socio-Economic Pathways (SSPs) and Representative Concentration Pathways (RCPs). Each SSP has country-level urban and rural population projections, while the RCPs are based on radiative forcing caused by greenhouse gases, aerosols and associated land-use change. In order for these projections to be applicable in earth system models, SSP and RCP population projections must be at the same spatial scale. Thus, a gridded population dataset that takes into account both RCP-based urban fractions and SSP-based population projection is needed. To support this need, an annual (2000–2100) high resolution (approximately 1km at the equator) gridded population dataset conforming to both RCPs (urban land use) and SSPs (population) country level scenario data were created.

Design Type(s)	data integration objective • population modeling objective • time series design
Measurement Type(s)	population data
Technology Type(s)	computational modeling technique
Factor Type(s)	
Sample Characteristic(s)	Homo sapiens • Africa • population

¹Department of Physical Geography and Ecosystem Science, Lund University, Sölvegatan 12, SE-223 62 Lund, Sweden. ²Department of Human Geography, Lund University, Sölvegatan 10, SE-223 62 Lund, Sweden. ³Swiss Federal Institute for Forest, Snow and Landscape research (WSL), Zürcherstr. 11, CH-8903 Birmensdorf, Switzerland. Correspondence and requests for materials should be addressed to N.B.-O. (email: Niklas.Boke-Olen@nateko.lu.se).

Background & Summary

The size and future trend of the human population on Earth has been a topic of scientific enquiry at least since Thomas R. Malthus wrote *An Essay on the Principle of Population* in 1798. Presently, the Population Division of the United Nations (UN) is one of several agencies or institutions that publish global population projections on a country-by-country basis at predefined intervals. The UN's projections are published in a biennial report called the World Population Prospects (WPP) with the 2015 revision projecting a remarkable 270% increase in the African population between 2015 and 2100 (ref. 1). This rapid population growth has a number of potentially associated effects that could fundamentally alter the continent's landscape. These include high rates of urbanization leading to unplanned expansion of cities, the spread of informal settlements that lack basic services and degradation of natural resources as a result of over-exploitation to meet rising food demand^{2,3}. Furthermore, a projected 4°C global warming by 2100 could have severe negative impacts on the rain-fed agro-ecosystems that are a main source of livelihood and nutrition in sub-Saharan Africa (SSA)^{3,4}. Altogether, this will lead to a reallocation of population from rural to urban areas, and create strong incentives for landscape transformation.

Population data has traditionally taken the form of estimates per administrative unit per unit time. The administrative units are often in the form of regional, national, or sub-national counts with temporal units at best at annual intervals but more commonly 5–10 years. From an analytical perspective this is troublesome. Since administrative units vary in size, shape, and usually are arbitrarily defined any study that uses administrative borders will obtain a very heterogeneous set of observations. Since the 1990s, there have been growing attempts to disaggregate population data into spatially explicit estimates distributed across a regular grid. Tobler, *et al.*⁵ produced a smoothed continuous map-grid of total population at a global scale for the year 1994. This work was later labeled as the first version of the Gridded Population of the World (GPWv1) by the Center for International Earth Science Information Network (CIESIN). The fourth, and latest, version, GPWv4, was published in 2015 (ref. 6) and includes population data at 5-year intervals between 2000 and 2020. As part of the AfriPop project, Linard *et al.*⁷ built a unique spatial database that combined census data across the continent with satellite imagery and land cover data in a dasytetric model. The AfriPop project was transformed into an open access archive and re-labeled WorldPop. Within this new framework, Sorichetta *et al.*⁸ developed a gridded population distribution dataset for the Caribbean and Latin America for 2000, 2015 and 2020. However, due to the coarse temporal resolution and limited time period available for these datasets none of them can be completely used as an accompanying dataset for analyses using projected 21st century data within Intergovernmental Panel on Climate Change (IPCC) Fifth Assessment Report (AR5) framework which is based on gridded climate projection data.

Here, we present a 30 arc-second, gridded population distribution projection for every year between 2000 and 2100 for the African continent conforming to both the Representative Concentration Pathways (RCPs) urban fractions⁹ and Shared Socio-Economic Pathways (SSPs) population (major characteristics presented in Table 1). To our knowledge the combination of RCPs and SSPs scenarios for gridded population projections is something that has not been done before. The RCPs and SSPs supersede the Special Report on Emissions Scenarios (SRES) and were adopted by the IPCC for its AR5 (refs 3,10). Unlike the SRES, the four RCPs are not based on socio-economic scenarios but on radiative forcing and the simulated influences of land use, greenhouse gas and aerosol emissions. Therefore, a set of five SSPs were used in conjunction with the RCPs to develop future country level population distribution scenarios¹¹. The development of society and the natural environment in SSPs are not explicitly taking climate change or the implementation of climate policies at the global scale during the 21st century into account. Each SSP scenario is adjoined with a population projection and a proportion of the country population living in urban areas. The presented gridded population dataset can be useful when performing future simulations dependent on gridded RCP land use and climate data, for example carbon flux studies or assessments of supply and demand of food.

Methods

The method can be summarized as a distribution of country level SSP urban and rural population projections onto a 30 arc seconds grid conforming to the urban fraction grid at 30 arc minutes. For this we used the African population for year 2000 at 30 arc-second spatial resolution from the WorldPop Project¹² as a starting dataset. Distance to road and to population centers of gravity were used to allow each pixel to be ranked uniquely into urban or no-urban (see below). A complete list of the included data sources can be found in Table 2.

SSP-RCP coupling in the baseline year 2000

The population distribution for Africa was modeled to follow the RCP-specific urban fraction dataset¹³ further described in Hurtt *et al.*⁹ and the country-specific SSP population and urban fraction scenarios from the SSP database¹⁴. The urban fraction data is provided at a spatial resolution of 30 arc-minutes (0.5 degrees or approximately 50 kilometers at the equator) and represents annual projected global land use and land cover patterns until the year 2100. It is developed with a Global Land-use Model (GLM)¹⁵ which estimates future land use transitions and patterns within each 30 arc-minute grid cell using an accounting based method by considering a range of parameters (i.e. spatial patterns, residency time, and land conversions)⁹. The five SSPs and four RCPs produce a set of 20 SSP-RCP scenario combinations that

Pathway	Key characteristics
RCP2.6	-Radiative forcing 2.6 W m ⁻² by 2100
	-Low GHG emissions
	-Medium-low air pollution
RCP4.5	-Radiative forcing 4.5 W m ⁻² by 2100
	-Very low baseline GHG emission with medium-low mitigation
	-Medium air pollution
RCP6.0	-Radiative forcing 6.0 W m ⁻² by 2100
	-Medium baseline GHG emission with high mitigation
	-Medium air pollution
RCP8.5	-Radiative forcing 8.5 W m ⁻² by 2100
	-High baseline GHG emission
	-Medium-High air pollution
SSP1	-Low population
	-High urbanization
	-High-Medium Economy
SSP2	-Medium population
	-Medium urbanization
	-Medium uneven economy
SSP3	-High population
	-Low urbanization
	-Slow economy
SSP4	-Medium-High population
	-High-Medium urbanization
	-Low-Medium economy
SSP5	-Low-Medium Population
	-High Urbanization
	-High Economy

Table 1. Main characteristics of RCP and SSP assumptions. RCP characteristics from Van Vuuren *et al.*¹⁰ and SSP characteristics from O'Neill *et al.*²⁴ and Kc & Lutz²⁵.

Name	Spatial domain	Temporal domain	Type	Source
SSP population scenarios	Country	2000–2100	Continuous	SSP Database ⁴
RCP Urban fraction	0.5 degree	2000–2100	Raster	Chini <i>et al.</i> ¹³
WorldPop Africa	30 arc-second	2000	Raster	http://www.worldpop.org/
Roads	Global	1980–2010	Polylines	gROADsv1 ²³
Water bodies mask	Global	2000	Polygons	GRUMPv1:National-Administrative-Boundaries ^{18,19}
Country Borders	Global	2008	Polygons	http://www.thematicmapping.org/downloads/

Table 2. Input datasets used to grid future populations.

deliver a reasonable basis for future scenarios. However, some combination (e.g., SSP1-RCP8.5) are very unlikely to occur in the future¹⁶ ($p < 0.01$). Consequently, we used the 15 most probable SSP-RCP combinations according to Engström *et al.*¹⁷.

The gridded population dataset for Africa for the year 2000 (ver. 3.020) from the WorldPop Project¹² was used as the starting point. The estimates of total number of people per grid cell across Africa are adjusted to match UN population division estimates. The national administrative boundaries dataset from GRUMPv1 (refs 18,19) were used to remove water bodies from the WorldPop data. This was done by converting the national boundaries to raster using ArcGIS 10 raster to polygon tool with 30 arc-seconds as the output resolution. The created raster was reclassified to include only ones and zeros for land and water bodies, respectively. Finally, it was matched to the spatial origin of WorldPop by using the resample (nearest neighbor) function within the raster package in R (R: A Language and Environment for Statistical Computing, <https://www.r-project.org/>). To classify each 30 arc-second pixel within each 0.5 degree pixel as urban or non-urban based on their population value the inverse distance to roads and inverse distance to center of gravity (COG) were each rescaled to lie between $1.0 \cdot 10^{-5}$ and $1.1 \cdot 10^{-5}$ and

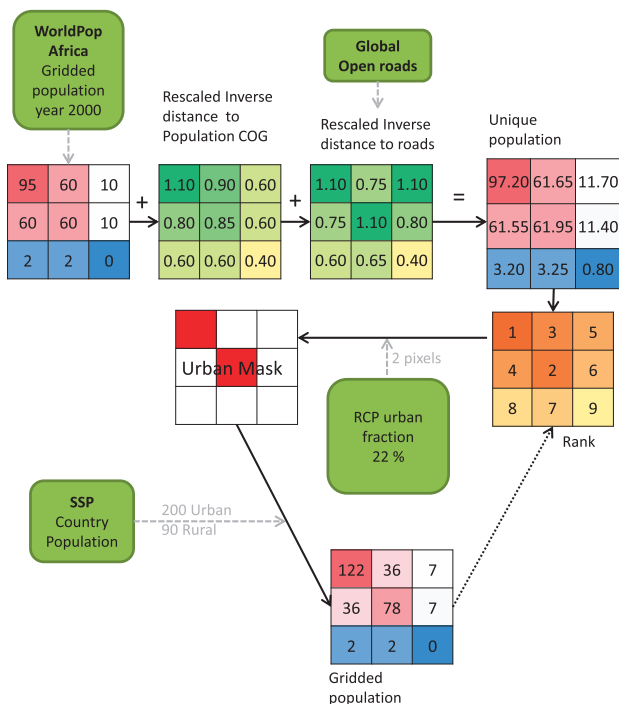


Figure 1. Flowchart and example of the method used to distribute the population. Example made with artificial numbers for visualization purposes. For simplicity the smaller grid cells each corresponds to one 30 arc second pixel and the full grid (9 × 9) represent one urban fraction grid cell (0.5 degree) and the full grid 9x9 corresponds to one country. The example highlights the need to add inverse distance to population center of gravity (COG) and inverse distance to roads to the population data to be able to uniquely rank the pixels. The country SSP population is distributed for rural and urban separately based on the urban mask and the gridded population from the year before or unique population for the first year. The green boxes with rounded corners indicate input data. Inverse distance to center of gravity and inverse distance to roads are for the small example not rescaled to the same range as done when processing the dataset.

added to the initial dataset (Fig. 1). Distance to roads and distance to population centers (COG) were chosen since their effect on the population distribution within an area have been demonstrated repeatedly^{8,20–22}. The distance to roads was calculated using Euclidian distance on the global roads open access data set²³. The COG was calculated on the WorldPop dataset for each 0.5 degree urban fraction pixel using the COgravity tool included in the R (R: A Language and Environment for Statistical Computing, <https://www.r-project.org/>) package SDMTools (<https://cran.r-project.org/web/packages/SDMTools/>). These operations are done to be able to more accurately classify pixels as urban or non-urban based on their unique population value and also to ensure that urban growth will be favored in proximity to population centers or roads. Our procedure requires ranking the pixels as non-urban or urban based on their population values. Hence a maximum of two arc-second pixels within each 30 arc-minute urban fraction grid cell were allowed to have the exact same value. This was achieved by addition of the rescaled inverse distance to road and COG, the result of that is from now on referred to as unique population dataset.

Population allotment per grid cell

The unique population dataset for year 2000 is used together with the RCP specific urban fraction for year 2000 to create the urban mask (Fig. 1). This is done by sorting the pixel values within each urban

fraction 0.5 degree grid cell and selecting the highest ones as urban until the urban fraction value is fulfilled (rounding the number of urban pixels within each 0.5 degree grid cell to the nearest integer). This is repeated for all 0.5 degree grid cells. Subsequently, the urban mask is used on a per country basis to distribute the urban and rural SSP population data and assuring that the unique population relationship is still valid. This means, for example, that a pixel with an initial value twice as large as another pixel will still have the same ratio under the condition that they are both located in the same country and are both either urban or rural pixels. The gridded population of the previous year is used as input to create the urban mask of the next year and to distribute the population thus creating a loop (Fig. 1). This ensures that the unique population for year 2000 will only be used once to create the dataset for year 2001 and thereafter the population from the year before will be used as the unique data set (Fig. 1). This meaning that the population from the previous year will be used to create a new urban mask based on the RCP urban fraction for that year. Hence the spatial distribution of the urban areas is based on the yearly RCP urban fraction and the gridded population from the year before using the ranking technique as shown in Fig. 1.

The population re-distributions are carried out for the 15 likely combinations of RCP and SSP scenarios from Engström *et al.*¹⁷ (Table 3). Hence, in total 15 different datasets with yearly population projections between 2000 and 2100 are created. An example of the population re-distribution for SSP 2 and RCP 4.5 for year 2050 can be seen in Fig. 2.

Code availability

The gridded population datasets were created using R3.3.0 (R: A Language and Environment for Statistical Computing, <https://www.r-project.org/>) and the scripts can be found on GitHub (https://github.com/niklasbokeolen/african_population/).

Data Records

The high resolution population projections for the RCP and SSP scenario combinations described here can be freely and publicly accessed at the DataGURU web site (Data citation 1) which also allows basic conversion/spatial and temporal cropping, thus enhancing the accessibility. The original data are stored as one geotiff (.tif) for each scenario combination and year with the datatype FLT4S and NA-value as -9999. They are in a longitude latitude projection with WGS84 as the datum and are created with the function writeRaster within the raster package (v2.5-2, <https://cran.r-project.org/web/packages/raster/>) in R 3.3.0 (R: A Language and Environment for Statistical Computing, <https://www.r-project.org/>).

To get an overview of the created dataset, parts of it can be explored with a shiny web application which provides an interactive visualization. It can be found in the below location: https://niklasbokeolen.shinyapps.io/Shiny_population/.

Note that the tool uses a re-projected version of the data to match the projection of the OpenStreetMap. For the official version of the gridded population dataset, the user is advised to download the original files via the DataGURU service which also provides the long term storage.

Technical Validation

The technical validation of the dataset is performed by comparing the SSP 1 country populations with the gridded population dataset (for SSP1/RCP 4.5) aggregated to country levels. This is done for year 2005 since both SSP population projections and RCP land use projections do not deviate until after that year. Accordingly, we performed the technical validation on only one RCP-SSP combination. We show that all the population is accounted for and every country lies on the one to one line (Fig. 3) with a coefficient of determination (r^2) of 1.0.

To further evaluate the created dataset we compared the 2000 to 2005 population change for the created gridded dataset with the change for UN (2015) adjusted Gridded Population of the World version 4 (GPWv4). This was done for a sample of six African countries (Benin, Madagascar, Morocco, Botswana, Ethiopia, and Tunisia) representing a wide variation in population density and spatial distribution. The population was aggregated to level 2 administrative regions within each country and only one SSP/RCP combination was used since the projections do not deviate until after year 2005. The result of the comparison to GPWv4 can be seen in Fig. 4. For most of the countries the change matches in general well but typically deviates more for a few of the level

	RCP 2.6	RCP 4.5	RCP 6	RCP 8.5
SSP 1	0.09	0.45	0.45	0.00
SSP 2	0.00	0.09	0.68	0.23
SSP 3	0.00	0.17	0.50	0.33
SSP 4	0.00	0.37	0.56	0.07
SSP 5	0.00	0.07	0.37	0.56

Table 3. RCP-SSP probability matrix as described by Engström *et al.*¹⁷

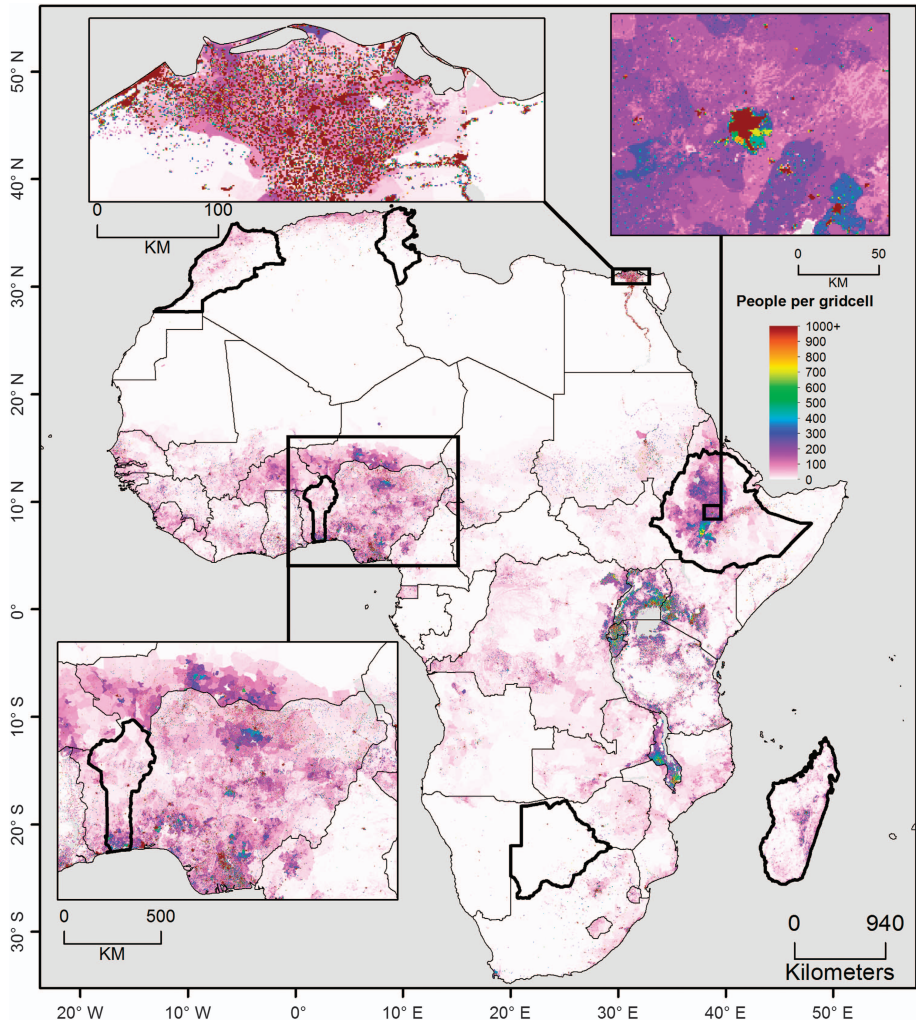


Figure 2. Map of year 2050 of the gridded population datasets for SSP 2 and RCP 4.5. Countries presented with bold borders are the countries used for a more in depth comparison (see technical validation section).

2 administrative regions. A summary of the comparison to GPWv4 for the validation countries and year 2005 can be seen in Table 4 where it can be observed that the total distributed populations (SSP countries population) are not exactly the same as the population for GPWv4. However, the coefficient of determination is high ($r^2 > 0.8$) for most of the countries and administrative levels indicating that the spatial pattern is captured between the regions. This indicates that the method is well suited to capture the spatially pattern. However, due to considerable differences in the total population between GPWv4 and the SSP population data we do not expect the change to match perfectly for all regions.

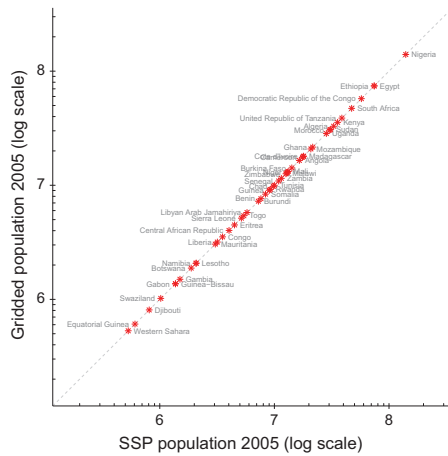


Figure 3. Country level validation of gridded dataset for year 2005. Gridded population aggregated to country totals and compared against SSP country population.

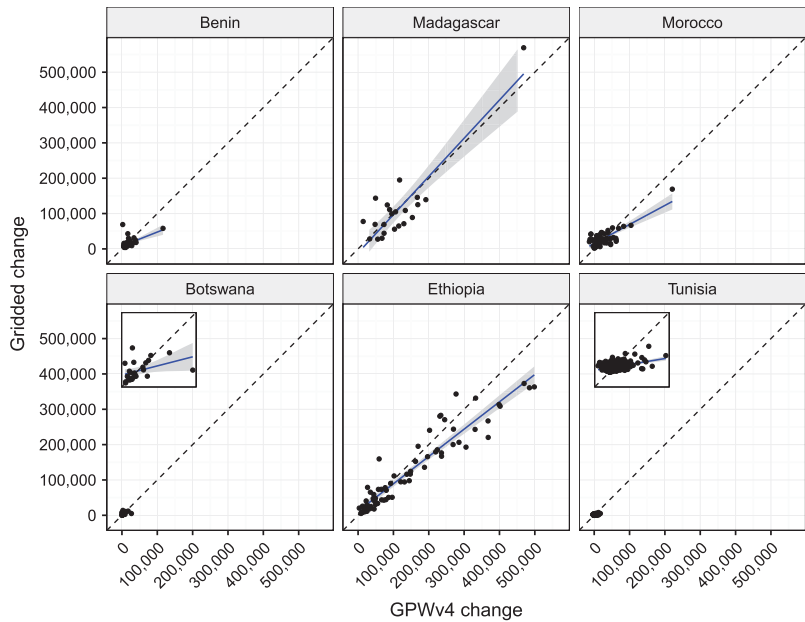


Figure 4. Validation result on administrative region at level 2. Plots show population change between year 2000 and 2005 for data set created in this paper (gridded change) and gridded population of the world v4 (GPWv4 change). A zoom of the Botswana and Tunisia data is included as an inset.

	n	r ²	RMSE	GPWv4 average population	Gridded average population	GPWv4 country population	SSP country population
<i>Benin</i>						8,203,291	7,630,000
<i>Adm1</i>	12	0.89	104,369	674,354	631,009		
<i>Adm2</i>	76	0.81	38,391	106,477	99,633		
<i>Madagascar</i>						18,200,149	17,900,000
<i>Adm1</i>	6	0.91	635,232	3,028,272	2,976,479		
<i>Adm2</i>	22	0.86	407,449	825,892	811,767		
<i>Morocco</i>						29,920,484	30,400,000
<i>Adm1</i>	15	0.79	587,860	1,988,823	2,015,600		
<i>Adm2</i>	54	0.91	312,416	552,451	559,889		
<i>Botswana</i>						1,860,717	1,880,000
<i>Adm1</i>	9	0.98	26,917	205,694	208,228		
<i>Adm2</i>	25	0.52	47,608	74,050	74,962		
<i>Ethiopia</i>						76,536,708	74 300 000
<i>Adm1</i>	11	0.99	1,162,510	6,953,130	6 749 082		
<i>Adm2</i>	72	0.94	229,176	1,062,284	1,031,110		
<i>Tunisia</i>						9,767,114	10,000,000
<i>Adm1</i>	24	0.83	174,471	404,435	414,169		
<i>Adm2</i>	268	0.48	26,375	36,218	37,090		

Table 4. Summary of gridded data (presented dataset) countries aggregated to administrative region level 1 and 2 for year 2005 and compared with GPWv4. SSP country population is the population from the SSP scenarios that the product is based on. The SSP population scenarios do not deviate until after year 2005. n indicates number of regions within each administrative level. r² is the coefficient of determination and RMSE is the root mean square error between GPWv4 and gridded population, aggregated to administrative level one or two.

Uncertainty

We used a deterministic method to produce the gridded population projections which means that the level of uncertainty in the created dataset is originating from uncertainty in the input data (Table 2). We would like to point out a possibly over-influence of roads in the created dataset. This is due to that WorldPop uses distance to roads and we further add the inverse distance to roads in order to create a unique population dataset as a starting point. However, since we rescale the distance to road to be between $1.0 \cdot 10^{-5}$ and $1.1 \cdot 10^{-5}$ we argue that this will only have an effect for pixels that were equal in the initial WorldPop dataset. Pixels (30 arc-seconds) with unequal population values in the initial dataset will have a very low probability of being affected by this small addition based on the distance to road.

References

- United Nations, Department of Economic and Social Affairs, Population Division (UNPD). *World Population Prospects: The 2015 Revision, Key Findings And Advance Tables*. (United Nations, 2015).
- United Nations Human Settlements Programme (UN-HABITAT). *The State Of African Cities 2010: Governance, Inequality And Urban Land Markets* (United Nations, 2010).
- Intergovernmental Panel on Climate Change (IPCC). *Climate Change 2014: Impacts, Adaptation, and Vulnerability. Part B: Regional Aspects. Contribution of Working Group II to the Fifth Assessment Report of the Intergovernmental Panel on Climate Change* (ed. Barros, V.R., Field, C.B., Dokken, D.J., Mastrandrea, M.D., Mach, K.J., Bilir, T.E., Chatterjee, M., Ebi, K.L., Estrada, Y. O., Genova, R.C., Girma, B., Kissel, E.S., Levy, A.N., MacCracken, S., Mastrandrea, P.R., White, L.L.) Ch 21-30 (Cambridge, United Kingdom and New York, NY, USA, 2014).
- World Bank. *Turn Down The Heat: Why A 4°C Warmer World Must Be Avoided* (International Bank for Reconstruction and Development/The World Bank, 2012).
- Tobler, W., Deichmann, U., Gottsegen, J. & Maloy, K. World population in a grid of spherical quadrilaterals. *Int. J. Popul. Geogr* **3**, 203–225 (1997).
- Doxsey-Whitfield, E. *et al.* Taking advantage of the improved availability of census data: a first look at the gridded population of the world, version 4. *Papers in Appl. Geography* **1**, 226–234 (2015).
- Linard, C., Gilbert, M., Snow, R. W., Noor, A. M. & Tatem, A. J. Population distribution, settlement patterns and accessibility across Africa in 2010. *PLoS ONE* **7**, e31743 (2012).
- Sorichetta, A. *et al.* High-resolution gridded population datasets for Latin America and the Caribbean in 2010, 2015, and 2020. *Sci. Data* **2**, 150045 (2015).
- Hurt, G. C. *et al.* Harmonization of land-use scenarios for the period 1500–2100: 600 years of global gridded annual land-use transitions, wood harvest, and resulting secondary lands. *Clim. Change* **109**, 117–161 (2011).
- van Vuuren, D. P. *et al.* The representative concentration pathways: an overview. *Clim. Change* **109**, 5–31 (2011).
- O'Neill, B. C. *et al.* A new scenario framework for climate change research: the concept of shared socioeconomic pathways. *Clim. Change* **122**, 387–400 (2014).
- Tatem, A. J. *et al.* Millennium development health metrics: where do Africa's children and women of childbearing age live? *Popul. Health Metr* **11**, 1–11 (2013).

13. Chini, L. P., Hurtt, G. C. & Frolking, S. Harmonized Global Land Use for Years 1500–2100, V1. *The Oak Ridge National Laboratory Distributed Active Archive Center*. doi:10.3334/ORNLDAAC/1248 (2014).
14. International Institute for Applied Systems Analysis (IIASA). SSP Database 2012–2015. *SSP Public Database*. <https://tntcat.iiasa.ac.at/SspDb/> (2015).
15. Hurtt, G. C. *et al.* The underpinnings of land-use history: three centuries of global gridded land-use transitions, wood-harvest activity, and resulting secondary lands. *Glob. Change Biol.* **12**, 1208–1229 (2006).
16. van Vuuren, D. P. *et al.* A new scenario framework for climate change research: scenario matrix architecture. *Clim. Change* **122**, 373–386 (2014).
17. Engström, K. *et al.* Assessing uncertainties in global cropland futures using a conditional probabilistic modelling framework. *Earth Syst. Dynam. Discuss* **7**, 893–915 (2016).
18. Balk, D. L. *et al.* Determining global population distribution: methods, applications and data. *Adv. in Parasitology* **62**, 119–156 (2006).
19. Center for International Earth Science Information Network (CIESIN) Columbia University, International Food Policy Research Institute (IFPRI), The World Bank & Centro Internacional de Agricultura Tropical (CIAT). Global Rural Urban Mapping Project, version 1 (GRUMPv1): National Administrative Boundaries. *Socioeconomic Data and Applications Center (SEDAC)* <http://sedac.ciesin.columbia.edu/data/set/grump-v1-national-admin-boundaries> (2011).
20. Reibel, M. & Bufalino, M. E. Street-weighted interpolation techniques for demographic count estimation in incompatible zone systems. *Environ. Plann. A* **37**, 127–139 (2005).
21. Linard, C., Tatem, A. J. & Gilbert, M. Modelling spatial patterns of urban growth in Africa. *Appl. Geogr.* **44**, 23–32 (2013).
22. Seto, K. C., Güneralp, B. & Hutyra, L. R. Global forecasts of urban expansion to 2030 and direct impacts on biodiversity and carbon pools. *Proc. Natl. Acad. Sci.* **109**, 16083–16088 (2012).
23. Center for International Earth Science Information Network (CIESIN) Columbia University & Information Technology Outreach Services (ITOS) University of Georgia. Global Roads Open Access Data Set, Version 1 (gROADSv1) *Socioeconomic Data and Application Center* <http://sedac.ciesin.columbia.edu/data/set/groads-global-roads-open-access-v1> (2013).
24. O'Neill, B. C. *et al.* The roads ahead: narratives for shared socioeconomic pathways describing world futures in the 21st century. Preprint at doi:10.1016/j.gloenvcha.2015.01.004 (2015).
25. Kc, S. & Lutz, W. The human core of the shared socioeconomic pathways: population scenarios by age, sex and level of education for all countries to 2100. Preprint at doi:10.1016/j.gloenvcha.2014.06.004 (2014).

Data Citation

1. Boke-Olén, N., Abdi, A. M., Hall, O. & Lehsten, V. *DataGURU* <http://dx.doi.org/10.18161/popcount.201610> (2016).

Acknowledgements

N.B.-O. is supported by Lund University Center for studies of Carbon Cycle and Climate Interactions (LUCCI) and Lund University and University of Gothenburg Biodiversity and Ecosystem Services in a Changing Climate (BECC). A.M.A. is funded by the Swedish National Space Board (Rymdstyrelsen) with support from LUCCI. V.L. is funded by the ERA-Net BiodivERsA, with the national funder FORMAS part of the 2012 BiodivERsA call for research proposals via the CONNECT project as well as from the Swiss National Science foundation. The funders had no role in study design, data collection and analysis, decision to publish, or preparation of the manuscript.

Author Contributions

N.B.-O. did data collection, analyses and produced the dataset. N.B.-O. and A.M.A. drafted the manuscript. O.H. and V.L. edited the manuscript. All authors read and approved the final version of the manuscript.

Additional Information

Competing financial interests: The authors declare no competing financial interests.

How to cite this article: Boke-Olén, N. *et al.* High-resolution African population projections from radiative forcing and socio-economic models, 2000 to 2100. *Sci. Data* **4**:160130 doi: 10.1038/sdata.2016.130 (2017).

Publisher's note: Springer Nature remains neutral with regard to jurisdictional claims in published maps and institutional affiliations.



This work is licensed under a Creative Commons Attribution 4.0 International License. The images or other third party material in this article are included in the article's Creative Commons license, unless indicated otherwise in the credit line; if the material is not included under the Creative Commons license, users will need to obtain permission from the license holder to reproduce the material. To view a copy of this license, visit <http://creativecommons.org/licenses/by/4.0>

Metadata associated with this Data Descriptor is available at <http://www.nature.com/sdata/> and is released under the CC0 waiver to maximize reuse.

© The Author(s) 2017

Paper IV

Evaluating water controls on vegetation growth in the semi-arid Sahel using field and Earth observation data

Abdulhakim M Abdi ^{1,*}, Niklas Boke-Olén ¹, David E Tenenbaum ¹, Torbern Tagesson ², Bernard Cappelaere ³, Jonas Ardö ¹

¹ Department of Physical Geography and Ecosystem Science, Lund University, Sölvegatan 12, 22362 Lund, Sweden

² Department of Geosciences and Natural Resource Management, University of Copenhagen, DK-1350 Copenhagen, Denmark

³ Institut de Recherche pour le Développement, HydroSciences Montpellier (CNRS, IRD, University of Montpellier), BP 64501, 34394 Montpellier, France

* Author to whom correspondence should be addressed; E-Mail: hakim.abdi@gmail.com

Abstract

Water loss is a crucial factor for vegetation in the semi-arid Sahel region of Africa. Global satellite-driven estimates of plant CO₂ uptake (gross primary productivity, GPP) have been found to not accurately account for Sahelian conditions, particularly the impact of canopy water stress. Here, we identify the main biophysical limitations that induce canopy water stress in Sahelian vegetation, and evaluate the relationships between field data and Earth observation-derived spectral products for up-scaling GPP. We find that plant available water and vapor pressure deficit together limit the GPP of Sahelian vegetation. Our results show that a multiple linear regression (MLR) GPP model that combines the Enhanced Vegetation Index, Land Surface Temperature, and the short-wave infrared reflectance (2105 – 2155 nm) of the Moderate Resolution Imaging Spectroradiometer satellite sensor was able to explain between 88% and 96% of the variability of eddy covariance flux tower GPP at three Sahelian sites (mean = 89%). The MLR GPP model presented here is scalable with estimates of GPP at a relatively high spatial resolution. Given the scarcity of field data on CO₂ fluxes in the Sahel, this scalability is important due to the low number of flux towers in the region.

1. Introduction

The Sahel is an arid and semi-arid region that stretches from the Atlantic Ocean in the west to the Red Sea in the east and separates the hyper-arid Sahara desert from the sub-humid and humid regions to the south (Figure 1). The Sahel has experienced a prolonged dry period from the mid-1960s through the late 1980s in which there were severe droughts that resulted in humanitarian crises (Ellis and Galvin, 1994). Recovery from this dry period was reported by Eklundh and Olsson (2003) who observed strong increases in seasonal satellite-derived NDVI (Normalized Difference Vegetation Index) from the mid-1980s onwards. This increase in vegetation greenness began to be referred to as the “greening of the Sahel” (Olsson et al., 2005), and is the result of increases in both herbaceous (Dardel et al.,

2014) and tree cover (Brandt et al., 2015). Seaquist et al. (2006) translated this greening into sequestered carbon (C) and found that 51 megatonnes of C (MtC) per year were taken up by Sahelian vegetation between 1982 and 1999 resulting in a net increase of 918 MtC over the 18-year period. The key suggested mechanism behind the greening is increased rainfall (Hickler et al., 2005), and, to a lesser extent, improved land use and migration-induced land abandonment (Olsson et al., 2005).

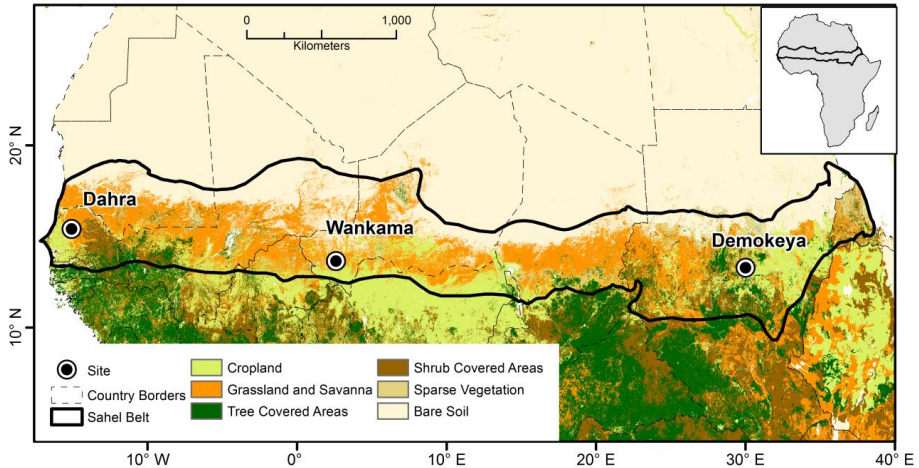


Figure 1. The location of the sites and the dominant land cover classes in Sahel. The Sahelian borders are based on the 150 and 700 mm annual rainfall isohyets. Dominant land cover types are according the Food and Agriculture Organization's 2014 Global Land Cover-SHARE database. Grassland and croplands together cover more than 67% of the total surface area of the Sahel.

Gross primary productivity (GPP) is the total amount of C plants extract from the atmosphere through photosynthesis. Some of this C goes to maintenance, and is thus lost through autotrophic respiration (R_a). The remaining C is stored as phytomass (net primary productivity, $NPP = GPP - R_a$). The capacity of Sahelian ecosystems to provide essential food, fuel and feed is a function of available NPP (Abdi et al., 2014). Since these ecosystem services are essential, evaluating the environmental controls that modulate GPP dynamics is essential for accurate accounting of primary productivity. The Sahel has a single growing season that starts in July and ends in October (Vrieling et al., 2013) with considerable inter-annual variability in the spatial distribution and quantity of rainfall (Nicholson, 2011; Philippon et al., 2014). The driest parts of the northern Sahel receive an annual average of 150 mm of rain, while the southern parts receive an annual average of ~750 mm (Le Houérou, 1989) (Figure 1).

The Sahel (Figure 1) is dominated by plants that have the C_4 photosynthetic pathway (Tagesson et al., 2016b), which are adapted to warm, arid environments and are composed mainly of grasses, herbs and crops. The mean tree canopy cover is approximately 7.3% and comprises trees that use the C_3 photosynthetic pathway (Hiernaux and Le Houérou, 2006; Brandt et al., 2016). It is well known that moisture availability controls C fluxes in drylands such as the Sahel, and several studies have attempted to explain the underlying mechanisms of its modulation of primary productivity in these

regions (Tucker et al., 1983; Prince, 1991; Verhoef et al., 1996; Moncrieff et al., 1997; Nicholson et al., 1998; Hickler et al., 2005; Sjöström et al., 2011). Merbold et al. (2009) found that mean annual rainfall is strongly correlated with maximum photosynthetic capacity and is the predominant factor driving C fluxes across Africa. With rainfall, the greening phase commences (Figure 2), soil moisture is replenished, which impacts the amount of energy partitioned into evapotranspiration (Sjöström et al., 2011; Nutini et al., 2014; Velluet et al., 2014). Rainfall also increases humidity, which lowers the difference between the vapor pressure deficit inside the leaf and that of the air. This difference in vapor pressure deficit was found to be a key factor affecting stomatal conductance of Sahelian plants (Boegh et al., 1999; Ago et al., 2015). The browning phase (Figure 2) begins with a decrease in soil moisture and increase in both surface temperature and vapor pressure deficit, which triggers the closure of the stomata to prevent water loss through transpiration. The closure of the stomata prohibits the flow of CO₂ into the leaf and thus reduces GPP.

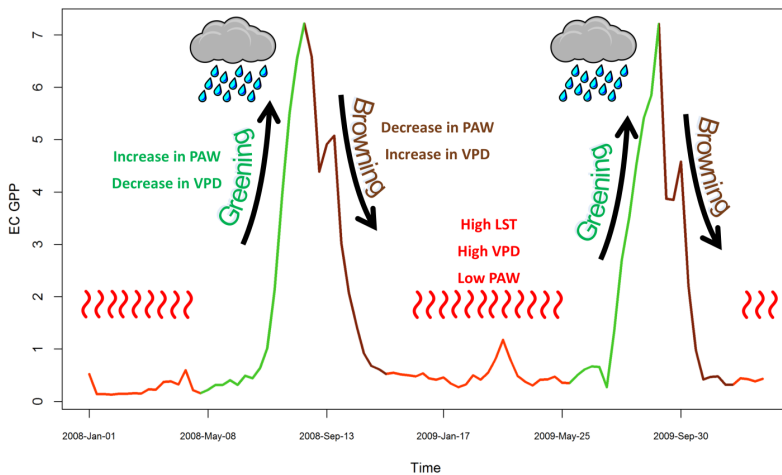


Figure 2. Conceptual diagram of the greening and browning processes present in the Sahel. The two peaks represent the uptake of CO₂ and the increase in GPP. The greening phase begins with the start of the rainy season and the increase in plant available water (PAW, section 3.3.1). During the greening phase vapor pressure deficit (VPD, section 3.3.2) decreases and so does land surface temperature (LST). The beginning of the browning phase starts with a reduction in PAW and increase in VPD and LST.

Most studies covering the Sahel base their results on a handful of sites, due to the scarcity of data on C fluxes over the region's 3.3 million km² of surface area (Ardö, 2016). Thus, Earth observation is an important tool for large-scale studies of the GPP of Sahelian ecosystems. The only global model of satellite-driven GPP estimates is the MOD17 production efficiency model (Running et al., 2000), which is based on the light-use efficiency concept (Monteith, 1972). However, this dataset has been shown to considerably underestimate GPP over semi-arid Sahelian ecosystems (Sjöström et al., 2011; Sjöström et al., 2013). Recent work by Sadeghi et al. (2015) found that the shortwave infrared spectral range of 2105 – 2155 nm provides optimal sensitivity to variations in soil moisture. Furthermore, aerosol effects are negligible because most aerosol particulates are smaller than that wavelength range (Liang et al., 2006). The drying and wetting processes that influence vegetative growth could be captured by satellite sensors that cover this spectral range because soil moisture at the top 1 – 2 cm of

soil significantly influences soil surface reflectance at these wavelengths (Lobell and Asner, 2002; Weidong et al., 2002). Another recent study by Tian and Philpot (2015) found that shortwave infrared radiation within the spectral range of 1850 – 2130 nm was sensitive to soil volumetric water content. Consequently, there is potential utility of this spectral range in C cycle studies that focus on Sahelian settings. This study has two objectives: (1) Identify the relative strengths of biophysical limitations that reduce CO₂ uptake in the Sahel, and (2) evaluate empirical relationships between Earth observation-derived spectral products that can account for these limitations to better explain the variability in EC GPP using Earth observation data.

2. Field Sites

We used three eddy covariance sites located in Sudan, Niger and Senegal. All three sites are within a narrow latitudinal band between 13°N and 15°N (Figure 1). A summary of the sites is presented below and summarized in Table 1.

2.1. Demokeya, Sudan

Demokeya (13.282°N, 30.478°E) is located in North Kordofan state. Mean annual air temperature is 30°C and mean annual precipitation is 320 mm. The landscape around the site is a typical Sahelian savanna, comprised of sparse trees, mainly *Acacia senegal* and *Acacia nilotica*, with a canopy cover of approximately 7%. The ground cover comprises annual grasses, primarily *Cenchrus biflorus*, *Eragrostis tremula*, and *Aristida pallida*. The sandy soils are poor in nutrients, have low soil organic C, and low cation exchange capacity (Olsson and Ardö, 2002). A complete description of Demokeya is provided in Ardö et al. (2008).

2.2. Wankama, Niger

The Wankama site is divided into two sub-sites, Wankama Millet (13.644°N, 2.629°E) and Wankama Fallow (13.647°N, 2.633°E), both of which are located in southwest Niger and within close proximity to each other. Mean annual air temperature is 30°C and mean annual precipitation is 479 mm. Only the fallow site has been used in this study. This site is composed of shrub and herbaceous layers; the shrub layer is primarily composed of *Guiera senegalensis* and the herbaceous layer is dominated by *Zornia glochidiata* (Boulain et al., 2009). The soils are mostly sandy with low nitrogen and phosphate content. A complete description of Wankama is provided in Cappelaere et al. (2009).

2.3. Dahra, Senegal

Dahra (15.402°N, 15.432°W) is located in the Louga province of northern Senegal. Long term mean annual air temperature is 29°C and mean annual precipitation is 416 mm. The vegetation around the site is grazed by livestock and dominated by annual grasses, particularly *Aristida adscensionis*, *Zornia latifolia*, *Eragrostis tremula*, *Dactyloctenium aegyptium*, and *Cenchrus biflorus*. The canopy cover is approximately 3% and comprises *Acacia Senegal*, *Acacia tortilis*, and *Balanites aegyptiaca*. The soils

are sandy with low water holding capacity and organic matter content. A complete description of Dahra is provided in Tagesson et al. (2015b).

Table 1. Basic site characteristics including location in decimal degrees (DD), vegetation and soil types, mean annual precipitation (MAP), and mean annual air temperature at 2 meters height (MAT). The DS and GS in the relative humidity column refer to Dry Season (Nov – Jun) and Growing Season (Jul – Oct), respectively.

Site	Country	Lon Lat (DD)	Vegetation Type	Soil Type	MAP (mm)	MAT (°C)	Rel. Hum. DS/GS (%)	Ref.
Demokeya	Sudan	30.47, 13.28	Sparse acacia savanna	Cambic Arenosols	320	30	16 / 57	Ardö et al. (2008)
Wankama Fallow	Niger	2.63, 13.64	Fallow shrubland	Sandy Ferruginous Arenosols	479	30	28 / 75	Cappelaere et al. (2009)
Dahra	Senegal	-15.43, 15.40	Open woody savanna	Luvic Arenosols	416	29	9 / 63	Tagesson et al. (2015b)

3. Data and Methods

3.1. Field Data

3.1.1. Eddy Covariance Gross Primary Productivity

The eddy covariance (EC) systems at all three sites are equipped with LI7500 open path infrared CO₂/H₂O analyzers (LI-COR Inc., Nebraska, USA) and GILL R3 triple-axis sonic anemometers (GILL Instruments, Lymington, UK). Eddy covariance data were recorded at 20 Hz and averaged over 30-minute periods. The EC method measures net ecosystem exchange of CO₂ (NEE) and following the approach in Tagesson et al. (2015a), NEE was partitioned into GPP and ecosystem respiration (R_{eco}) using a non-linear asymptotic regression with incoming photosynthetically active radiation and vapor pressure deficit as independent variables. Gaps in the time series of NEE, GPP and R_{eco} were consequently gap-filled, again following the method outlined in Tagesson et al. (2015a).

3.1.2. Climatic Variables, Soil Moisture and Temperature

Air temperature (°C) and relative humidity (%) at 2 m were monitored using MP100A Temperature and Relative Humidity Probe (Rotronic) in Demokeya, with Vaisala HMP45C probes (Vaisala Oyj, Helsinki, Finland) in Wankama, and Campbell CS215 (Campbell Scientific, Utah, USA) in Dahra.

Precipitation (mm) was recorded using ARG100 tipping buckets (Campbell Scientific, Utah, USA) at all three sites. Volumetric soil moisture was recorded using CS616 water content reflectometers (Campbell Scientific) in Demokeya and Wankama, and HH2 probe (Delta T Devices) in Dahra. These parameters were recorded every 10 – 30 seconds and averaged for every 30 minutes. Measurement depths varied with site and were dependent on the field campaign. Volumetric soil moisture was summed from top of soil to 50 cm depth in Dahra and Wankama, and to 60 cm depth in Demokeya in order to compute plant available water (see section 3.3.1).

3.2. Earth Observation Data

The Moderate Resolution Imaging Spectroradiometer (MODIS) sensor on board NASA’s Terra and Aqua satellites has a viewing swath width of 2,330 km and images the entire surface of the Earth every one to two days. The MCD43A4 Nadir Bidirectional Reflectance Distribution Function Adjusted Reflectance (NBAR) product is preferable over the other surface reflectance products (MOD09A1/MYD09A1) because it is adjusted using a bidirectional reflectance distribution function to model at-nadir values (Schaaf et al., 2002). The Collection 5.1 MCD43A4 NBAR Level 3 and MOD17 8-day GPP product (MOD17A2) products were downloaded for each site from the Oak Ridge National Laboratory Distributed Active Archive Center (ORNL-DAAC, daac.ornl.gov/modisglobal). These data are provided as ASCII files containing observations within a specified radius around a particular point of interest. We selected a 3 x 3 km radius around each flux tower site based on footprint analysis conducted in Demokeya by Sjöström et al. (2009) and in Dahra by Tagesson et al. (2015c). Land surface temperature (LST) has been found to strongly influence ecosystem respiration (Vancutsem et al., 2010; Jägermeyr et al., 2014) and has been used estimate vapor pressure deficit (Hashimoto et al., 2008). Sims et al. (2008) used LST to characterize temperature and drought stress in a modeling framework that used MODIS enhanced vegetation index (EVI) as a predictor of GPP. In order to test the applicability of LST for improving GPP modeling, we downloaded the MOD11A2/MYD11A2 Level 3 LST product (Collection 5.1) from the ORNL-DAAC database (daac.ornl.gov/modisglobal).

Table 2. Field capacity, soil texture and permanent wilting point (PWP) at the three sites. Soil texture data was included with the soil moisture data provided by the International Soil Monitoring Network (ISMN) (Dorigo et al., 2011). This information was verified against site descriptions provided by the principal investigator at each site. Field capacity and PWP was derived from the Africa Soil Profiles Database (v1.2) (Leenaars et al., 2014) based on the soil texture configuration at each site.

Site	Field Capacity, %	Soil Texture, % (Sand / Silt / Clay)		Permanent Wilting Point, %	
		0 – 30 cm	30 – 100 cm	0 – 30 cm	30 – 100 cm
Demokeya	15	89 / 6 / 5	90 / 5 / 5	2	3
Wankama Fallow	16	90 / 5 / 5	88 / 5 / 7	3	3
Dahra	7	89 / 6 / 5	89 / 5 / 6	2	4

3.3. Methods

3.3.1. Plant Available Water

Plant available water (PAW) is the amount of water present in the soil that can be extracted by roots. PAW is a function of soil type, soil water content at field capacity (moisture left over after percolation) and permanent wilting point (soil moisture that is unavailable to plants). It is an important parameter in the terrestrial water cycle and may have a considerable influence on GPP (Pappas et al., 2013). PAW was calculated as:

$$PAW = (SWC \times 100) - PWP \times D \quad (1)$$

where PAW is plant available water (mm); SWC is volumetric soil water content at field capacity ($\text{m}^3 \text{m}^{-3}$); PWP is the soil texture-dependent permanent wilting point (%) from Table 2; D (mm) is the depth at which the soil moisture measurements were made. The PWP is a biophysical parameter that quantifies the condition where the force exerted by a plant to remove water from the soil (-1500 kPa) is countered by the forces binding the water to the soil (Zotarelli et al., 2010). At this point plant roots cannot extract further water from the soil and sustain growth leading to wilting.

3.3.2. Vapor Pressure Deficit

When plants transpire, the mixture of air and water exiting the stomata is saturated at a relative humidity of ~100% (Dingman, 2015). The maximum amount of water vapor the air can hold at a particular temperature is a function of temperature, so there is potential for higher transpiration at higher temperatures. The climate of the Sahel is generally hot with a mean annual air temperature of 30°C across the three sites. The average relative humidity (RH) across the three sites is 18% in the dry season and 65% in the growing season according to the field measurements. Vapor pressure deficit (VPD) (Anderson, 1936) is the difference between the amount of water in the air and the maximum amount of water the air can hold when it is saturated, and is a limiting factor for Sahelian GPP (Maroco et al., 1997; Boegh et al., 1999; Ago et al., 2015). VPD was calculated from field-measured air temperature (T_a , °C) and relative humidity (RH, %) following the approach described in Ward et al. (2015):

$$e_s = 0.611 \times \exp \left[17.27 \times \frac{T_a}{T_a + 237.3} \right] \quad (2)$$

where e_s is the saturation vapor pressure (kPa) at a certain T_a . Then, the actual vapor pressure (e_a , kPa) is calculated from RH and e_s :

$$e_a = \left(\frac{RH}{100} \right) \times e_s \quad (3)$$

Finally, VPD (kPa) is estimated as the difference between the two:

$$VPD = e_s - e_a \quad (4)$$

3.3.3. Antecedent Precipitation Index

The timing, quantity and effects of previous rainfall on vegetation are important because it takes time for water to percolate through soil and become available for plants. When precipitation occurs, soil moisture conditions evolve as a function of its current degree of saturation. Antecedent precipitation index (API) (Kohler and Linsley, 1951) has been previously used to characterize the influence of past rainfall events on vegetation (Choudhury and Golus, 1988). The formulation of API used here follows Heggen (2001):

$$API = \sum_{P \geq 1}^{n=8} P_t k^{-a} \quad (5)$$

where *API* is the antecedent precipitation index in mm per 8 days; *P_t* is the observed precipitation amount on period *t*; the decay constant, *k*, ranges between 0.80 and 0.98 (Hong et al., 2007) and a value of 0.90 has been applied in this study; *a* is the number of antecedent days.

3.3.4. Enhanced Vegetation Index

The Enhanced Vegetation Index (EVI) (Gao et al., 2000; Huete et al., 2002) utilizes three spectral bands that summarize radiometric and biophysical vegetation characteristics. EVI includes the blue band in addition to the vegetation-sensitive red and near-infrared bands. A set of coefficients and the blue band enhances the vegetation signal by reducing the influence of soil reflectance and atmospheric scattering. Sjöström et al. (2011) and Ma et al. (2013) found that EVI follows the seasonal dynamics of EC GPP better than the MODIS-derived GPP in Sahelian and Australian xeric savannas, respectively.

$$EVI = 2.5 \times \frac{NIR_{B2} - RED_{B1}}{NIR_{B2} + 6 \times RED_{B1} - 7.5 \times BLUE_{B3} + 1} \quad (6)$$

where RED, NIR and BLUE represent MCD43A4 NBAR Level 3 surface reflectance acquired in the red, near infrared and blue portions of the electromagnetic spectrum, respectively. The subscripts denote MODIS NBAR Band 1 (B1), Band 2 (B2), and Band 3 (B3).

3.3.5. Statistical Analysis

Data processing, statistical analysis and visualization were performed in R 3.1.1 (www.r-project.org). Both linear and multiple linear regression (MLR) were used to examine the relationships between VPD, PAW, LST, EVI, NBAR Band 7, and EC GPP. The relationships were used to build GPP models composed of field metrics of water stress and vegetation indices as input data. Additionally partial correlations were performed on both the field and Earth-observation variables

during the greening and browning phases using Spearman's rank order correlation (Spearman, 1904). This was done to assess the relationship of each variable with EC GPP while keeping the influence of the other variables constant. Within each year, the greening phase was delineated as the period from the lowest to the highest GPP value, and the browning was delineated as the following period from maximum GPP to its lowest value. The coefficient of determination (R^2) was calculated as a measure of the amount of EC GPP variance explained by each set of predictor variables. Bayesian information criterion (BIC) (Schwarz, 1978) was chosen to identify the model which best describes the EC GPP data. BIC considers both the goodness of fit and the number of parameters that achieve a certain degree of fit by levying a penalty term $q\log(n)$ on increasing the number of parameters to prevent overfitting:

$$BIC = 2\log(L) + q\log(n) \quad (7)$$

where L is the maximum value log likelihood function, q is the total number of parameters and n is the number of sample points. Root-mean-square error (RMSE) was calculated to evaluate the performance of each model output to EC GPP. RMSE calculates the square root of the variance and smaller values denote better model performance. An RMSE of 0.0 indicates perfect simulation of the EC GPP data.

$$RMSE = \sqrt{\frac{\sum_{i=1}^n (OBS - PRED)^2}{n}} \quad (8)$$

where PRED is the model-estimated GPP ($\text{g C m}^{-2} \text{ day}^{-1}$), OBS is the EC GPP ($\text{g C m}^{-2} \text{ day}^{-1}$), and n is the number of sample points.

4. Results and Discussion

4.1. Seasonal dynamics and inter-annual variability of field data

Mean 8-day rainfall across all three sites was 12 mm in the growing season and 1 mm in the dry season (Figure 3). Growing season average EC GPP was highest in Dahra at $8.6 \text{ g C m}^{-2} \text{ d}^{-1}$, followed by Demokeya at $3.9 \text{ g C m}^{-2} \text{ d}^{-1}$ and Wankama Fallow with $3.5 \text{ g C m}^{-2} \text{ d}^{-1}$. EC GPP was tightly coupled with the unimodal rains and soil moisture. The greening phase was dominated by a rapid decrease in VPD and an increase in the amount of PAW. Growing season EC GPP was attained across all sites when PAW was generally above 25 mm ($\sim 0.04 \text{ m}^3 \text{ m}^{-3}$) and when VPD was below 2 kPa, which is comparable to studies conducted in similar environments (Merbold et al., 2009; Zhao and Ji, 2016). The decline in PAW and the onset of high VPD during times of drought reduces plant photosynthetic capacity by causing closure of stomata to prevent moisture loss (Kutsch et al., 2008). Thus, a decrease in moisture during the growing season, as happened in Dahra in 2011, where there was 42% decrease in rainfall and 46% decrease in soil moisture from the previous year, could cause a reduction in GPP. Indeed, EC GPP in Dahra during the 2011 growing season was 72% less than the previous year. A similar pattern of decline was observed in Demokeya during the 2009 growing season when there was a 25% decrease in rainfall, 14% decrease in soil moisture, and a 9% decrease in GPP from the previous year (Figure 3 a). When rainfall resumes to previous levels, as happened in 2012 in Dahra (Figure 3 c), the herbaceous vegetation respond rapidly to changes in the soil water regime resulting in increased C uptake (Tagesson et al., 2016b). The speed of vegetation response to the resumption in rainfall could be due to land memory effects (Schwinning et al., 2004).

The seasonal variability of the field parameters, PAW, VPD and EC GPP, was fairly consistent across all sites (Figure 3). However, Dahra had the highest average EC GPP during the growing season ($8.6 \text{ g C m}^{-2} \text{ d}^{-1}$) despite having similar climatic and subsurface conditions as the other two sites (Table 1). A recent study by Tagesson et al. (2016a) provided two plausible reasons for the higher photosynthetic capacity at Dahra: (1) 80% of the vegetative cover at Dahra is comprised of herbaceous C_4 plants, signifying a higher concentration of plants that are more productive under optimal climatic conditions (i.e. during the growing season), and (2) intense grazing disturbance causes plants to develop strategies that allocate more C to leaves thereby increasing their leaf area index and leading to increase in absorbed photosynthetically active radiation and C assimilation. A third plausible reason for the high EC GPP at Dahra is linked to the increase in relative humidity which ranges from 9% in the dry season to 63% in the growing season (Table 1). This is connected to the movement of the inter-tropical convergence zone (ITCZ) and the West African Monsoon, which transports moist air from the Gulf of Guinea to West Africa (Steiner et al., 2009; Tagesson et al., 2015b; Tagesson et al., 2016b). This large influx of humid air could allow the stomata to remain open longer during the growing season, thus enabling enhanced C uptake without increased water loss through transpiration. Growing season (July – October) API in Dahra was 153% higher than Demokeya and 57% higher than Wankama Fallow, and had higher intra-seasonal variability (standard deviation = 171%). This is also probably due to West African Monsoon, which causes higher amounts of rainfall at Dahra (Sultan et al., 2003; Messenger et al., 2004; Steiner et al., 2009; Browne and Sylla, 2012).

Table 3. Summary of the regression analysis between EC GPP and three field-measured water stress controls: plant available water (PAW), vapor pressure deficit (VPD) and antecedent precipitation index (API) for each site.

Response = EC GPP		Statistics		
Demokeya	RMSE	R²	n	BIC
API	1.61	0.28	97	382.04
VPD	1.22	0.59	95	321.88
PAW	1.19	0.62	89	298.27
VPD + API	1.22	0.59	95	326.36
API + PAW	1.19	0.62	89	301.82
PAW + VPD	1.12	0.66	89	291.87
Wankama Fallow	RMSE	R²	n	BIC
API	1.54	0.33	159	605.44
VPD	0.96	0.74	157	448.70
PAW	0.91	0.76	132	365.07
VPD + API	0.94	0.75	156	445.64
API + PAW	0.91	0.77	131	366.92
PAW + VPD	0.77	0.83	129	318.23
Dahra	RMSE	R²	n	BIC
API	2.91	0.38	161	815.93
PAW	2.51	0.59	154	736.34
VPD	1.99	0.75	146	631.43
API + PAW	2.28	0.64	147	680.49
VPD + API	1.92	0.77	146	624.80
VPD + PAW	1.88	0.77	139	590.21
All Sites	RMSE	R²	n	BIC
API	2.37	0.33	417	1888.05
PAW	2.27	0.36	375	1780.69
VPD	2.21	0.43	398	1779.50
VPD + API	2.22	0.44	390	1697.36
API + PAW	2.18	0.45	367	1652.43
PAW + VPD	2.06	0.47	364	1624.53

Table 4. Summary of the partial correlation analysis between EC GPP and field and Earth observation variables during the greening and browning phases. r_s is Spearman's Rho, t_s is the test statistic, and P is the significance of the test statistic

Response = EC GPP	Greening Phase n = 106			Browning Phase n = 75		
	r_s	t_s	P	r_s	t_s	P
PAW	0.44	4.950	< 0.01	0.16	0.156	0.18
VPD	-0.24	-2.525	0.01	-0.52	-0.523	< 0.01
EVI	0.61	7.776	< 0.05	0.60	6.289	< 0.01
LST	-0.28	-2.957	< 0.05	-0.34	-3.074	< 0.01
BAND 7	0.32	3.426	< 0.05	0.22	1.920	0.06

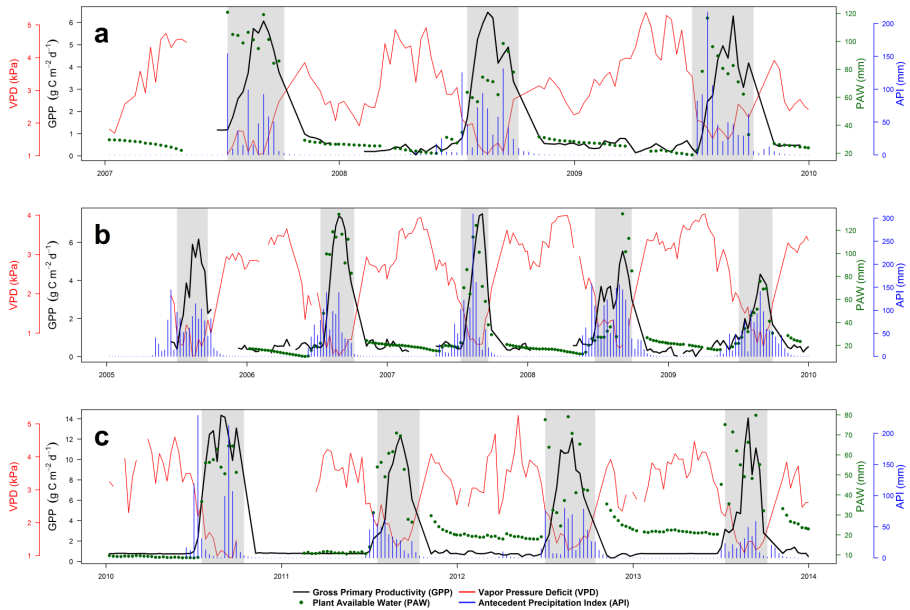


Figure 3. Site-level 8-day data for surface and subsurface conditions in (a) Demokeya, (b) Wankama Fallow, (c) Dahra. The shading indicates the growing season (July – October).

Table 5. Summary of the regression analysis between EC GPP, land surface temperature (LST), Enhanced Vegetation Index (EVI), and MODIS NBAR bands.

Response = EC GPP		Statistics			
Demokeya	RMSE	R²	n	BIC	
BAND 7	1.70	0.20	97	392.13	
LST	1.44	0.40	94	349.51	
EVI	0.60	0.89	97	184.09	
MOD17 GPP	0.89	0.77	95	262.10	
EVI + LST	0.58	0.89	94	180.95	
EVI + BAND 7	0.51	0.93	97	161.24	
EVI + BAND7 + LST	0.48	0.93	94	155.54	
Wankama Fallow	RMSE	R²	n	BIC	
LST	1.55	0.33	155	592.58	
BAND 7	1.36	0.50	158	559.78	
EVI	0.96	0.74	158	450.78	
MOD17 GPP	1.43	0.44	123	452.12	
EVI + LST	0.94	0.76	154	444.33	
EVI + BAND 7	0.90	0.78	158	435.56	
EVI + BAND7 + LST	0.67	0.88	154	344.91	
Dahra	RMSE	R²	n	BIC	
BAND 7	2.73	0.38	156	772.01	
LST	2.35	0.58	163	747.90	
EVI	1.00	0.91	156	459.54	
MOD17 GPP	1.35	0.86	166	587.48	
EVI + LST	0.96	0.92	153	442.79	
EVI + BAND 7	0.93	0.93	156	440.53	
EVI + BAND7 + LST	0.85	0.96	153	414.90	
All Sites	RMSE	R²	n	BIC	
BAND 7	2.18	0.32	411	1826.60	
LST	2.03	0.42	412	1767.47	
EVI	1.04	0.83	411	1220.91	
MOD17 GPP	1.39	0.76	384	1362.45	
EVI + LST	0.96	0.86	401	1131.69	
EVI + BAND 7	0.91	0.88	411	1112.77	
EVI + BAND7 + LST	0.84	0.89	401	1023.90	

4.2. Relationship between field data and eddy covariance gross primary productivity

Cross-site relationships of PAW and VPD with EC GPP were fairly moderate ($R^2 = 0.36$ and 0.43 , respectively). The relationships at the individual sites were varied with R^2 values of VPD ranging between 0.59 and 0.75 and those of PAW between 0.59 and 0.76 (Table 3). API was the worst performing variable averaging a cross-site R^2 of 0.33 . The combination of PAW and VPD explained the largest variance across all three sites ($R^2 = 0.47$, $RMSE = 2.06 \text{ g C m}^{-2} \text{ d}^{-1}$), with the highest R^2 and lowest RMSE at Wankama Fallow ($R^2 = 0.83$, $RMSE = 0.77 \text{ g C m}^{-2} \text{ d}^{-1}$) (Table 3).

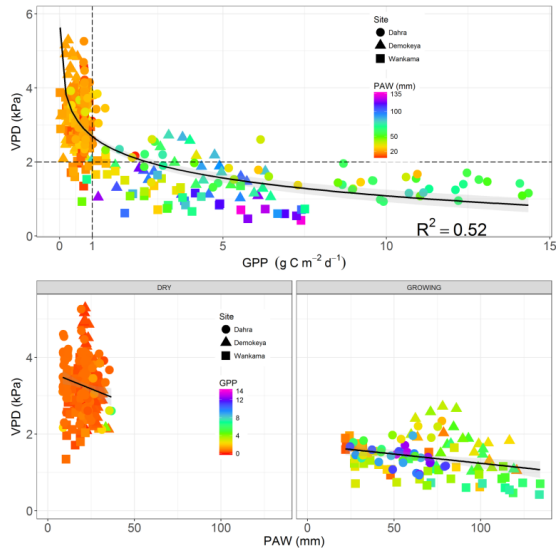


Figure 4. Top: Comparison of VPD and EC GPP, with coloring that indicates corresponding values of PAW for each site. Values to the left of the vertical dotted line ($\text{GPP} < 1 \text{ g C m}^{-2} \text{ d}^{-1}$) and above the horizontal dotted line ($\text{VPD} > 2 \text{ kPa}$) represent the dry season. Bottom: Relationship between the VPD and PAW per corresponding GPP values during the dry and growing seasons. The solid black line is the regression line with 95% confidence interval in light gray shading.

An overview of the relationship between EC GPP, VPD and PAW across all sites is shown in Figure 4. The dry season is characterized by high VPD ($> 2 \text{ kPa}$), which is linked to the reduction in evapotranspiration due to low PAW. With the reduction/closure of stomatal conductance, plants deactivate metabolic activity in the shoots to reduce consumption of water (and subsequent transpiration) while simultaneously enhancing uptake of water and nutrients by the roots to mitigate the effect of the dry season (Gargallo-Garriga et al., 2014). In the wetter savanna systems of the humid region ($> 750 \text{ mm MAP}$), it has been shown that a considerable amount of C is stored in the roots at the start of the dry season and is subsequently used by the herbaceous vegetation to re-sprout at the start of the next growing season (Otieno et al., 2010). If the dry season is intense, prolonged, or both, this memory effect allows vegetation to tap into these C reserves and maintain root respiration (Hasibeder et al., 2015). A recent global study by Murray-Tortarolo et al. (2016) lends support to this, finding that the intensity and duration of the dry season has a larger impact on annual primary productivity than increased rainfall in the rainy season. Thus, a similar mechanism may take place in

the poorer soils of the Sahel, where the herbaceous species are specialized to grow quickly at the beginning of the rainy season (Tagesson et al., 2016b). These subsurface mechanisms can in turn be influenced by anthropogenic activity as soil moisture amount and availability are influenced by land management practices (Ardö and Olsson, 2004; Ardö et al., 2008).

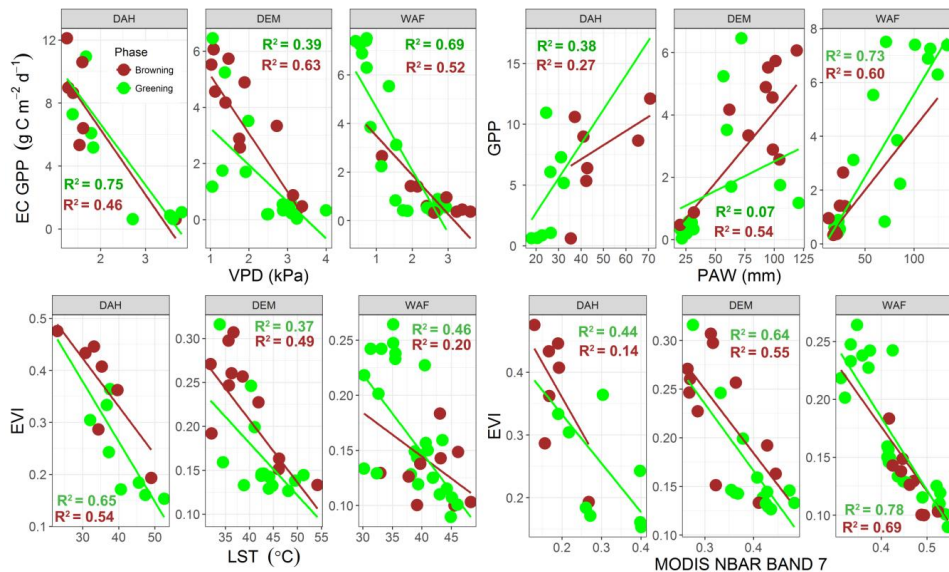


Figure 5. Scatterplots of the relationships between the field variables EC GPP, PAW and VPD (top row) and MODIS-derived variables (bottom row) during the greening (green color) and browning (brown color) on a per-site basis. (DAH = Dahra, DEM = Demokeya, WAF = Wankama Fallow).

When the rainy season commences, not only is soil water replenished and root water uptake increased, but VPD is reduced due to humid air masses from the northward movement of the ITCZ. In Wankama Fallow, maximum EC GPP is reached when PAW is greater than 125 mm and VPD is below 1.5 kPa, while in Demokeya maximum EC GPP occurs when PAW is above 90 mm and VPD is below 2 kPa. At Dahra maximum EC GPP was reached at VPD levels similar to Demokeya and Wankama Fallow, however, PAW was relatively low compared to the other two sites at ~60 mm. The partial correlation analysis revealed that the increase in C uptake during the greening phase, shortly after the onset of the first rains, is governed by the availability of PAW and a reduction in VPD (Table 4). The increase in soil moisture also decreases LST ($r_s = -0.28$) due to evaporative cooling. These are further illustrated by scatterplot in Figure 5. The browning phase is characterized by a steep decrease in GPP and a reduction in PAW due to a cessation of the rains. The relationship of EC GPP, VPD and PAW were generally strong during both the greening and browning phases (Figure 5). The mechanism by which VPD and PAW interact is further illustrated in Figure 6, which uses the 2009 growing season in Demokeya as an example. The first rains occurred on July 4th, however, the relative humidity began to increase from a mean of 15% in April and May, which is typical of the dry season, to 32% in June. Between July 4th and September 1st (the larger shaded area in Figure 6), the mean relative humidity was 64%. The effect of the increase in relative humidity, and decrease in VPD, a full month before the

first rains is particularly interesting. This can play the role of an anticipatory mechanism for vegetation that enables it to begin photosynthesis rapidly at, or shortly before, the onset of rain (De Bie et al., 1998). The second GPP peak (smaller shaded area in Figure 6) can be explained by the second, smaller, rainfall event of that year, which was not sufficient enough to replenish PAW to previous levels. However, it created enough reduction in VPD that stimulated the vegetation to resume C assimilation (Figure 6).

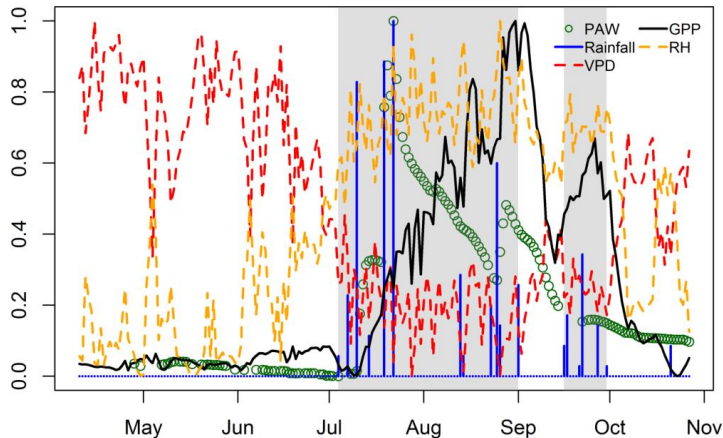


Figure 6. A narrowed-down example of a typical Sahelian growing season exemplified here by the 2009 growing season in Demokeya. Relative humidity (RH) begins to increase and vapor pressure deficit (VPD) begins to decrease a full month before the onset of the rainy season. Once the rains fall, plant available water (PAW) is replenished and GPP begins to increase commencing the greening phase. Although PAW has been gradually decreasing during the growing season, the decrease in rainfall prompts a decrease in RH and an increase in VPD, which sharply reduced GPP due to stomatal closure. All variables have been normalized to between zero and one for visual purposes.

4.3. Eddy covariance gross primary productivity and MODIS-derived data

EVI was strongly correlated with EC GPP across all sites ($R^2 = 0.83$, $RMSE = 1.04 \text{ g C m}^{-2} \text{ d}^{-1}$) (Table 5). The partial correlation of the MODIS data showed that the EVI was closely coupled with EC GPP during both greening and browning phases (Table 4). The decline in PAW during the browning phase leads to a reduction in transpiration and latent heat flux and an increase in sensible heat flux and LST ($r_s = -0.34$) (Table 4, Figure 5). MODIS NBAR Band 7 exhibits a positive response during the greening ($r_s = 0.32$) and browning phases ($r_s = 0.22$), probably due to the band's sensitivity to changes in soil moisture during the wetting and drying phases. The relationship between EVI, LST, and MODIS NBAR Band 7 is shown in Figure 7. The slope of the regression line during the dry season ($\beta_1 = -0.24$) shows a rapid increase MODIS NBAR Band 7 for each unit decrease in EVI, whereas the change is more gradual during the growing season (Figure 7). Both MODIS NBAR Band 7 ($0.20 < R^2 < 0.50$) and LST ($0.33 < R^2 < 0.58$) had generally moderate relationships with EC GPP. However, when LST and MODIS NBAR Band 7 were included in an MLR model together with EVI, the combination was able to consistently explain higher variance ($R^2 \geq 0.88$) across all sites (Figure 8).

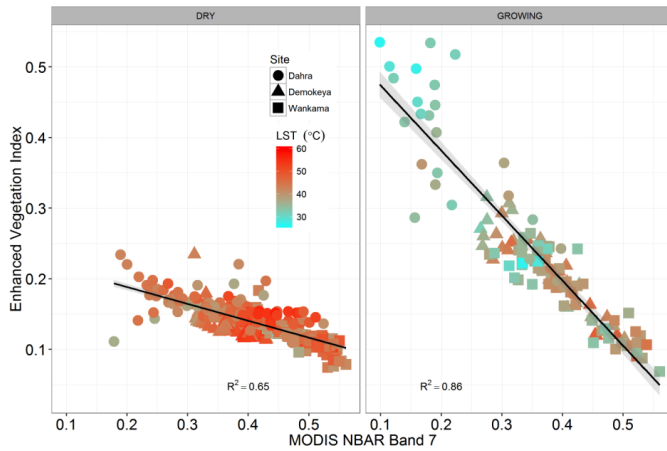


Figure 7. Comparison of EVI and MODIS NBAR Band 7, with coloring that indicates corresponding values of LST for each site during the growing (July – October) and dry season (November – June). The solid black line is the regression line with 95% confidence interval in light gray shading.

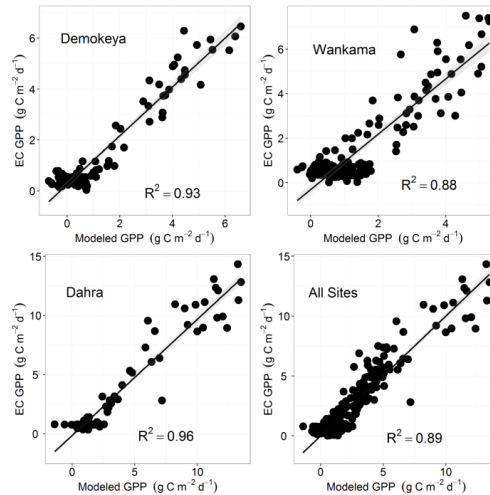


Figure 8. Cross-site relationship between the MLR GPP model (\sim EVI+Band7+LST) and 8-day EC GPP. The solid black line is the regression line with 95% confidence interval in light gray shading.

Both EVI and MLR GPP follow the seasonal progression of EC GPP well, but the MLR GPP model tracks the dry season EC GPP better than EVI (Figure 9). The inclusion of LST and MODIS NBAR Band 7 improves the variance explained by 6.7% from 0.83 for EVI to 0.89 for the MLR model comprising EVI, LST and MODIS NBAR Band 7 while decreasing the BIC from 1221 to 1024 (Table 5). When the data is split into the individual sites, a similar pattern emerges with the explained

variance of MLR model over EVI increasing between 4.3% in Demokeya to 15.9% in Wankama (Table 5). The MLR GPP model for all the sites is shown in Equation 6:

$$GPP = -4.28 + [(34.51 \times EVI) + (-0.06 \times LST) + (7.81 \times BAND7)] \quad (6)$$

The ability of the MLR model to explain cross-site variability in EC GPP was improved (from 85% to 89%) when data from both the growing and dry seasons were included in the model. Although, there is no green herbaceous vegetation during the dry season, the small C fluxes that were observed could be due to the sparse tree cover (Ardö et al., 2008). It is reasonable to assume that the dry season signal contains information about land memory effects (Fontaine et al., 2007; Dirmeyer et al., 2009). However, it is unlikely that such effects would be passed on through soil moisture since upper layer dries out within two months of the start of the dry season (Shinoda and Yamaguchi, 2003). Thus, such a memory could be retained in the dormant seeds, roots and foliage (Hiernaux et al., 1994; Schwinning et al., 2004).

The spectral range of MODIS NBAR Band 7 is most sensitive to surface soil water content in general, and the rate of evaporation during the dry season in particular (Tian and Philpot, 2015). This is discernible in the relatively rapid increase of the surface reflectance of MODIS NBAR Band 7 compared to the decrease in EVI in response to the decline of the vegetative cover during the dry season (Figure 7). On the other hand, LST is linked to VPD due to the feedback between land (vegetated or bare) and near-surface air (Hashimoto et al., 2008). This is clearly shown in the relationship between EVI and LST during both the greening and browning phases in Figure 5. There have been other recent attempts to model GPP in water limited regions using EVI combined with other variables. For example, in a tropical xeric savanna ecosystem, Ma et al. (2014) were able to explain 88% of the variability in EC GPP by parameterizing ecosystem light use efficiency using MODIS EVI and top-of-atmosphere photosynthetically active radiation. In another study, Sjöström et al. (2011) found that the combination of MODIS EVI with flux tower-derived evaporative fraction, as a proxy of water availability, and photosynthetically active radiation significantly improved the modeling of EC GPP for seven African sites, including Demokeya and Wankama Fallow, with up to 73% of the variance explained. Using only Earth observation data, our model is able to explain 89% of the variance in EC GPP across the three Sahelian sites.

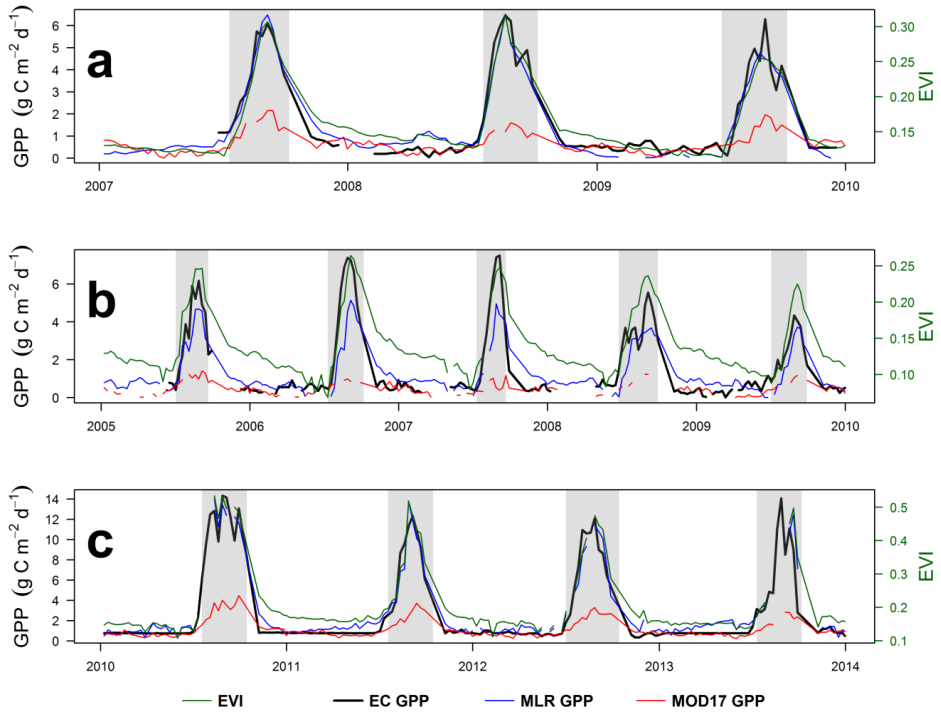


Figure 9. Cross-site comparison of 8-day EC GPP, EVI, the MLR GPP model, and MOD17 GPP for (a) Demokeya, (b) Wankama Fallow and (c) Dahra. The shading indicates the growing season (July – October).

5. Conclusions

Hydrological processes generally control vegetation dynamics at multiple spatial and temporal scales. This is particularly true for the Sahel, where the short unimodal rainy season induces a net CO_2 uptake that is driven mainly by the herbaceous canopy (Tagesson et al., 2016b). Except in highly humid environments, all plants undergo photosynthesis at the expense of losing moisture to the atmosphere. This moisture loss is particularly significant for dryland vegetation where an imbalance can occur between the amount of water plants require and the limited amount that is available in the ecosystem. In this study, we found that the two main moisture-related biophysical limitations, PAW and VPD together control plant CO_2 uptake in the semi-arid conditions. With the start of the dry season in November, low PAW is present in the drying soils of the Sahel, which leads to decreased availability of water for uptake by plant roots (Figures 3 and 4). This, in turn, reduces evapotranspiration (latent heat) due to drier soils and plants close their stomata to prevent moisture loss.

Considering both the importance of drylands in the global C cycle (Ahlström et al., 2015) and the dependence of human livelihoods on the products of photosynthesis (Abdi et al., 2014), it is essential account for water stress controls in order to better model primary productivity in this region. This is particularly important considering the fact that there is a chronic lack of field data on C fluxes in the Sahel. We found that the combination of MODIS NBAR Band 7 as a proxy for soil moisture variability, LST as a proxy for VPD, and EVI as a proxy of photosynthetic activity in an MLR model was able to explain 89% of the variability of EC GPP across the three Sahelian sites (Figures 8 and 9). Since EVI, LST, and MODIS NBAR Band 7 are based on Earth observation data, the MLR model presented here is potentially scalable with repeatable estimates of GPP at relatively high spatial and temporal resolutions. Moreover, the availability of standardized EC flux measurements, such as the recently released FLUXNET2015 database, can potentially eliminate variability in systematic and processing-induced uncertainties between sites. This can further improve model estimates when relating EC GPP with Earth observation data. Studies of the C cycle often focus on the growing season as it is the principal period where C assimilation takes place, however, the inclusion of dry season dynamics can potentially improve the explanatory capacity of GPP models by accounting for land memory effects. Further evaluation of this approach using more dryland sites from the FLUXNET2015 database as well as other types of in-situ validation data is required to test its efficiency in modeling GPP in water-limited areas.

Acknowledgments

AMA received support from the Lund University Center for Studies of Carbon Cycle and Climate Interactions (LUCCI) and the Royal Physiographic Society in Lund. Data for the Wankama (Niger) site were produced through the AMMA-CATCH regional observatory, funded by the French IRD and INSU national research institutes. Funding for this project was provided by the Swedish National Space Board (contract no. 100/11 to JA).

Author contributions

AMA conceived and designed the study, conducted the analysis, interpreted the results, and wrote the paper. JA, DET and TT assisted with the study design and the interpretation of the results. NBO contributed to the analysis and the interpretation of the results. BC provided site data for Wankama and approved the final manuscript. All authors discussed the results and revised the manuscript.

Competing interests

The authors declare that they have no competing interests.

References

- Abdi AM, Seaquist J, Tenenbaum DE, et al. (2014) The supply and demand of net primary production in the Sahel. *Environmental Research Letters* 9: 094003.
- Ago EE, Serça D, Agbossou EK, et al. (2015) Carbon dioxide fluxes from a degraded woodland in West Africa and their responses to main environmental factors. *Carbon Balance and Management* 10: 1-16.
- Ahlström A, Raupach MR, Schurgers G, et al. (2015) The dominant role of semi-arid ecosystems in the trend and variability of the land CO₂ sink. *Science* 348: 895-899.
- Anderson DB. (1936) Relative Humidity or Vapor Pressure Deficit. *Ecology* 17: 277-282.
- Ardö J. (2016) Increasing the Confidence of African Carbon Cycle Assessments. *EGU General Assembly Conference Abstracts*. 10008.
- Ardö J, Molder M, El-Tahir BA, et al. (2008) Seasonal variation of carbon fluxes in a sparse savanna in semi arid Sudan. *Carbon Balance Manag* 3: 7.
- Ardö J and Olsson L. (2004) Soil Carbon Sequestration in Traditional Farming in Sudanese Dry Lands. *Environmental Management* 33: S318-S329.
- Boegh E, Soegaard H, Hanan N, et al. (1999) A Remote Sensing Study of the NDVI–Ts Relationship and the Transpiration from Sparse Vegetation in the Sahel Based on High-Resolution Satellite Data. *Remote Sensing of Environment* 69: 224-240.
- Boulain N, Cappelaere B, Ramier D, et al. (2009) Towards an understanding of coupled physical and biological processes in the cultivated Sahel – 2. Vegetation and carbon dynamics. *Journal of Hydrology* 375: 190-203.
- Brandt M, Hiernaux P, Rasmussen K, et al. (2016) Assessing woody vegetation trends in Sahelian drylands using MODIS based seasonal metrics. *Remote Sensing of Environment* 183: 215-225.
- Brandt M, Mbow C, Diouf AA, et al. (2015) Ground- and satellite-based evidence of the biophysical mechanisms behind the greening Sahel. *Global Change Biology* 21: 1610-1620.
- Browne NAK and Sylla MB. (2012) Regional Climate Model Sensitivity to Domain Size for the Simulation of the West African Summer Monsoon Rainfall. *International Journal of Geophysics* 2012: 1-17.
- Cappelaere B, Descroix L, Lebel T, et al. (2009) The AMMA-CATCH experiment in the cultivated Sahelian area of south-west Niger – Investigating water cycle response to a fluctuating climate and changing environment. *Journal of Hydrology* 375: 34-51.
- Choudhury BJ and Golus RE. (1988) Estimating soil wetness using satellite data. *International Journal of Remote Sensing* 9: 1251-1257.
- Dardel C, Kergoat L, Hiernaux P, et al. (2014) Re-greening Sahel: 30 years of remote sensing data and field observations (Mali, Niger). *Remote Sensing of Environment* 140: 350-364.
- De Bie S, Ketner P, Paasse M, et al. (1998) Woody plant phenology in the West Africa savanna. *Journal of Biogeography* 25: 883-900.
- Dingman SL. (2015) *Physical Hydrology: Third Edition*: Waveland Press.
- Dirmeyer PA, Schlosser CA and Brubaker KL. (2009) Precipitation, Recycling, and Land Memory: An Integrated Analysis. *Journal of Hydrometeorology* 10: 278-288.
- Dorigo WA, Wagner W, Hohensinn R, et al. (2011) The International Soil Moisture Network: a data hosting facility for global in situ soil moisture measurements. *Hydrol. Earth Syst. Sci.* 15: 1675-1698.
- Eklundh L and Olsson L. (2003) Vegetation index trends for the African Sahel 1982 - 1999. *Geophys. Res. Lett.* 30: 1430.
- Ellis J and Galvin KA. (1994) Climate patterns and land-use practices in the dry zones of Africa. *BioScience* 44: 340-349.
- Fontaine B, Louvet S and Roucou P. (2007) Fluctuations in annual cycles and inter-seasonal memory in West Africa: rainfall, soil moisture and heat fluxes. *Theoretical and applied climatology* 88: 57-70.

- Gao X, Huete AR, Ni W, et al. (2000) Optical–Biophysical Relationships of Vegetation Spectra without Background Contamination. *Remote Sensing of Environment* 74: 609-620.
- Gargallo-Garriga A, Sardans J, Pérez-Trujillo M, et al. (2014) Opposite metabolic responses of shoots and roots to drought. *Scientific Reports* 4: 6829.
- Hashimoto H, Dungan JL, White MA, et al. (2008) Satellite-based estimation of surface vapor pressure deficits using MODIS land surface temperature data. *Remote Sensing of Environment* 112: 142-155.
- Hasibeder R, Fuchslueger L, Richter A, et al. (2015) Summer drought alters carbon allocation to roots and root respiration in mountain grassland. *New Phytologist* 205: 1117-1127.
- Heggen RJ. (2001) Normalized Antecedent Precipitation Index. *Journal of Hydrologic Engineering* 6: 377-381.
- Hickler T, Eklundh L, Seaquist JW, et al. (2005) Precipitation controls Sahel greening trend. *Geophysical Research Letters* 32: L21415.
- Hiernaux P, Cissé M, Diarra L, et al. (1994) Fluctuations saisonnières de la feuillaison des arbres et des buissons sahéliens. Conséquences pour la quantification des ressources fourragères. *Revue d'élevage et de médecine vétérinaire des pays tropicaux* 47: 117-125.
- Hiernaux P and Le Houérou HN. (2006) Les parcours du Sahel. *Science et changements planétaires/Sécheresse* 17: 51-71.
- Hong Y, Adler RF, Hossain F, et al. (2007) A first approach to global runoff simulation using satellite rainfall estimation. *Water Resources Research* 43: n/a-n/a.
- Huete A, Didan K, Miura T, et al. (2002) Overview of the radiometric and biophysical performance of the MODIS vegetation indices. *Remote Sensing of Environment* 83: 195-213.
- Jägermeyr J, Gerten D, Lucht W, et al. (2014) A high-resolution approach to estimating ecosystem respiration at continental scales using operational satellite data. *Global Change Biology* 20: 1191-1210.
- Kohler M and Linsley R. (1951) Predicting the runoff from storm rainfall. *US Weather Bureau Research Papers*. Washington, DC: National Oceanic and Atmospheric Administration.
- Kutsch WL, Hanan N, Scholes B, et al. (2008) Response of carbon fluxes to water relations in a savanna ecosystem in South Africa. *Biogeosciences* 5: 1797-1808.
- Le Houérou HN. (1989) Definition, Geographical Limits, Contacts with Other Ecoclimatic Zones. *The Grazing Land Ecosystems of the African Sahel*. Berlin, Heidelberg: Springer Berlin Heidelberg, 1-16.
- Leenaars J, van Oostrum A and Ruiperez Gonzalez M. (2014) Africa Soil Profiles Database, version 1.2. A compilation of geo-referenced and standardised legacy soil profile data for sub-Saharan Africa (with dataset). *Africa Soil Information Service (AfSIS) Project*. Wageningen, the Netherlands: ISRIC – World Soil Information.
- Liang S, Zhong B and Fang H. (2006) Improved estimation of aerosol optical depth from MODIS imagery over land surfaces. *Remote Sensing of Environment* 104: 416-425.
- Lobell DB and Asner GP. (2002) Moisture Effects on Soil Reflectance. *Soil Science Society of America Journal* 66: 722-727.
- Ma X, Huete A, Yu Q, et al. (2013) Spatial patterns and temporal dynamics in savanna vegetation phenology across the North Australian Tropical Transect. *Remote Sensing of Environment* 139: 97-115.
- Ma X, Huete A, Yu Q, et al. (2014) Parameterization of an ecosystem light-use-efficiency model for predicting savanna GPP using MODIS EVI. *Remote Sensing of Environment* 154: 253-271.
- Maroco J, Attilde P, et al. (1997) Stomatal Responses to Leaf-to-Air Vapour Pressure Deficit in Sahelian Species. *Functional Plant Biology* 24: 381-387.
- Merbold L, Ardö J, Arneith A, et al. (2009) Precipitation as driver of carbon fluxes in 11 African ecosystems. *Biogeosciences* 6: 1027-1041.
- Messenger C, Gallée H and Brasseur O. (2004) Precipitation sensitivity to regional SST in a regional climate simulation during the West African monsoon for two dry years. *Climate Dynamics* 22: 249-266.

- Moncrieff JB, Monteny B, Verhoef A, et al. (1997) Spatial and temporal variations in net carbon flux during HAPEX-Sahel. *Journal of Hydrology* 188: 563-588.
- Monteith JL. (1972) Solar radiation and productivity in tropical ecosystems. *Journal of Applied Ecology* 9: 747-766.
- Murray-Tortarolo G, Friedlingstein P, Sitch S, et al. (2016) The dry season intensity as a key driver of NPP trends. *Geophysical Research Letters* 43: 2632-2639.
- Nicholson SE. (2011) *Dryland Climatology*: Cambridge University Press.
- Nicholson SE, Tucker CJ and Ba M. (1998) Desertification, drought, and surface vegetation: An example from the West African Sahel. *Bulletin of the American Meteorological Society* 79: 815-830.
- Nutini F, Boschetti M, Candiani G, et al. (2014) Evaporative Fraction as an Indicator of Moisture Condition and Water Stress Status in Semi-Arid Rangeland Ecosystems. *Remote Sensing* 6: 6300.
- Olsson L and Ardö J. (2002) Soil carbon sequestration in degraded semiarid agro-ecosystems-perils and potentials. *AMBIO: A Journal of the Human Environment* 31: 471-477.
- Olsson L, Eklundh L and Ardö J. (2005) A recent greening of the Sahel—trends, patterns and potential causes. *Journal of Arid Environments* 63: 556-566.
- Otieno DO, K'Otuto GO, Maina JN, et al. (2010) Responses of ecosystem carbon dioxide fluxes to soil moisture fluctuations in a moist Kenyan savanna. *Journal of Tropical Ecology* 26: 605-618.
- Pappas C, Fatichi S, Leuzinger S, et al. (2013) Sensitivity analysis of a process-based ecosystem model: Pinpointing parameterization and structural issues. *Journal of Geophysical Research: Biogeosciences* 118: 505-528.
- Philippon N, Martiny N, Camberlin P, et al. (2014) Timing and Patterns of the ENSO Signal in Africa over the Last 30 Years: Insights from Normalized Difference Vegetation Index Data. *Journal of Climate* 27: 2509-2532.
- Prince SD. (1991) Satellite remote sensing of primary production: comparison of results for Sahelian grasslands 1981-1988. *International Journal of Remote Sensing* 12: 1301-1311.
- Running SW, Thornton PE, Nemani RR, et al. (2000) Global terrestrial gross and net primary productivity from the Earth Observing System. In: Sala OE, Mooney HA and Howarth RW (eds) *Methods in Ecosystem Science*. Springer-Verlag, New York, 44-57.
- Sadeghi M, Jones SB and Philpot WD. (2015) A linear physically-based model for remote sensing of soil moisture using short wave infrared bands. *Remote Sensing of Environment* 164: 66-76.
- Schaaf CB, Gao F, Strahler AH, et al. (2002) First operational BRDF, albedo nadir reflectance products from MODIS. *Remote Sensing of Environment* 83: 135-148.
- Schwarz G. (1978) Estimating the Dimension of a Model. *The Annals of Statistics* 6: 461-464.
- Schwinning S, Sala OE, Loik ME, et al. (2004) Thresholds, memory, and seasonality: understanding pulse dynamics in arid/semi-arid ecosystems. *Oecologia* 141: 191-193.
- Seaquist J, Olsson L, Ardö J, et al. (2006) Broad-scale increase in NPP quantified for the African Sahel, 1982–1999. *International Journal of Remote Sensing* 27: 5115-5122.
- Shinoda M and Yamaguchi Y. (2003) Influence of Soil Moisture Anomaly on Temperature in the Sahel: A Comparison between Wet and Dry Decades. *Journal of Hydrometeorology* 4: 437-447.
- Sims DA, Rahman AF, Cordova VD, et al. (2008) A new model of gross primary productivity for North American ecosystems based solely on the enhanced vegetation index and land surface temperature from MODIS. *Remote Sensing of Environment* 112: 1633-1646.
- Sjöström M, Ardö J, Arneth A, et al. (2011) Exploring the potential of MODIS EVI for modeling gross primary production across African ecosystems. *Remote Sensing of Environment* 115: 1081-1089.
- Sjöström M, Ardö J, Eklundh L, et al. (2009) Evaluation of satellite based indices for gross primary production estimates in a sparse savanna in the Sudan. *Biogeosciences* 6: 129-138.
- Sjöström M, Zhao M, Archibald S, et al. (2013) Evaluation of MODIS gross primary productivity for Africa using eddy covariance data. *Remote Sensing of Environment* 131: 275-286.

- Spearman C. (1904) The Proof and Measurement of Association between Two Things. *The American Journal of Psychology* 15: 72-101.
- Steiner AL, Pal JS, Rauscher SA, et al. (2009) Land surface coupling in regional climate simulations of the West African monsoon. *Climate Dynamics* 33: 869-892.
- Sultan B, Janicot S and Diedhiou A. (2003) The West African Monsoon Dynamics. Part I: Documentation of Intraseasonal Variability. *Journal of Climate* 16: 3389-3406.
- Tagesson T, Ardö J, Guiro I, et al. (2016a) Very high CO₂ exchange fluxes at the peak of the rainy season in a West African grazed semi-arid savanna ecosystem. *Geografisk Tidsskrift-Danish Journal of Geography* 116: 93-109.
- Tagesson T, Fensholt R, Cappelaere B, et al. (2016b) Spatiotemporal variability in carbon exchange fluxes across the Sahel. *Agricultural and Forest Meteorology* 226–227: 108-118.
- Tagesson T, Fensholt R, Cropley F, et al. (2015a) Dynamics in carbon exchange fluxes for a grazed semi-arid savanna ecosystem in West Africa. *Agriculture, ecosystems & environment* 205: 15-24.
- Tagesson T, Fensholt R, Guiro I, et al. (2015b) Ecosystem properties of semiarid savanna grassland in West Africa and its relationship with environmental variability. *Global Change Biology* 21: 250-264.
- Tagesson T, Fensholt R, Huber S, et al. (2015c) Deriving seasonal dynamics in ecosystem properties of semi-arid savanna grasslands from in situ-based hyperspectral reflectance. *Biogeosciences* 12: 4621-4635.
- Tian J and Philpot WD. (2015) Relationship between surface soil water content, evaporation rate, and water absorption band depths in SWIR reflectance spectra. *Remote Sensing of Environment* 169: 280-289.
- Tucker CJ, Vanpraet C, Boerwinkel E, et al. (1983) Satellite remote sensing of total dry matter production in the Senegalese Sahel. *Remote Sensing of Environment* 13: 461-474.
- Vancutsem C, Ceccato P, Dinku T, et al. (2010) Evaluation of MODIS land surface temperature data to estimate air temperature in different ecosystems over Africa. *Remote Sensing of Environment* 114: 449-465.
- Velluet C, Demarty J, Cappelaere B, et al. (2014) Building a field- and model-based climatology of local water and energy cycles in the cultivated Sahel – annual budgets and seasonality. *Hydrol. Earth Syst. Sci.* 18: 5001-5024.
- Verhoef A, Allen SJ, Bruin HAR, et al. (1996) Fluxes of carbon dioxide and water vapour from a Sahelian savanna. *Agric For Meteorol.* 80.
- Vrieling A, de Leeuw J and Said M. (2013) Length of Growing Period over Africa: Variability and Trends from 30 Years of NDVI Time Series. *Remote Sensing* 5: 982-1000.
- Ward AD, Trimble SW, Burckhard SR, et al. (2015) *Environmental Hydrology, Third Edition*: CRC Press.
- Weidong L, Baret F, Xingfa G, et al. (2002) Relating soil surface moisture to reflectance. *Remote Sensing of Environment* 81: 238-246.
- Zhao W and Ji X. (2016) Spatio-temporal variation in transpiration responses of maize plants to vapor pressure deficit under an arid climatic condition. *Journal of Arid Land* 8: 409-421.
- Zotarelli L, Dukes MD and Morgan KT. (2010) Interpretation of Soil Moisture Content to Determine Soil Field Capacity and Avoid Over-Irrigating Sandy Soils Using Soil Moisture Sensors. *Agricultural and Biological Engineering Department Series*. Gainesville, Florida: UF/IFAS Extension.

Paper V

Estimating gross primary productivity in semi-arid Africa using the plant phenology index

A M Abdi ^{1*}, N Boke-Olén ¹, H Jin ¹, L Eklundh ¹, T Tagesson ², V Lehsten ^{1,3}, J Ardö ¹

¹ Department of Physical Geography and Ecosystem Science, Lund University, Sölvegatan 12, SE-223 62 Lund, Sweden

² Department of Geosciences and Natural Resource Management, University of Copenhagen, DK-1350 Copenhagen, Denmark

³ Swiss Federal Institute for Forest, Snow and Landscape research (WSL), Zürcherstr. 11, CH-8903 Birmensdorf, Switzerland

* Author to whom correspondence should be addressed; E-Mail: hakim.abdi@gmail.com

Abstract

The importance of drylands in the global carbon cycle as a sink for CO₂ emissions has recently been highlighted. Thus, accurate estimation of the spatiotemporal dynamics of carbon assimilation in drylands is necessary. In this letter, the efficacy Plant Phenology Index (PPI) is examined and compared against three Earth observation-based models of gross primary productivity (GPP). PPI which was originally designed for boreal coniferous forests and provides improved estimates for seasonality metrics in those ecosystems. Since PPI was designed to capture green leaf area index, it could potentially be used in estimating GPP. Results show that a PPI-based GPP model was able to capture the magnitude of in situ GPP relatively well ($R^2 = 0.75$, RMSE = 1.39 g C m⁻² d⁻¹) compared to the other tested models. However, this correlation could be further improved by accounting for total chlorophyll content to estimate GPP in semi-arid systems.

Introduction

The uptake of CO₂ by terrestrial vegetation through photosynthesis, termed gross primary productivity (GPP), is the largest flux of the global carbon cycle (Le Quere et al., 2009). Globally, GPP accounts for 120 petagrams of carbon (PgC) and its spatiotemporal variability is not fully understood owing to the complexity of processes related to plant physiology and environmental controls on photosynthesis (Xia et al., 2015). Several modeling approaches attempted to describe the process whereby solar radiation is converted into carbon (McCallum et al., 2009; Anav et al., 2015). One of the most common approaches, called light use efficiency (LUE), was first described by Monteith (1972). The concept is based on the premise that GPP is proportional to the absorbed photosynthetically active radiation (APAR), which equals incoming PAR multiplied by the fraction of absorbed PAR (fPAR), and an LUE factor (ϵ) that translates absorbed energy into assimilated carbon (Equations 1).

$$GPP = APAR \times \epsilon \quad (1)$$

Presently, the Moderate Resolution Imaging Spectroradiometer (MODIS) onboard the Terra and Aqua satellites is the only Earth observation (EO) platform that provides near-real-time estimates of terrestrial carbon uptake. At the core is the MOD17 algorithm (Running et al., 2004) that uses MODIS spectral data and climatic drivers in an LUE model (Heinsch et al., 2003). In sub-Saharan Africa, Sjöström et al. (2013) found that, of the 12 eddy covariance savanna sites in their study, MOD17 underestimated ϵ for 10 of them by an average of 1.2 g C MJ⁻¹. Thus, MOD17 primary productivity over African drylands may not be fully representative of field conditions. The potential of the Enhanced Vegetation Index (EVI) to model GPP in African ecosystems and its comparison to MOD17 GPP (v. 5.0) was further explored by Sjöström et al. (2011). They found that a GPP model based on EVI and factors related to water availability and PAR to be an improvement over MOD17 GPP in African ecosystems. However, in a recent review, Tang et al. (2016) expressed concern whether spectral vegetation indices can really capture the primary productivity cycle since they represent the endpoint of plant physiological process such as assimilation, respiration and phytomass accretion. These concerns underscore the notion that vegetation indices are not reduced to zero during periods of drought and thus do not explicitly show when photosynthesis ends (Walther et al., 2016). Considering these

shortcomings, Jin and Eklundh (2014) developed a physically-based vegetation index in an effort to achieve a higher consistency of EO-based vegetation indices that better explain the relationship between canopy development and GPP. This index, called the Plant Phenology Index (PPI), is linear to the green leaf area of the vegetation canopy and thus may be able to better represent carbon assimilation (Jin and Eklundh, 2014). PPI was originally designed for boreal coniferous forests as a solution to the influence of snow in phenology metrics that affect EVI, and the saturation that affects the Normalized Difference Vegetation Index (NDVI) at high LAI values. The efficacy of PPI has not been tested in the semi-arid ecosystems of sub-Saharan Africa. Therefore, the principal objective of this letter is to provide a first assessment on the performance of PPI in estimating the GPP of these drylands.

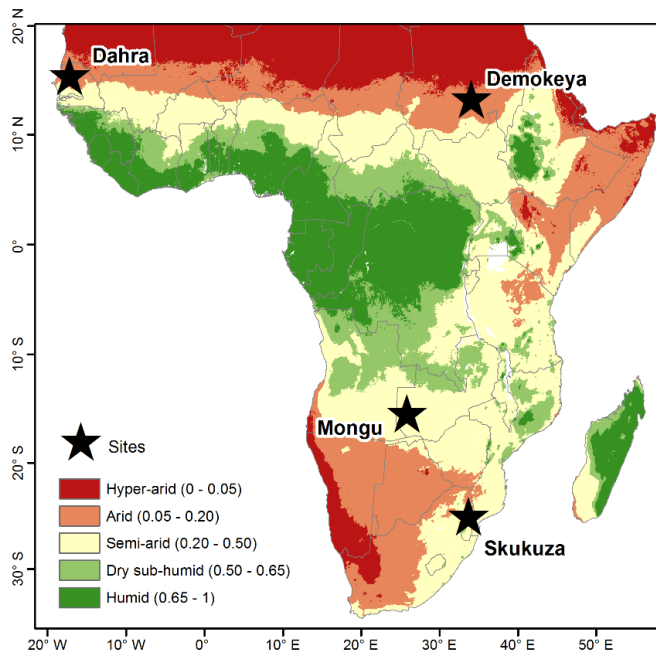


Figure 1: Location of the study sites and the aridity zones in the study region. Data on precipitation from Funk et al. (2015) and potential evapotranspiration from Mu et al. (2011) averaged for the period 2000 – 2014 were used to produce this figure

Data and Methods

Study Sites

This study focused on four eddy covariance flux tower sites in semi-arid Africa, two in the Sahel and two in southern Africa (Figure 1). The sites have mean annual precipitation (MAP) ranging between 320 – 879 mm and mean annual temperature (MAT) between 22 – 30 °C (Table 1).

Table 1: Descriptions and physical characteristics of the sites included in this study including the location in decimal degree (D), mean annual precipitation (MAP), and mean annual temperature (MAT).

Site, Country	Lon, Lat (DD)	Ecosystem Type	MAP (mm)	MAT (°C)	Measurement Years	Reference
Demokeya, Sudan	30.47, 13.28	Sparse acacia savanna	320	30	2007 – 2009	Ardö et al. (2008)
Dahra, Senegal	-15.43, 15.40	Open woody savanna	416	29	2010 – 2013	Tagesson et al. (2015)
Skukuza, South Africa	31.49, -25.01	Wooded grassland	547	22	2001 – 2005	Kutsch et al. (2008)
Mongu, Zambia	23.25, -15.43	Kataba forest	879	25	2008 – 2009	Scanlon and Albertson (2004)

Eddy Covariance Flux Tower Data

The field data for each site are part of FLUXNET2015 (fluxnet.fluxdata.org/data/fluxnet2015-dataset), which is a harmonized global dataset of micrometeorological, energy, net ecosystem exchange of CO₂ between the atmosphere and terrestrial biosphere. The data processing pipeline in the FLUXNET2015 dataset ensures intercomparability and quality assurance and control

across multiple sites. Daily data of two parameters were extracted for each site (Table 2). These data are all Tier-1 level under the fair-use data policy of the FLUXNET2015 Dataset, meaning that the data are open and free for scientific purposes (fluxnet.fluxdata.org/data/data-policy). Vapor pressure deficit (VPD) (Anderson, 1936), the difference between the amount of moisture in the air and the maximum amount of moisture the air can hold when it is saturated, has been found to be a limiting factor for GPP (Maroco et al., 1997; Ago et al., 2015). Therefore, we selected VPD along with daytime-partitioned GPP from the FLUXNET2015 database.

Table 2: Parameters extracted from the FLUXNET2015 dataset for each site.

Variable	Description	Units
GPP_DT_CUT_MEAN	Gross primary production using the daytime partitioning method (Lasslop et al., 2010), average of GPP versions.	$\text{g C m}^{-2} \text{ d}^{-1}$
VPD_F	Vapor Pressure Deficit consolidated from VPD_F_MDS and VPD_ERA methods	hPa

Earth Observation Data

The MOD17 8-day GPP product (MOD17A2) within a 3 x 3 km radius around each flux tower site was downloaded for each of the four sites from the Oak Ridge National Laboratory Distributed Active Archive Center (ORNL-DAAC, daac.ornl.gov/modisglobal) (ORNL DAAC, 2008). The Collection 5 daytime Land Surface Temperature (LST) (MOD11A2), Leaf Area Index (LAI) and Fraction of Photosynthetically Active Radiation (FPAR) (MOD15A2) were also downloaded from ORNL-DAAC. The Plant Phenology Index (PPI) for each site was acquired from the DataGURU (dataguru.lu.se). Then, PPI values were averaged over a 3 x 3 km radius around each flux tower to facilitate comparability with the MOD17A2 data.

Plant Phenology Index

Leaf area index (LAI), the one-sided leaf area per unit ground surface area ($\text{m}^2 \text{m}^{-2}$), represents the total leaf surface area that intercepts incoming photosynthetically active radiation (PAR). Additionally, LAI describes the potential leaf surface area that is available for gas exchange between the terrestrial biosphere and the atmosphere (Cowling and Field, 2003). LAI can also be subdivided into photosynthetic (green) and non-photosynthetic (brown) LAI, the latter being the LAI of dry or senescent vegetation (Pinter et al., 1983). PPI is able to capture green LAI and was expressed by Jin and Eklundh (2014) as:

$$PPI = -K \times \ln \left(\frac{M - DVI}{M - DVI_S} \right) \quad (2)$$

where PPI is in LAI units ($\text{m}^2 \text{m}^{-2}$); K is a gain factor that is dependent on sun zenith angle, the geometry of leaf angular distribution, and the instantaneous diffuse fraction of solar radiation (Jin and Eklundh, 2014); DVI is the difference between the near infrared and red bands resulting in the Difference Vegetation Index ($DVI = NIR - Red$) (Richardson and Wiegand, 1977); M is pixel-specific canopy maximum DVI; DVI_S is the DVI of the soil based on 41 soil samples from the ASTER spectral library (Baldrige et al., 2009). See Jin and Eklundh (2014) for a detailed description of PPI.

Model Formulation

Leaf chemical processes are likely to be influenced by the feedback between canopy and near-surface air, and actual leaf temperature (Hashimoto et al., 2008; Sims et al., 2008). EO-derived LST has been found to correlate well with VPD and has been used as an environmental scalar in modeling GPP (Hashimoto et al., 2008; Sims et al., 2008; Wu et al., 2010). VPD was derived from daytime LST using Equation 3:

$$VPD_{LST} = -2.74 + (2.57 * 1.06^{LST_{Day}}) \quad (3)$$

where VPD_{LST} is the vapor pressure deficit derived from LST; LST_{Day} is the 8-day MOD11A2 product. In previous study, Abdi et al. (2017) showed that GPP is significantly reduced in

Sahelian ecosystems when it is above 2 kPa. Therefore, following the approach described in Sims et al. (2008), we used VPD instead of LST as a direct control on GPP. This was done by scaling VPD_{LST} so that GPP is reduced when $VPD > 20$ hPa:

$$VPD_{Scaled} = \min \left[5.22 - (0.14 \times VPD_{LST}); \frac{VPD_{LST}}{20} \right] \quad (4)$$

We define GPP as the product of PPI and VPD_{Scaled} :

$$GPP_{PPI} = PPI \times VPD_{Scaled} \quad (5)$$

We compared this model to two other vegetation index-based models: the ‘‘Temperature-Greenness’’ (T-G) model (Sims et al., 2008) and the ‘‘Greenness-Radiation’’ (G-R) model (Gitelson et al., 2006). We also compared it to the MOD17A2 GPP product. The T-G model was originally developed for North America and uses the product of scaled LST and EVI (scaledLST * scaledEVI) to estimate GPP. It is based on the idea that GPP has generally strong correlation with EVI, and that LST accounts for temperature controls on GPP. The LST scaling factor reduces scaledLST to 1 when LST = 30°C and to 0 when LST = 0, or reaches 50°C, while the EVI scaling factor reduces GPP to zero when EVI ≈ 0.1 (Sims et al., 2008). The G-R model is based on the idea that total chlorophyll content of a canopy is the primary factor influencing the amount of PAR absorbed by green vegetation (Gitelson et al., 2006). It originally formulated GPP as the product of total chlorophyll (Chl) and top-of-canopy PAR (PAR_{TOC}), but was modified by Wu et al. (2011) who replaced Chl with EVI for scalability using EO data.

Statistical analysis

All the EO data were smoothed with a Savitzky-Golay filter (Savitzky and Golay, 1964) in the software package TIMESAT (Jönsson and Eklundh, 2004) using: fitting method = 1, window size = 5, and seasonal parameter = 1. The full dataset containing all four sites was randomly split 50/50 into calibration (297 samples) and evaluation (297 samples) subsets. In order to compare the GPP models against EC GPP, we used the coefficient of determination (R^2) in an ordinary least-squares regression analysis. We also computed the root-mean-square error (RMSE) to assess their accuracy in relation to EC GPP.

Results and Discussion

Inter-annual and seasonal variations in the eddy covariance-derived variables

EC GPP was seasonal with distinct growing and non-growing periods (Figure 2). This seasonality corresponded well with the seasonal and inter-annual pattern of VPD, which is high during the dry season and low during the growing season. The LST seasonality matched that of VPD at all sites except at the southernmost site, Skukuza (Figure 2 c), where VPD was somewhat erratic.

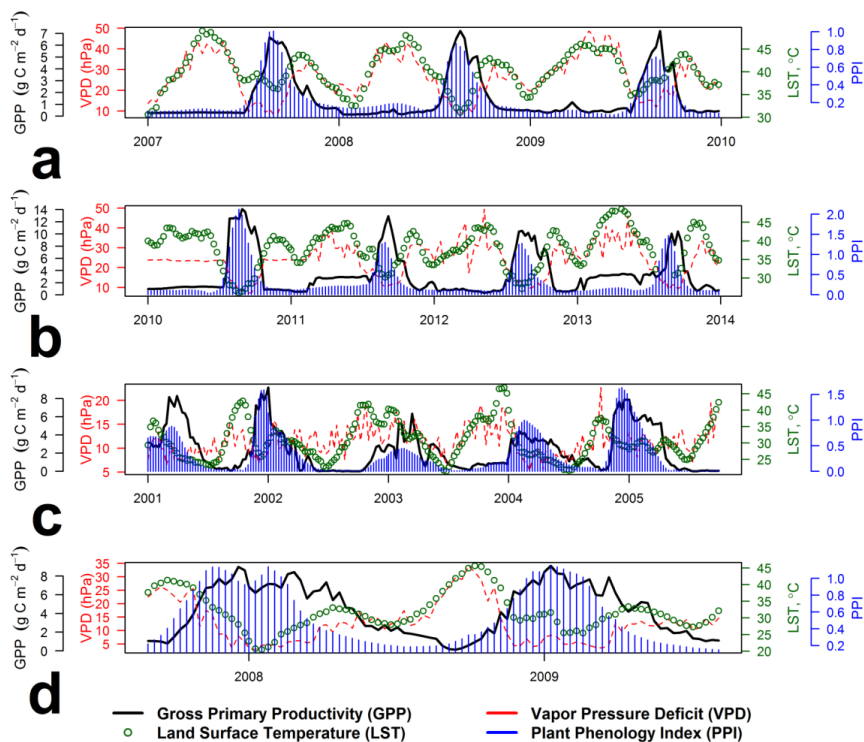


Figure 2: Seasonality and inter-annual variability of 8-day averaged PPI and MOD11A2 LST, and the FLUXNET2015 derived EC GPP and VPD for (a) Demokeya, (b) Dahra, (c) Skukuza, (d) Mongu. Note the differences in scaling of the y-axes.

PPI followed the seasonal progression of EC GPP generally well across all sites. Though, at the forested site, Mongu, the green-up and brown-down phases had a distinct offset (Figure 2 d). Maximum EC GPP during the growing season was between $7.5 - 9.5 \text{ g C m}^{-2} \text{ d}^{-1}$ at most sites except Dahra, which had a maximum of $14 \text{ g C m}^{-2} \text{ d}^{-1}$, despite possessing considerably less tree canopy cover ($\sim 3\%$) than either Skukuza (30%) or Mongu (65%). The reasons for the high GPP at Dahra are caused by higher photosynthetic capacity at the site due to site characteristics (higher fraction of C4 plants), anthropogenic influence (grazing-induced compensatory growth) and climatic factors (West African Monsoon) (Tagesson et al., 2016a; Tagesson et al., 2016b).

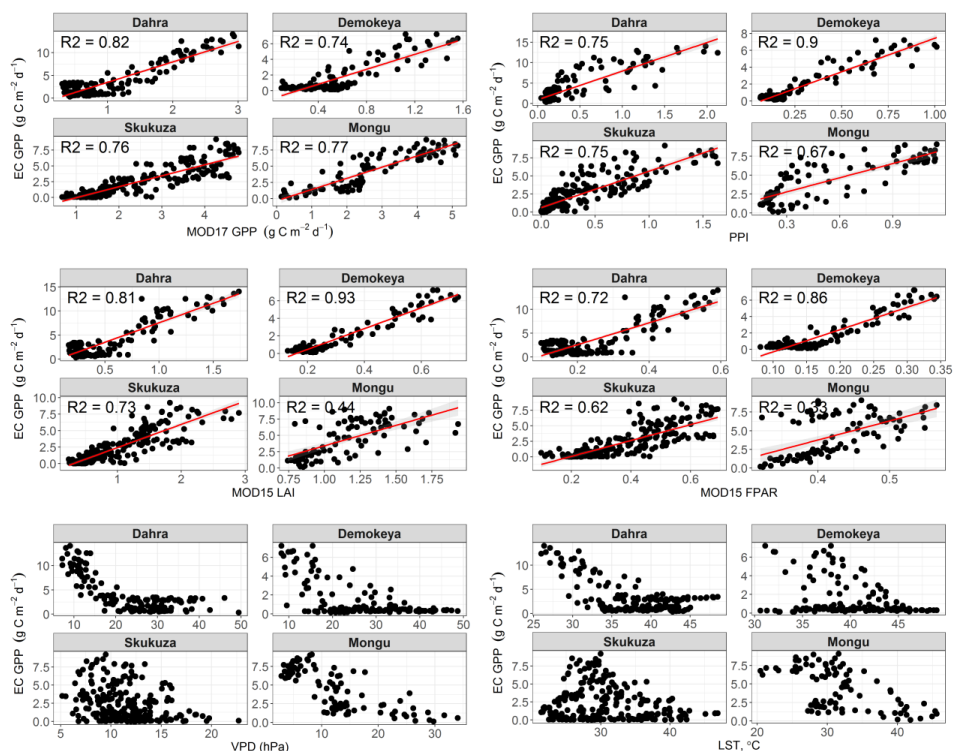


Figure 3: Scatterplots of individual site-based relationships between the 8-day EO-derived data and 8-day EC GPP. The solid red line is the regression line.

Relationship between field and EO data

Comparison between EC GPP, PPI and the different MODIS vegetation products are shown in Figure 3. PPI performed well across all the sites with the highest correlation with EC GPP in Demokeya ($R^2 = 0.90$), and the lowest in Mongu ($R^2 = 0.67$). Although MOD17 GPP performed fairly well across the four sites, with an average R^2 of 0.77 it consistently underestimated EC GPP by an average of $1.12 \text{ g C m}^{-2} \text{ d}^{-1}$. The probably reason for this is the low LUE specification in biome properties look-up table, as specified in Sjöström et al. (2013). The correlation between EC GPP and MOD15 fPAR and LAI products was generally high for most sites ($0.62 < R^2 < 0.93$) except at Mongu where the R^2 was 0.33 and 0.44, respectively. The sites with higher percent canopy cover, Skukuza and Mongu, displayed some hysteresis in the relationship between EC GPP and PPI, EVI, fPAR and APAR. Hysteresis is a disproportionate increase-decrease pattern that creates the appearance of a loop in the scatterplot caused when the greening and browning phases have a distinctly different behavior. In dryland systems this behavior could be due to the coupled action of plant available water and vapor pressure deficit during the two phases (Abdi et al., 2017). The scatterplot of EC GPP and VPD shows the seasonal peak EC GPP corresponds with $\text{VPD} < 2 \text{ hPa}$.

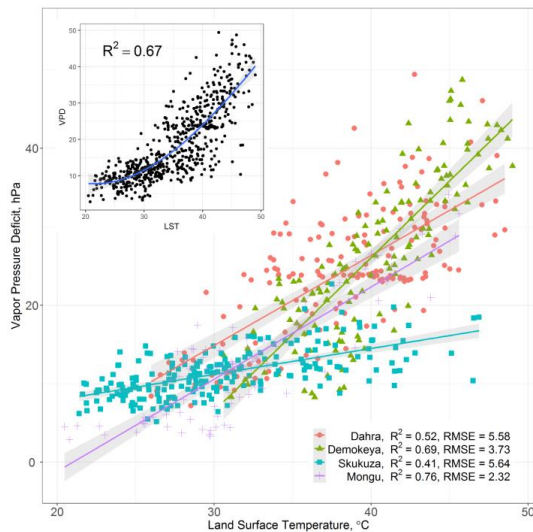


Figure 4: Individual and cross-site (inset) relationships between 8-day VPD and LST.

EC GPP had low correlations with LAI ($R^2 = 0.44$) and fPAR ($R^2 = 0.33$) at Mongu (Figure 3). VPD and LST had a generally strong relationship across all the sites ($R^2 = 0.67$) (Figure 4), due to the connection of LST with VPD, surface moisture conditions and the partitioning of latent and sensible heat fluxes. Generally, the rainy season in African drylands has a lower LST than the dry season due to increased vegetative cover, and the incoming energy is rapidly utilized by evapotranspiration (Nutini et al., 2014).

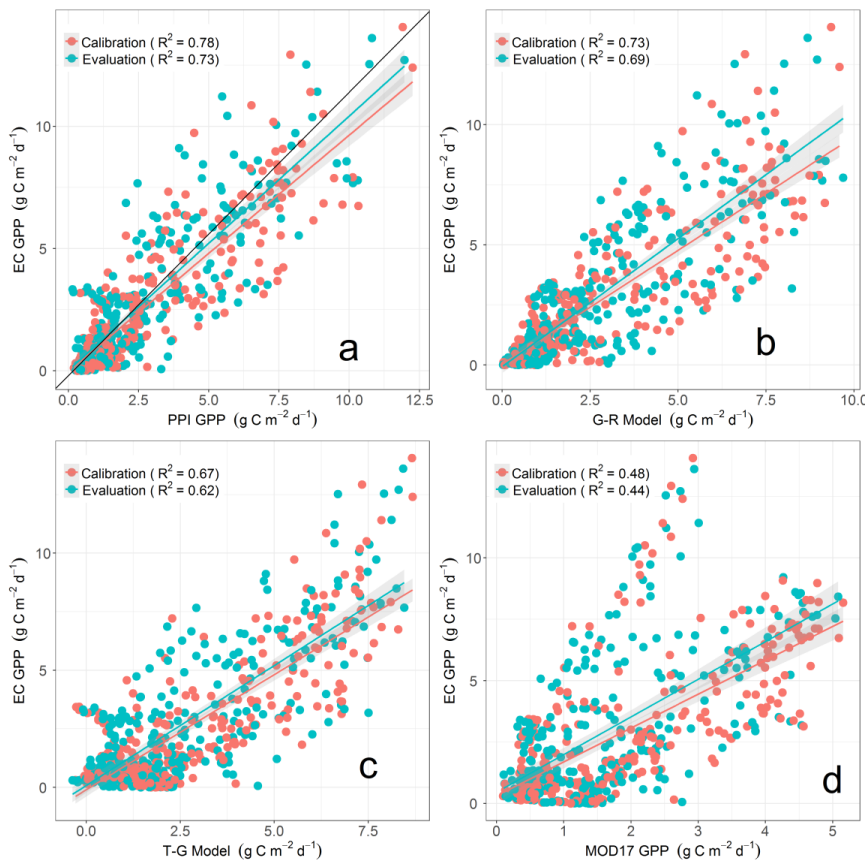


Figure 5: Cross-site relationships between EC GPP and each of the four GPP models (a – d, see Table 4). The calibration and evaluation dataset each has the same quantity of data points ($n = 297$). The red and green lines are the regression line for calibration and evaluation, respectively, with 95% confidence interval in light gray shading.

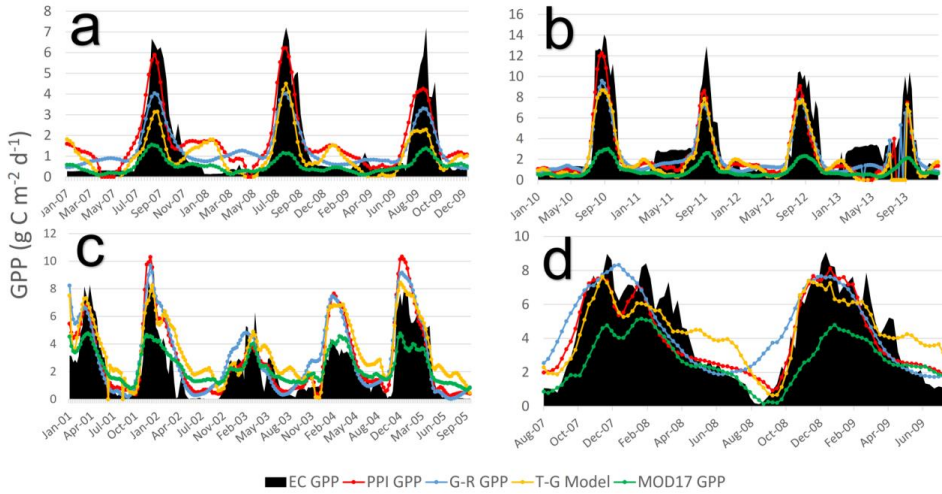


Figure 6: Time series comparison between the four GPP models (see Table 3) at each site: **(a)** Demokeya, **(b)** Dahra, **(c)** Skukuza, and **(d)** Mongu.

Table 3: A full dataset ($n = 594$) summary of the regression coefficients between EC GPP and four models across the four sites. F is the F-statistic, DF is the degrees of freedom, S.E. is the standard error, and RMSE is the root-mean-square error in $\text{g C m}^{-2} \text{d}^{-1}$.

	β_0	β_1	R^2	F	DF	S.E.	RMSE
PPI GPP	0.1248	2.9330	0.75	1867	611	0.067	1.39
T-G Model	-0.4744	18.0335	0.64	1107	618	0.5420	1.70
G-R Model	-1.4524	1.2311	0.70	1481	622	0.0319	1.54
MOD17	0.4277	1.4291	0.43	471	629	0.0658	2.14

Comparison of GPP models

The calibration and evaluation output produced by the PPI GPP model were comparable with GPP modeled using other methods (Figure 5 a). MOD17 GPP underestimated EC GPP and displayed two distinct slopes, a higher slope ($\beta_1 = 4.5$) and lower slope ($\beta_1 = 1.74$) (Figure 5 d). The data points within the higher slope belong to the two Sahelian sites, and the lower slope includes the two southern African sites. This split could be attributed to MOD17's reliance on the MOD12Q1 land cover product (Friedl et al., 2010). MOD12Q1 classifies Mongu as "Savanna", a class that has a maximum possible tree canopy cover of 30% according to Hansen et al. (2000), which is roughly half of the canopy cover at Mongu. The calibration and evaluation R^2 results of the G-R model (Gitelson et al., 2006) underperformed in comparison to the PPI GPP model (Figure 5 a b), leading to a lower overall performance of that model (RMSE = 1.54 vs. 1.39 g C m⁻² d⁻¹) (Table 3). Additionally, the slopes of the regression lines in Figure 5, show that the PPI GPP model displayed the closest value to the 1:1 line. This suggests that PPI GPP model exhibits a relatively strong ability to estimate the magnitude of EC GPP compared to the G-R model. The PPI GPP model also outperformed the T-G model in both the calibration (RMSE = 1.30 vs. 1.60 g C m⁻² d⁻¹) and evaluation (RMSE = 1.47 vs. 1.76 g C m⁻² d⁻¹) datasets (Figure 5 c). The sites classified as "drought sites" in Sims et al. (2008) are considerably cooler than Sahelian sites (12°C vs 30°C), so the LST scaling factor in the T-G model cannot account for the environmental conditions in this warm region. However, the T-G model performed well at Skukuza ($R^2 = 0.74$), which is probably because it has a lower mean LST (29°C) that is within the optimal threshold set in the T-G model (Sims et al., 2008). The full PPI GPP model used was:

$$GPP_{PPI} = 0.12 + 2.93 \times (PPI \times VPD_{Scaled})^{0.70} \quad (6)$$

A time series comparison of the four GPP models (PPI, G-R, T-G, and MOD17) and EC GPP for each site is shown in Figure 6. The PPI GPP model tracked the seasonal and inter-annual development of EC GPP well. Furthermore, it managed to capture the amplitude of EC GPP reasonable well, which is further confirmed by the slope close to the 1:1 line in Figure 5 a. At Demokeya, the PPI model over-estimated GPP during the dry season, but captured the start and end of the growing season for all sites in-line with EC GPP except at Mongu (Figure 6 d). The

MOD17 model underestimated GPP at all sites but was able to follow the greening and browning phases of Skukuza (30% canopy cover) and Mongu (65% canopy cover), suggesting that this model does better in tree-dominated areas than savanna. The T-G model either excessively underestimated (Figure 6 a b) or overestimated (Figure 6 c) peak GPP at most sites.

Conclusions

The Plant Phenology Index (PPI) was originally designed for boreal coniferous forests as a solution to suppressing the influence of snow in phenology metrics that affect the EVI, and the saturation that affects the Normalized Difference Vegetation Index (NDVI) at high LAI values. In this study, we evaluated the performance of a PPI-based model in predicting the GPP at four semi-arid sites in sub-Saharan Africa with a wide canopy cover range (3 – 65%). We found that PPI is able to capture EC GPP reasonably well ($R^2 = 0.75$, $RMSE = 1.39 \text{ g C m}^{-2} \text{ d}^{-1}$) due to its sensitivity to green LAI. It further managed to capture the magnitude of EC GPP relatively well compared to the other tested models. However, the performance of PPI can be further improved through the inclusion of total chlorophyll content as it is a principal factor influencing carbon assimilation. Canopy foliage remains green during the growing season despite considerable variability in total chlorophyll content between the beginning and end of the season. Accounting for total chlorophyll content, perhaps through the inclusion of chlorophyll-sensitive vegetation indices, could further enhance the ability of PPI to estimate GPP in semi-arid systems.

Acknowledgments

AMA received support from the Lund University Center for Studies of Carbon Cycle and Climate Interactions (LUCCI) and the Royal Physiographic Society in Lund. Funding for this project was provided by the Swedish National Space Board (contract no. 100/11 to JA).

References

- Abdi AM, Boke-Olén N, Tenenbaum DE, et al. (2017) Evaluating water controls on vegetation growth in the semi-arid Sahel using field and Earth observation data. *Submitted to Remote Sensing*.
- Ago EE, Serça D, Agbossou EK, et al. (2015) Carbon dioxide fluxes from a degraded woodland in West Africa and their responses to main environmental factors. *Carbon Balance and Management* 10: 1-16.
- Anav A, Friedlingstein P, Beer C, et al. (2015) Spatiotemporal patterns of terrestrial gross primary production: A review. *Reviews of Geophysics* 53: 785-818.
- Anderson DB. (1936) Relative Humidity or Vapor Pressure Deficit. *Ecology* 17: 277-282.
- Ardö J, Molder M, El-Tahir BA, et al. (2008) Seasonal variation of carbon fluxes in a sparse savanna in semi arid Sudan. *Carbon Balance Manag* 3: 7.
- Baldridge AM, Hook SJ, Grove CI, et al. (2009) The ASTER spectral library version 2.0. *Remote Sensing of Environment* 113: 711-715.
- Cowling SA and Field CB. (2003) Environmental control of leaf area production: Implications for vegetation and land-surface modeling. *Global Biogeochemical Cycles* 17: 7-1-7-14.
- Friedl MA, Sulla-Menasse D, Tan B, et al. (2010) MODIS Collection 5 global land cover: Algorithm refinements and characterization of new datasets. *Remote Sensing of Environment* 114: 168-182.
- Funk C, Peterson P, Landsfeld M, et al. (2015) The climate hazards infrared precipitation with stations—a new environmental record for monitoring extremes. *Scientific Data* 2: 150066.
- Gitelson AA, Viña A, Verma SB, et al. (2006) Relationship between gross primary production and chlorophyll content in crops: Implications for the synoptic monitoring of vegetation productivity. *Journal of Geophysical Research: Atmospheres* 111: n/a-n/a.
- Hansen M, DeFries R, Townshend JR, et al. (2000) Global land cover classification at 1 km spatial resolution using a classification tree approach. *International Journal of Remote Sensing* 21: 1331-1364.
- Hashimoto H, Dungan JL, White MA, et al. (2008) Satellite-based estimation of surface vapor pressure deficits using MODIS land surface temperature data. *Remote Sensing of Environment* 112: 142-155.
- Heinsch FA, Reeves M, Bowker C, et al. (2003) GPP and NPP (MOD17A2/A3) Products NASA MODIS Land Algorithm. *MOD17 User's Guide*: 1-57.
- Jin H and Eklundh L. (2014) A physically based vegetation index for improved monitoring of plant phenology. *Remote Sensing of Environment* 152: 512-525.
- Jönsson P and Eklundh L. (2004) TIMESAT—a program for analyzing time-series of satellite sensor data. *Computers & Geosciences* 30: 833-845.
- Kutsch WL, Hanan N, Scholes B, et al. (2008) Response of carbon fluxes to water relations in a savanna ecosystem in South Africa. *Biogeosciences* 5: 1797-1808.
- Lasslop G, Reichstein M, Papale D, et al. (2010) Separation of net ecosystem exchange into assimilation and respiration using a light response curve approach: critical issues and global evaluation: separation of net into GPP and Reco. *Glob Change Biol.* 16.
- Le Quere C, Raupach MR, Canadell JG, et al. (2009) Trends in the sources and sinks of carbon dioxide. *Nature Geosci* 2: 831-836.
- Maroco J, Attille, P. o, et al. (1997) Stomatal Responses to Leaf-to-Air Vapour Pressure Deficit in Sahelian Species. *Functional Plant Biology* 24: 381-387.
- McCallum I, Wagner W, Schimullius C, et al. (2009) Satellite-based terrestrial production efficiency modeling. *Carbon Balance and Management* 4.
- Monteith JL. (1972) Solar radiation and productivity in tropical ecosystems. *Journal of Applied Ecology* 9: 747-766.
- Mu Q, Zhao M and Running SW. (2011) Improvements to a MODIS global terrestrial evapotranspiration algorithm. *Remote Sensing of Environment* 115: 1781-1800.

- Nutini F, Boschetti M, Candiani G, et al. (2014) Evaporative Fraction as an Indicator of Moisture Condition and Water Stress Status in Semi-Arid Rangeland Ecosystems. *Remote Sensing* 6: 6300.
- ORNL DAAC. (2008) MODIS Collection 5 Land Products Global Subsetting and Visualization Tool. In: DAAC O (ed). Oak Ridge, Tennessee, USA.
- Pinter PJ, Jackson RD, Idso SB, et al. (1983) Diurnal Patterns of Wheat Spectral Reflectances. *IEEE Transactions on Geoscience and Remote Sensing* GE-21: 156-163.
- Richardson AJ and Wiegand C. (1977) Distinguishing vegetation from soil background information. *Photogrammetric engineering and remote sensing* 43: 1541-1552.
- Running SW, Nemani RR, Heinsch FA, et al. (2004) A Continuous Satellite-Derived Measure of Global Terrestrial Primary Production. *BioScience* 54: 547-560.
- Savitzky A and Golay MJE. (1964) Smoothing and Differentiation of Data by Simplified Least Squares Procedures. *Analytical Chemistry* 36: 1627-1639.
- Scanlon TM and Albertson JD. (2004) Canopy scale measurements of CO₂ and water vapor exchange along a precipitation gradient in southern Africa. *Glob Change Biol.* 10.
- Sims DA, Rahman AF, Cordova VD, et al. (2008) A new model of gross primary productivity for North American ecosystems based solely on the enhanced vegetation index and land surface temperature from MODIS. *Remote Sensing of Environment* 112: 1633-1646.
- Sjöström M, Ardö J, Arneth A, et al. (2011) Exploring the potential of MODIS EVI for modeling gross primary production across African ecosystems. *Remote Sensing of Environment* 115: 1081-1089.
- Sjöström M, Zhao M, Archibald S, et al. (2013) Evaluation of MODIS gross primary productivity for Africa using eddy covariance data. *Remote Sensing of Environment* 131: 275-286.
- Tagesson T, Ardö J, Guiro I, et al. (2016a) Very high CO₂ exchange fluxes at the peak of the rainy season in a West African grazed semi-arid savanna ecosystem. *Geografisk Tidsskrift-Danish Journal of Geography* 116: 93-109.
- Tagesson T, Fensholt R, Cappelaere B, et al. (2016b) Spatiotemporal variability in carbon exchange fluxes across the Sahel. *Agricultural and Forest Meteorology* 226–227: 108-118.
- Tagesson T, Fensholt R, Guiro I, et al. (2015) Ecosystem properties of semiarid savanna grassland in West Africa and its relationship with environmental variability. *Global Change Biology* 21: 250-264.
- Tang J, Körner C, Muraoka H, et al. (2016) Emerging opportunities and challenges in phenology: a review. *Ecosphere* 7: e01436-n/a.
- Walther S, Voigt M, Thum T, et al. (2016) Satellite chlorophyll fluorescence measurements reveal large-scale decoupling of photosynthesis and greenness dynamics in boreal evergreen forests. *Global Change Biology* 22: 2979-2996.
- Wu C, Chen JM and Huang N. (2011) Predicting gross primary production from the enhanced vegetation index and photosynthetically active radiation: Evaluation and calibration. *Remote Sensing of Environment* 115: 3424-3435.
- Wu C, Munger JW, Niu Z, et al. (2010) Comparison of multiple models for estimating gross primary production using MODIS and eddy covariance data in Harvard Forest. *Remote Sensing of Environment* 114: 2925-2939.
- Xia J, Niu S, Ciaia P, et al. (2015) Joint control of terrestrial gross primary productivity by plant phenology and physiology. *Proceedings of the National Academy of Sciences* 112: 2788-2793.

**Avhandlingar från Institutionen för naturgeografi och ekosystemanalys (INES),
Lunds universitet**

**Dissertations from Department of Physical Geography and Ecosystem Science,
University of Lund**

Martin Sjöström, 2012: Satellite remote sensing of primary production in semi-arid Africa.

Zhenlin Yang, 2012: Small-scale climate variability and its ecosystem impacts in the sub-Arctic.

Ara Toomanian, 2012: Methods to improve and evaluate spatial data infrastructures.

Michal Heliasz, 2012: Spatial and temporal dynamics of subarctic birch forest carbon exchange.

Abdulghani Hasan, 2012: Spatially distributed hydrological modelling : wetness derived from digital elevation models to estimate peatland carbon.

Julia Bosiö, 2013: A green future with thawing permafrost mires? : a study of climate-vegetation interactions in European subarctic peatlands. (Lic.)

Anders Ahlström, 2013: Terrestrial ecosystem interactions with global climate and socio-economics.

Kerstin Baumanns, 2013: Drivers of global land use change : are increasing demands for food and bioenergy offset by technological change and yield increase? (Lic.)

Yengoh Genesis Tambang, 2013: Explaining agricultural yield gaps in Cameroon.

Jörgen Olofsson, 2013: The Earth : climate and anthropogenic interactions in a long time perspective.

David Wårlind, 2013: The role of carbon-nitrogen interactions for terrestrial ecosystem dynamics under global change : a modelling perspective.

Elin Sundqvist, 2014: Methane exchange in a boreal forest : the role of soils, vegetation and forest management.

Julie Mari Falk, 2014: Plant-soil-herbivore interactions in a high Arctic wetland : feedbacks to the carbon cycle.

Finn Hedefalk, 2014: Life histories across space and time : methods for including geographic factors on the micro-level in longitudinal demographic research. (Lic.)

Sadegh Jamali, 2014: Analyzing vegetation trends with sensor data from earth observation satellites.

Cecilia Olsson, 2014: Tree phenology modelling in the boreal and temperate climate zones : timing of spring and autumn events.

Jing Tang, 2014: Linking distributed hydrological processes with ecosystem vegetation dynamics and carbon cycling : modelling studies in a subarctic catchment of northern Sweden.

Zhang Wenxin, 2015: The role of biogeophysical feedbacks and their impacts in the arctic and boreal climate system.

Lina Eklund, 2015: “No Friends but the Mountains” : understanding population mobility and land dynamics in Iraqi Kurdistan.

Stefan Olin, 2015: Ecosystems in the Anthropocene : the role of cropland management for carbon and nitrogen cycle processes.

Thomas Möckel, 2015: Hyperspectral and multispectral remote sensing for mapping grassland vegetation.

Hongxiao Jin, 2015: Remote sensing phenology at European northern latitudes : from ground spectral towers to satellites.

Bakhtiyor Pulatov, 2015: Potential impact of climate change on European agriculture : a case study of potato and Colorado potato beetle.

Christian Stiegler, 2016: Surface energy exchange and land-atmosphere interactions of Arctic and subarctic tundra ecosystems under climate change.

Per-Ola Olsson, 2016: Monitoring insect defoliation in forests with time-series of satellite based remote sensing data : near real-time methods and impact on the carbon balance.

Jonas Dalmayne, 2016: Monitoring biodiversity in cultural landscapes : development of remote sensing- and GIS-based methods.

Balathandayuthabani Panneer Selvam, 2016: Reactive dissolved organic carbon dynamics in a changing environment : experimental evidence from soil and water.

Kerstin Engström, 2016: Pathways to future cropland : assessing uncertainties in socio-economic processes by applying a global land-use model.

Finn Hedefalk, 2016: Life paths through space and time : adding the micro-level geographic context to longitudinal historical demographic research.

Ehsan Abdolmajidi, 2016: Modeling and improving Spatial Data Infrastructure (SDI).

Giuliana Zanchi, 2016: Modelling nutrient transport from forest ecosystems to surface waters.

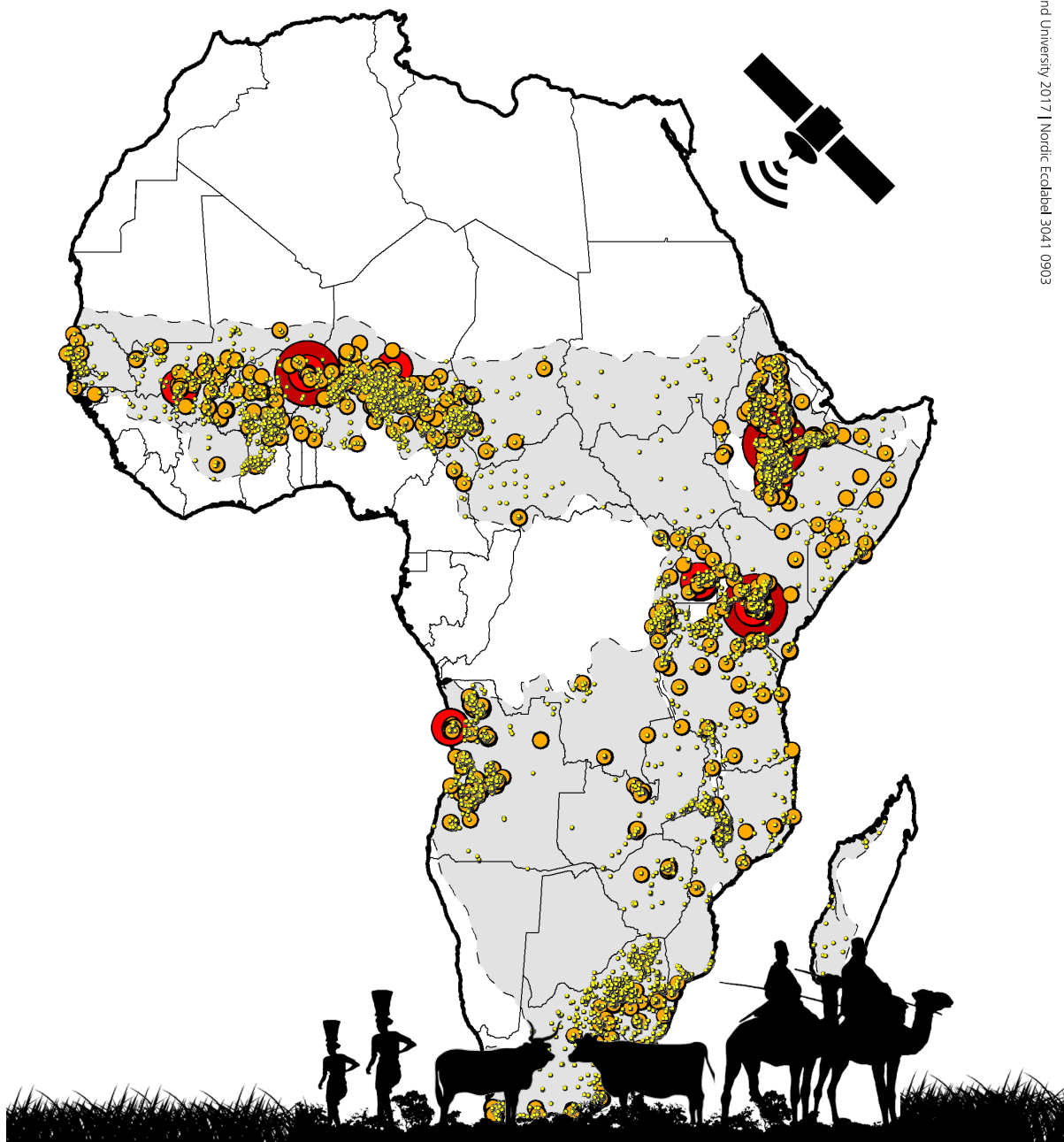
Florian Sallaba, 2016: Biophysical and human controls of land productivity under global change : development and demonstration of parsimonious modelling techniques.

Norbert Pirk, 2017: Tundra meets atmosphere : seasonal dynamics of trace gas exchange in the High Arctic.

Minchao Wu, 2017: Land-atmosphere interactions and regional Earth system dynamics due to natural and anthropogenic vegetation changes.

Niklas Boke-Olén, 2017: Global savannah phenology : integrating earth observation, ecosystem modelling, and PhenoCams.

Abdulhakim M. Abdi, 2017: Primary production in African drylands: quantifying supply and demand using earth observation and socio-ecological data.



LUND UNIVERSITY
Faculty of Science
Department of Physical Geography
and Ecosystem Science
ISBN 978-91-85793-77-8

